LAPPEENRANTA UNIVERSITY OF TECHNOLOGY
School of Engineering Science
Master's Program in Chemical and Process Engineering

Yinusa, Adeola McSteven

INFLUENCE OF PULSED-ELECTRIC FIELD IRRADIATION IN CRYSTALLIZATION

Examiner: Professor Marjatta Louhi-Kultanen
Supervisor: Johanna Puranen M. Sc.(Tech.)

ABSTRACT

Lappeenranta University of Technology
School of Engineering Science
Master's Program in Chemical and Process Engineering

Yinusa, Adeola McSteven

Influence of Pulsed-Electric Field Irradiation in Crystallization

Master's thesis

2015

51 pages, 33 figures, 6 tables and 4 appendices.

Examiner: Professor Marjatta Louhi-Kultanen
Supervisor: Johanna Puranen M. Sc.(Tech.)

Keywords: Glycine polymorphism, cooling crystallization, crystal morphology, PEF, XRD, FTIR

The growing pharmaceutical interest, among others, in the polymorphic composition of the emerging solid end-products from production processes has been traced to the need for attainment of high product purity. This is more so as the presence of different polymorphs may constitute physical impurity of the product. Hence, the need for optimization of the yield of desired product component(s) through controlled crystallization kinetics for instance.

This study was carried out to investigate the impact of pulsed electric field (PEF) irradiation on the crystal morphology of glycine obtained by cooling crystallization (without seeding) from commercial glycine sample in distilled deionized water solution. In doing so, three different pulse frequencies (294, 950 and 145 Hz) and a case without PEF were studied at three cooling rates (5, 10 and 20 ºC/h). The crystal products obtained were analyzed for polymorphic composition by powder x-ray diffraction (PXRD) and Fourier transform infrared (FTIR) spectroscopy while the particles characterization was done on Morphologi G3.

The results obtained from this study showed that pulsed electric field irradiation had significant impact on metastability of the aqueous solution as well as on the polymorphic composition of the end product. With increasing PEF frequency applied, nucleation started earlier and the γ-glycine polymorph content of the product crystals increased. These were found to have been aided by cooling rate, as the most significant effect was observed at 5 ºC/h. It was also discovered that PEF application had no measurable impact on the pH of the aqueous solution as well as the size distribution of the particles. Cooling on the contrary was believed to be responsible for the broadening of the particle size distribution with a downward shift of the lower limit of the raw material from about 100 μm to between 10 and 50 μm.

ACKNOWLEDGEMENTS

I would like to firstly thank God and Prof. Marjatta Louhi-Kultanen for offering me the opportunity to carry out this study as my Master's Thesis. In addition, to this first offer, her active guidance throughout the period of this work was immensely useful and profoundly appreciated. To Johanna Puranen, my supervisor, I definitely cannot quantify the wisdom in your professional counsel and moral support towards the success of this work. I therefore say, a very big thank you.

I would also like to express my appreciation to Liisa Puro and Toni Väkiparta for their assistance with my analysis. My colleagues, lecturers and technical support staff at LUT throughout the period of my study, I sincerely appreciate your individual and collective contributions to this day. My deep appreciation also goes to LUT Foundation for its financial contribution towards the success of this project.

Finally, my unending appreciation goes to my family at home and abroad; my mum, siblings, wife and daughters. Your moral support and understanding, particularly with respect to my need for absence in order to ensure focus on this work. And to that brother-in-friend from my Bachelor degree days, Ghali, I say thank you for everything and best of luck in all your endeavors.

January 2015, Lappeenranta

Yinusa, Adeola McSteven

TABLE OF CONTENTS

APPENDICES

Appendix I: PXRD spectra of individual measurements

Appendix II: FT-IR spectra of individual measurements

Appendix III: Morphologi G3 particle images of individual measurements

Appendix IV: Particle characterization data plots

NOMENCLATURE

Symbols

Cd_temp	digitally displayed coolant temperature	, ºC
Cm_temp	manually determined coolant temperature	, ºC
c_p	specific heat capacity of water	, J/(kg·K)
D	impeller diameter	, m
d	treatment gap or distance between electrodes	, m
E	electric field intensity or strength	, kV/cm
m	total mass of treated sample	, kg
N	impeller rotation speed	, rpm
P	estimated heating effect of the electric field	, W
PN	crystallization conducted without electric field	, -
P2	pulse frequency at pulse setting 2	, Hz
P3	pulse frequency at pulse setting 3	, Hz
P4	pulse frequency at pulse setting 4	, Hz
S_temp	temperature of the aqueous solution	, ºC
t	time corresponding to temperature rise of solution	, s
U	applied voltage	, V
ΔT	temperature increase	, ºC
α	alpha glycine polymorph	, -
β	beta glycine polymorph	, -
δ	delta glycine polymorph	, -
γ	gamma glycine polymorph	, -
ε	sigma glycine polymorph	, -

Abbreviations

DC	Direct current
DSC	Differential scanning calorimetry
FTIR	Fourier transform infrared spectroscopy
KBr	Potassium bromide
KDP	Potassium dihydrogen phosphate
PEF	Pulsed electric field
PXRD	Powder X-ray diffraction
TG/DTA	Thermal gravimetry/differential thermal analyzer
UV-vis	Ultraviolet visible spectroscopy

1. INTRODUCTION

The role of crystallization as a process-step in broad applications of relevance to day-to-day industrial processes, such as wastewater treatment, food processing and pharmaceuticals, cannot be over-emphasized. Taking an instance of its pharmaceutical application significance, wherein physical impurity of the product can be occasioned by its heterogeneous polymorphic composition (Louhi-Kultanen et al. 2006), adequate knowledge of crystallization as to the identification, control and modification of the constituent polymorphs will be highly valuable to attaining the desired final product quality (Devi et al. 2014; Boldyreva et al. 2003).

Quite a lot of effort have been put into the control of the end product quality through modification of the crystallization kinetics as well as the operational crystallization conditions (Louhi-Kultanen et al. 2006) leading to the attainment of the target product. To this extent, ultrasound has been extensively studied and proven to be relatively favorable to the process but not much has been heard or even documented of the impact of pulsed-electric field irradiation. The first dc-field induced crystallization of glycine aqueous solution was reported by Aber et al. (2005).

In a classic case of unseeded batch cooling crystallization, the width of the metastable zone generated by the supersaturation of the solution is expected to pose a major influence on the nucleation mechanism of the eventual crystal product. This metastability depends on such operational factors as the mixing conditions; cooling profile and solution composition among others (Palosaari, et al. 2007). Devi, et al. (2014) demonstrated the significance of cooling in their study of unstable β-polymorph nucleation attainment, and for a simple homogenous system; the impact of mixing conditions with respect to the geometry and operating speed of the choice impeller arouses additional interest.

In this work, the effect of pulsed electric field to be employed in the investigation of glycine end product from cooling crystallization (without seeding) of commercial glycine sample is to be evaluated. Three different pulse frequencies and cooling profiles

would be studied and compared with a corresponding case without PEF. The product crystals from the experimental study therefore, would be analyzed for polymorphic composition by Powder X-ray diffraction and Fourier Transform Infrared spectroscopy while the crystal size distribution is to be executed on Morphologi G3.

2. GLYCINE

2.1 Glycine and its polymorphs

Glycine, NH_2CH_2COOH, is a protein-secreted amino acid that has been extensively reported to exist in living organisms (Srinivasan 2008). It is known to be the simplest molecule of the group (Devi et al. 2014) and is not considered to be an essential amino acid due to the ability of the body to synthesize it from other chemicals (Faculty 2009). It may be found as a neutral molecule in gaseous state but in both liquid and solid states, it exists as a crystal-hardness-favoring zwitterion as shown in Figure 1 (Sankar et al. 2010).

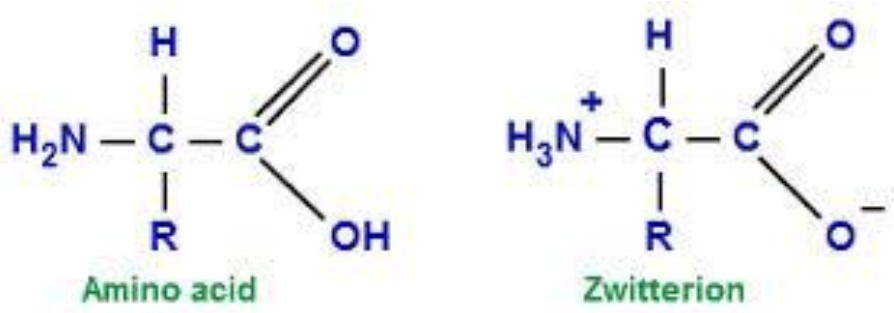

Figure 1. General structural forms of amino acid and zwitterion (Pearson 2014).

Several studies carried out on glycine have revealed that three major polymorphs, namely α-, β- and γ-, exist of the compound with a stability ranking of the order $\beta < \alpha < \gamma$ at atmospheric conditions (Srinivasan 2008; Boldyreva et al. 2003). However, two additional polymorphs, δ- and ε- have also been reportedly discovered at high pressure conditions but this has not been sufficiently substantiated (Sankar et al. 2010). α- and β- are known to exist in monoclinic form while γ- is trigonal / hexagonal, but a clearer distinction in these three identified major polymorphs can be further established in the

linkage manner of their zwitterions via hydrogen bonds (Boldyreva et al. 2003). While in α-polymorphs the zwitterions are linked as double anti-parallel layers held by van der Waals, in β-polymorphs they exist as individual parallel polar layers held in a three-dimensional structure and in γ-polymorphs they are found as three-dimensional network of connected polar helixes. It is perhaps as a result of the unstable nature of β-glycine polymorph that its crystal image, unlike those of α- and γ-polymorphs (Fig. 2), has rarely been captured in the literature.

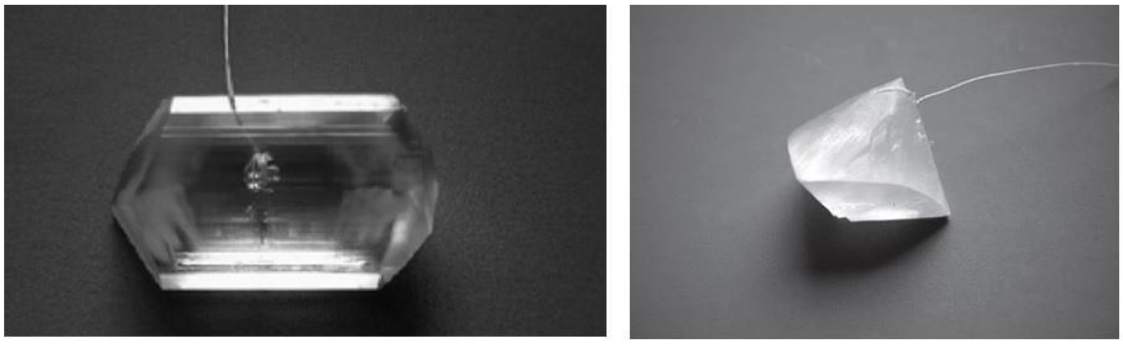

Figure 2. Images of α-glycine polymorph (left) and γ-glycine polymorph (right) crystals (Srinivasan 2008).

Although numerous studies have been carried out on glycine and its polymorphs, Boldyreva et al. (2003) opines that comparison of the reported data on its evaluated properties can be difficult and misleading due to lack of adequate information on the original composition of the studied glycine samples. Though, commercial brands of glycine are mostly packaged as α-polymorphs, there is the likelihood of its 'contamination' by the other two polymorphs, depending on the production process employed. This also goes a long way in influencing the composition of the crystallized end product and should therefore be adequately considered when dealing with commercial glycine samples.

While Figure 3 presents the solubility curve of a typical commercial glycine sample, Figure confirms the dominant proportion of α-glycine polymorphs to those of γ-glycine polymorphs in most commercial grades of glycine. It may also be noteworthy that variations in polymorphic composition have been established among packages under the

same production (Boldyreva et al. 2003) and this may further complicate the use of reported analytical data.

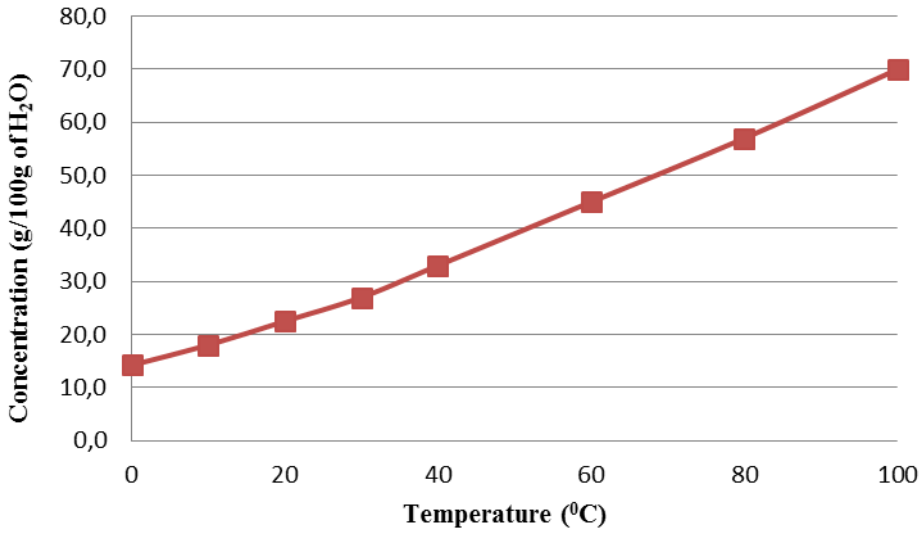

Figure 3. Solubility phase diagram of glycine (Mullin 2001).

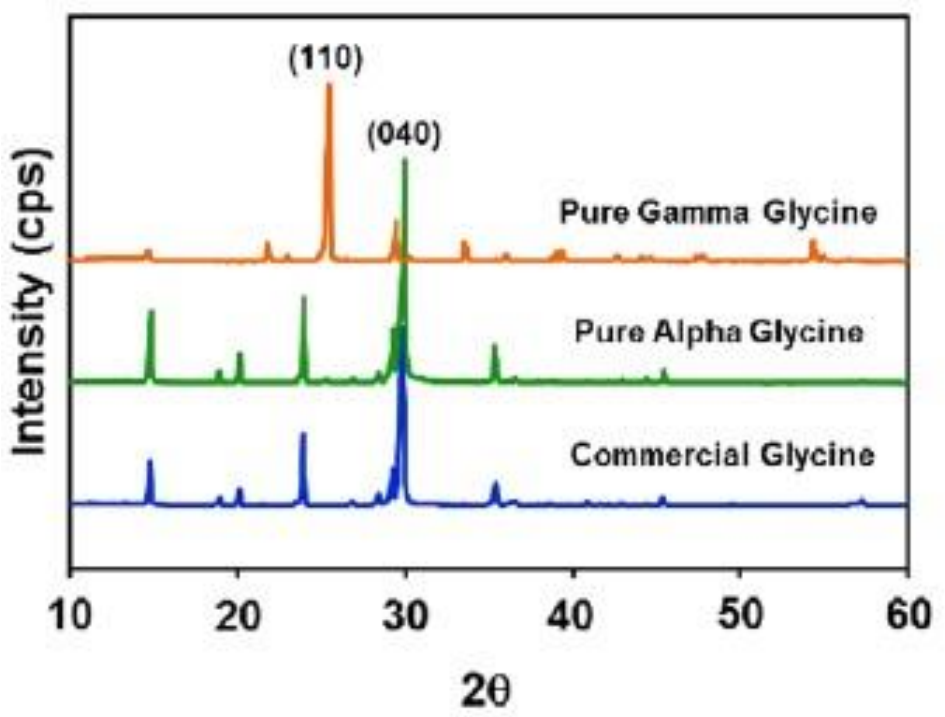

Figure 4. PXRD patterns of commercial glycine, pure α-glycine and pure γ-glycine (Devi & Srinivasan 2014).

2.2 Production processes of glycine polymorphs

It has been established in literature that the resultant crystallization product from any commercial glycine sample is largely dependent on the initial polymorphic composition of the sample. This implies that a pure α-polymorph-based glycine sample, for example, would ideally yield α-crystals unless the crystallization kinetics is doctored towards the modification of the base crystals into other polymorphic forms (Boldyreva et al. 2003). However, for most commercial grades of glycine, the synthesis of these three documented polymorphs is intertwined and could be simultaneous or concurrent (Fig. 5) as it may be observed under sophisticated in-situ monitoring (Boldyreva et al. 2003). It is for this reason, that the attainment of pure polymorph yield is very challenging.

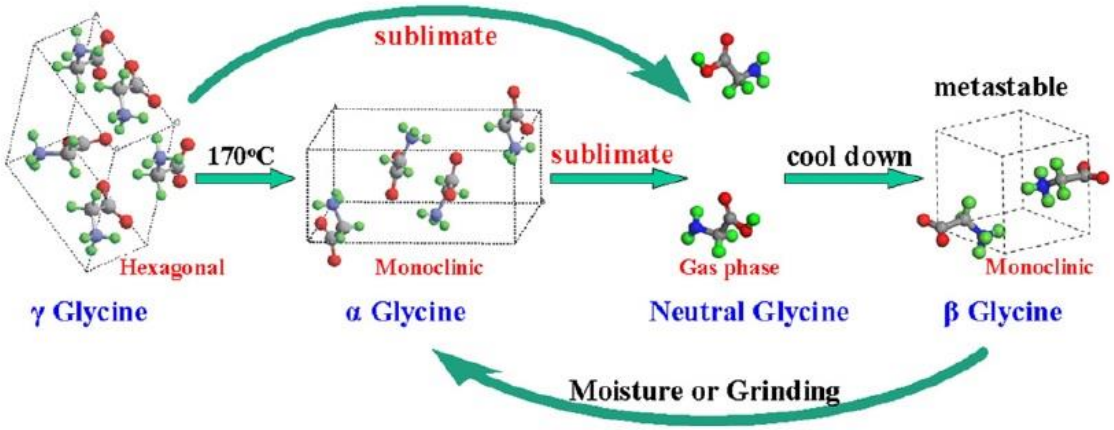

Figure 5. The transformation of glycine under sublimation (Liu et al. 2008).

While α-glycine is readily obtainable via spontaneous crystallization from its pure aqueous solutions (Srinivasan 2008), β-glycine can be obtained through precipitation of the aqueous solution by ethanol, while γ-glycine is only achievable from the aqueous medium through pulse irradiation inducement or in the presence of a selective additive (Boldyreva et al. 2003). The unstable β-glycine polymorph has hitherto been mostly synthesized through ethanol-aided anti-solvent crystallization (Nii & Takayanagi, 2014). This has been achievable with the knowledge of alcohol addition effect on aqueous glycine solution. This tends to lower the solubility of the aqueous solution with a corresponsing increase in supersaturation which results in increased concentration of solvated glycine monomers in relation to hydrogen bonded dimers (Devi et al. 2014).

But in a novel effort and departure from the most documented afore-mentioned synthesis path, Liu et al. (2008) prepared β-glycine polymorphs from vaporised forms of either of the thermodynamically more stable (α- and γ-) polymorphs. And more recently had Devi et al. (2014) reported that a metastable form β-glycine polymorphs is also achievable in dry ambient conditions through rapid dewatering and dry storage aimed at hindering the spontaneous conversion of β- to α-polymorphs. These β-polymorphs, when subjected to solution-mediated phase transformation under atmospheric conditions, produce the metastable α-polymorphs (Fig. 6) (Nii & Takayanagi 2014; Srinivasan 2008) which in turn yield the stable γ-polymorphs under high atmospheric humidity (Liu et al. 2008). However, at temperature of about 170 ^{0}C, the stable γ-polymorphs revert back into the metastable α-form (Liu et al. 2008; Srinivasan 2008).

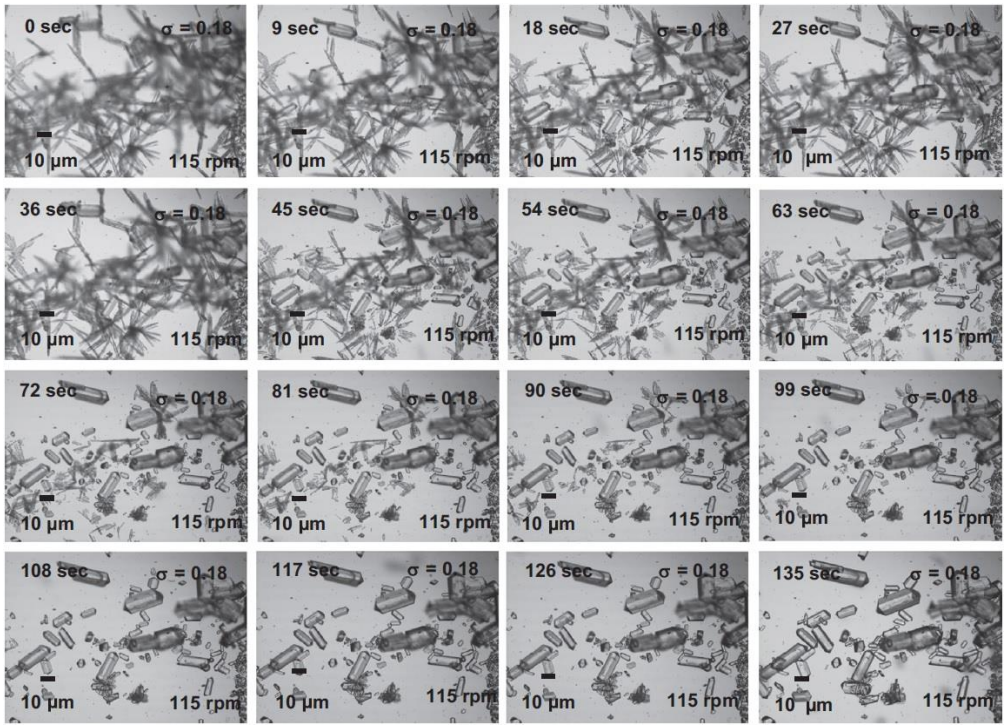

Figure 6. Solution-mediated transformation of β- to α-polymorph observed at 0.18 supersaturation and 115 rpm mixing speed (Devi et al. 2014).

In further demonstration of the significance of charged ions in aqueous glycine solution to the formation of α and γ glycine polymorphs, as could be seen in Figure 7, α-glycine

polymorphs were readily formed as dimers in the solution by self-ionic charge compensation. However, from the same solution, γ-glycine polymorphs were derived through the introduction of induced charge compensator (e.g. sodium acetate, sodium nitrate, sodium hydroxide) which prevented the spontaneous formation of the α-polymorphs favoured dimers. (Devi & Srinivasan 2014; 2013)

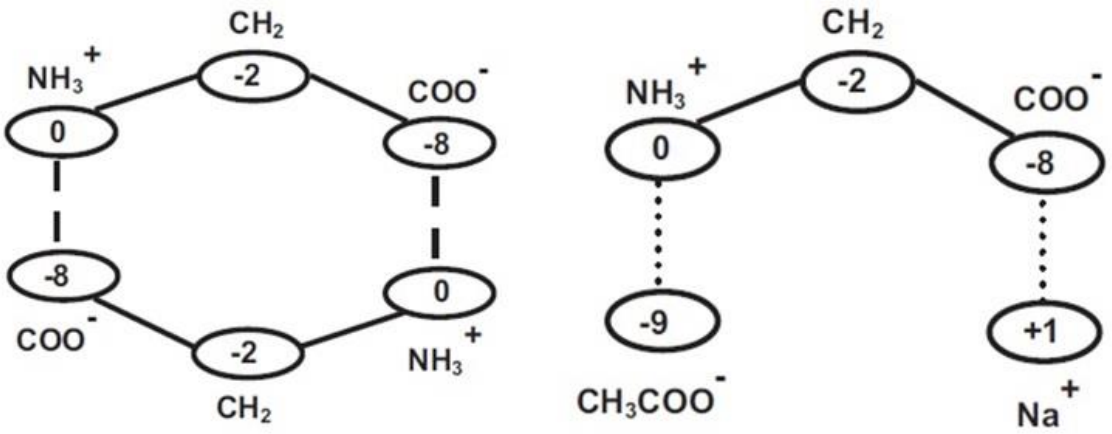

Figure 7. Self-charge compensated dimer (left) and sodium acetate compensated monomer (right) showing the net positive and negative charges in each case (Devi & Srinivasan 2013).

This induced charge compensator transforms the ionic state of the solution. When dosed increasingly beyond its critical point, it stops the erstwhile dominant self-ionic charge compensation mechanism in favour of induced-ionic charge compensation that produces the stable γ-glycine polymorphs. An alternative reasoning to this is that, the acidic nature of the selective additive (i.e. ionic charge compensator) unavoidably lowers the pH (or the basic nature causes a corresponding pH rise) of the solution thereby making the zwitterions become de-protonated (or protonated) and preventing the formation of dimers (Sankar et al. 2010).

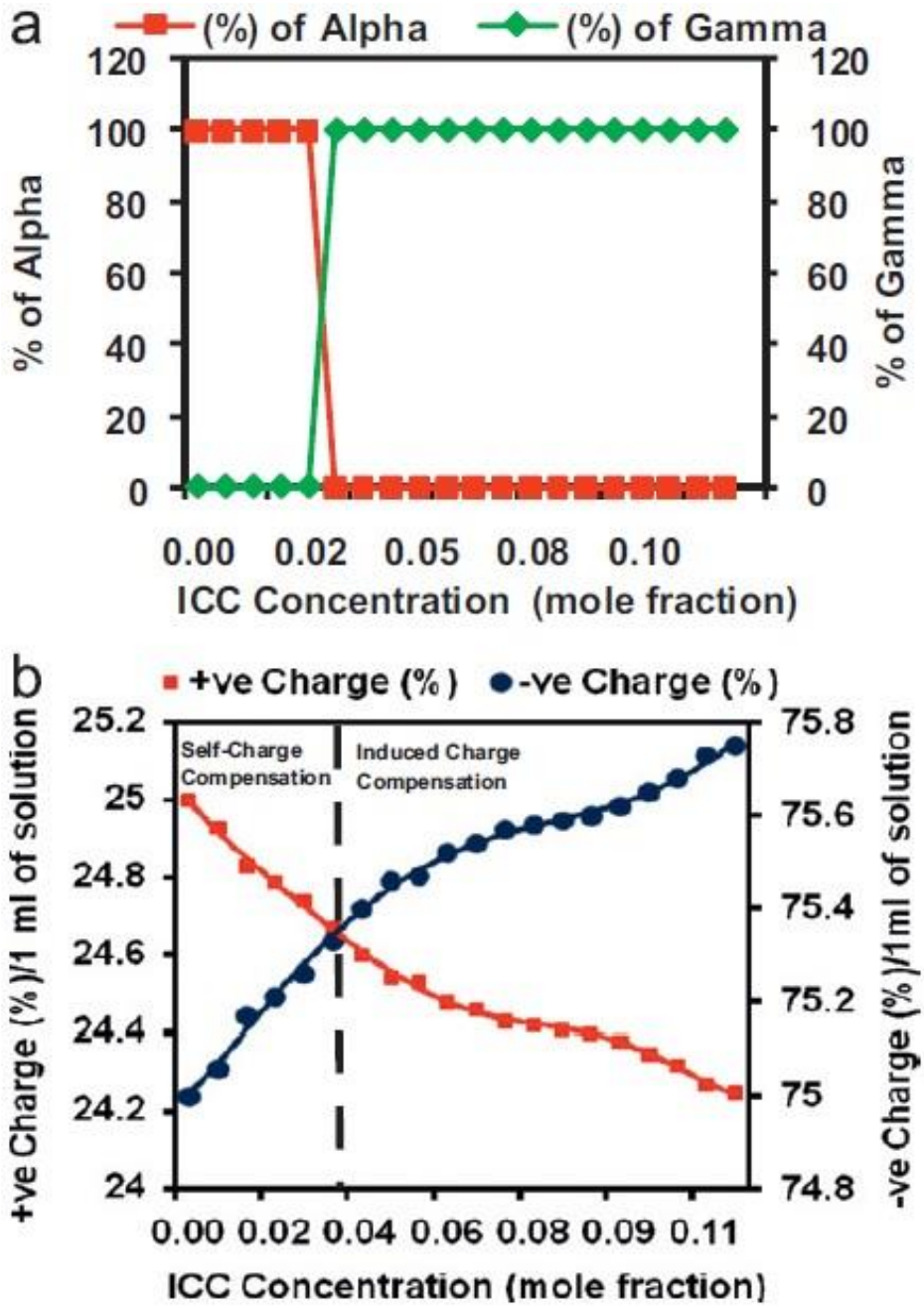

Figure 8. Percentage of polymorph nucleation (a) and net ionic charges in solution (b) at different concentrations of the induced charge compensator used to hinder the spontaneous formation of α-polymorph dimers (Devi & Srinivasan 2013).

Illustrated graphically in Figure is the effect of the sodium acetate employed as the induced charge compensator in Devi & Srinivasan (2013) to distort the spontaeous crystallization of the α-polymorphs in favour of the γ-polymorphs. It can be seen also clearly, that the composition of these two polymorphs broke-even at critical dosage of

the induced charge compensator and beyond this point, the γ- fraction increased with a corresponsing decrease of the α-fraction.

2.3 Industrial applications of glycine

Glycine has been mostly applied in medicine and in conjunction with other compounds. It has recorded proven success as a nutritional safe antacid in combination with calcium carbonate in buffer solutions. It is also known to be an important component of intravenous fluids (Yuki Gosei Kogyo Co. Ltd 2006). It has also been utilized in the treatment of schizophrenia, leg ulcers and ischemic stroke caused by blockage of blood vessel in the brain. It is also believed to hold prospects for memory enhancement and treatment of neurobehavioral disorders, benign prostatic hyperplasia (BPH), liver and kidney protection as well as cancer prevention (EBSCO Publishing 2013; Therapeutic Research Faculty 2009).

In food processing, advantage of the sweetish taste of glycine is being taken to improve the taste quality of food through seasoning, as an ingredient in pet food formulation or for smoothening of such effects as saltiness, sourness or bitterness. It is also employed either alone or in combination with other preservatives to further extend the shelf-life of foods, a feat achieved through the bacteriostatic effect of glycine which ensures the inhibition bacterial cell-wall biosynthesis during growth. As a colorant and flavor additive for food, glycine is also reportedly used in combination with reducing sugars (Fig. 9). This leads to pH and temperature elevation which when undesired is avoided by the replacement of the latter with sugar alcohols. (Yuki Gosei Kogyo Co. Ltd 2006).

Figure 9. Glycine as food additive in bean jam (Yuki Gosei Kogyo Co. Ltd 2006).

Other industrial uses of glycine include its adoption as a washing agent in the removal of metal ions through its chelating action that helps to improve the solubility of these metal ions. It is also used as an ingredient in culture media due to its effectiveness in the control of the carbon-nitrogen ratio that is reputed for the proliferation of bacteria in the medium (Yuki Gosei Kogyo Co. Ltd 2006). Kumar et al. (2011) and Srinivasan & Arumugan (2007) also justified γ-glycine as a vital non-linear optical material thereby qualifying it for application in optoelectronics, fiber optics communication and optical modulation.

3. PEF IRRADIATION AND CRYSTALLIZATION

3.1 Pulsed electric field irradiation: general principle

Pulsed electric field irradiation has been broadly utilized in food and mineral processing with positive testimonies. It belongs to the non-thermal category of emerging technologies for treatment and preservation of food and dairy products and is applicable on both continuous and batch scales (Barbosa-Canovas 2002), with long or short pulses as may be deemed necessary (Mikhaylin et al. 2014).

It is generally reputed for shortening of treatment or processing duration, reduced heating effect, minimal energy losses from heating and quality preservation among others (Verma 2012). In general principle, it is the application of high electric field intensity to a system (i.e. solution or treatment media), with the goal of setting the system into disturbance through the travel of pulse current between the electrodes. This pulse current could be of exponentially-decaying, square-wave, bi-polar or oscillatory forms (U.S. Food and Drug Administration 2011; Ramaswamy et al. 2005).

An integrated PEF system, as shown in Figure 10, comprises of a fluid handling unit, electronically monitored and controlled high voltage pulse generator, PEF treatment chamber and the product handling section. The electrodes in the PEF treatment chamber

are usually made of inert materials like titanium and are immersed into the system, such that the largest component molecule to be treated is smaller than the treatment gap of the chamber (Ramaswamy et al. 2005).

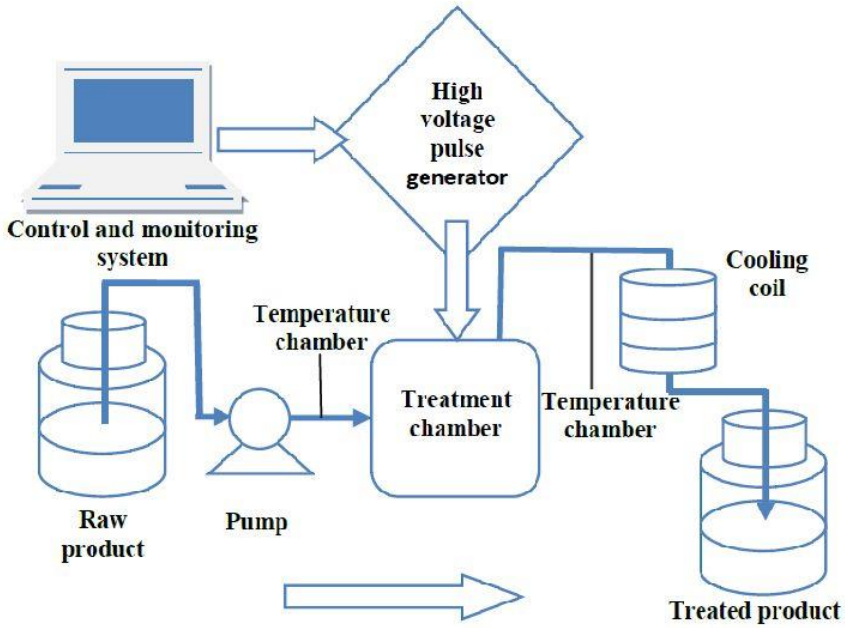

Figure 10. Schematic outline of a typical integrated PEF set-up (Verma 2012).

While the schematic illustration of Figure 10 applies to typical food processing, a direct semblance of it applies in batch cooling crystallization for instance, particularly with respect to the major components of the set-up. The fluid handling unit compares with the thermostat water-bath; the electronic monitor over the high voltage pulse generator is the same as the mixed signal oscilloscope; the PEF treatment chamber is the crystallizer or reactor; while the product handling section compares with the post-processes of filtration and product drying.

3.2 The impact of metastability on crystallization

The metastability in crystallization is characterized by a supersaturation-driven region, known as the metastable zone, in which the nucleation and consequent growth of crystals occur. Nucleation is signaled by the appearance of crystal(s) in the solution. In the case of cooling crystallization of glycine, according to Bonnin-Paris et al. (2011), it

is a consequence of the cooling of the saturated solution which leads to decrease in glycine solubility and consequent exceeding of the supersaturation limit of the solution. Crystal growth on the other hand is observed once the initial crystal(s) exceed a critical size or on addition of seed crystals and is sustained for as long as the solution remains supersaturated (Bonnin-Paris et al. 2011).

The concentration in this metastable zone is higher than in saturation but lower than that at which spontaneous nucleation occurs (Palosaari et al. 2007). Hence, it could be said that the width of this zone is defined by these boundaries. The significance of the width of this zone therefore necessitates the mention of operating conditions such as cooling rate, mixing conditions, state of the solution and presence of impurities as potential contributing factors to its size. And because the quality of product crystals are considered to be better when processed within this zone, adequate knowledge of these parameters is believed to be critical to the control of the metastable limits (Bonnin-Paris et al. 2011; Palosaari et al. 2007).

Figure 11 therefore presents a general relation between the solubility curve and metastable zones with the different nucleation possibilities in crystallization. It further depicts the ease of practical accomplishment of crystallization in the order of secondary, heterogeneous and homogeneous crystallizations (Palosaari et al. 2007).

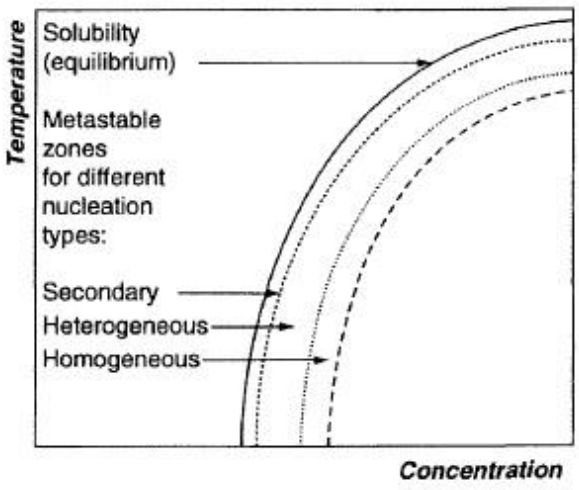

Figure 11. Schematic illustration of metastability (Palosaari et al. 2007).

The metastable zone width of aqueous glycine solution has been reported by Bonnin-Paris et al. (2011), to be greatly dependent on the cooling rate utilized. As could be seen in Figure 12, the zone widens with increasing speed of cooling. But though no mention was made of other likely process parameters aiding this observation, it is not in doubt that narrower metastable zone width was obtainable under slower cooling rates.

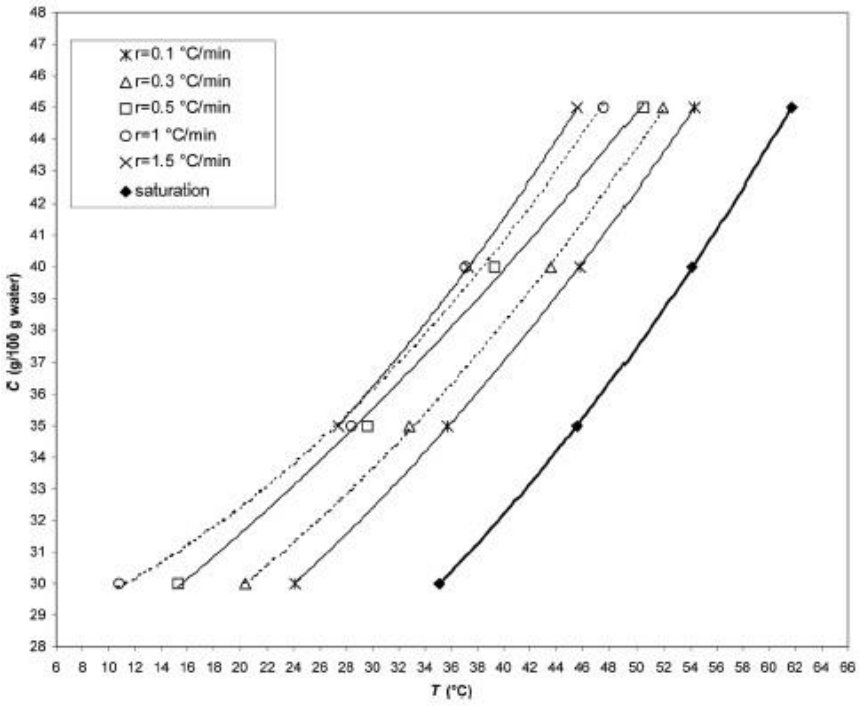

Figure 12. Cooling rate impact on metastable zone width (Bonnin-Paris et al. 2011).

3.3 Crystallization of glycine by PEF irradiation

Because glycine belongs to the family of compounds with strong permanent electric dipole moments, its solute molecules should conform to the same arrangement under the influence of the applied electric field (Fig. 13) as against the random order. This effect results in a change in the effective collisions preceding the attachment of molecules to the nucleus. Molecules with the same orientation collide with the nucleus in a specific order, which if similar to that of existent molecules in the nucleus causes the number and frequency of successful attachments to rise. (Radácsi 2012)

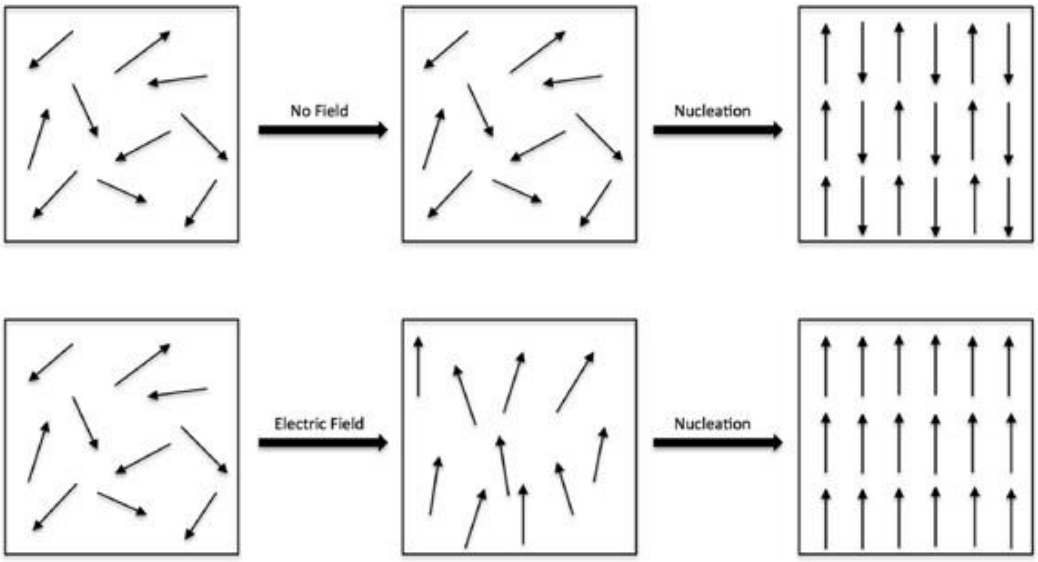

Figure 13. Electric field effect on molecules with strong electric permanent dipole moment (Radácsi 2012).

Motivated by an earlier discovery of the ability of laser beam to induce the crystallization of supersaturated aqueous glycine solutions into α- and γ- polymorphs, depending on the polarization state of the beam, Aber et al. (2005) decided to verify the theoretical evidence of a strong dc-electric field inducing glycine crystallization. One of such evidence is the molecular dynamics simulation that have shown that supercooled water could be induced to crystallize by a dc-electric field intensity of about 5000 kV/cm. They were therefore of the opinion that since glycine exists as zwitterions in aqueous solutions and possesses far more enormous permanent electric dipole moment than water, its crystallization should then be more easily induced by dc-electric field.

This hypothesis was then verified by subjecting aqueous glycine solutions (aged for 2 to 5 weeks) to dc-electric field treatment at about 6 kV/cm intensity in quiescent state (i.e. without agitation) for a period of 10 minutes. Under this circumstance, dc-electric field was reportedly found to indeed induce nucleation. At higher supersaturations (1.8 and above), γ-polymorph crystals were observed with increasing population as supersaturation increased. However, with experiments conducted under agitation, up to supersaturation of about 2.4, only α-polymorphs were obtained and traces of γ-polymorphs could only be identified thereafter. These crystallized γ-polymorphs were also found to be needle-like as against their ideal pyramid form and also grow faster.

3.4 Important parameters in crystallization with PEF

The utilization of pulsed electric field in processes has been informed by its prospects for enhancing such processes. With its recorded feat in food and mineral processing, the optimism for a similar achievement in crystallization may be justified and hence the motivation for its impact assessment. However, the efficiency of pulsed electric field in application has been established to depend on such critical factors as the electric field intensity, pulse wave-shape and treatment medium conditions (U.S. Food and Drug Administration 2011; Cueva 2009).

3.4.1 Electric field intensity

The electric field intensity is a strength indicator of the electric field on the treatment medium. It is an inverse relation between the applied voltage and the distance between the electrodes otherwise known as the treatment gap. Hence, the higher the applied voltage over a short treatment gap, the greater the pulsed electric field effect (Barbosa-Canovas 2002) which could be as much as 80 kV/cm and can be calculated according to equation (1) (Verma 2012). It is also suspected that with strong enough electric field intensity, of the magnitude of 6 kV/cm or more, all solute molecules can be orientated parallel to the direction of the electric field and this could ultimately improve the γ-glycine polymorph fraction of the crystallized product (Radácsi 2012; Aber et al. 2005).

$$E = \frac{U}{d} \quad , \tag{1}$$

where E electric field intensity
U applied or peak voltage
d treatment gap.

The processing time, when required, is determined as the product of the number of pulses and the effective pulse duration (Verma 2012) while the heating effect of the electric field can be determined accordingly from the general equation:

$$P = m \cdot c_p \cdot \Delta T / t \quad , \tag{2}$$

where P estimated heating effect of the electric field

m total mass of treated sample

c_p specific heat capacity

ΔT temperature difference resulting from heating

t corresponding time of temperature rise.

3.4.2 The pulse wave-shape

Square-wave, exponential-decay and oscillatory-decay pulses (Fig. 14) are the typical pulse waveforms obtainable in pulsed electric field applications. Of these three, oscillatory-decay pulse has been identified to be the least impacting in view of its hindrance to adequate exposure of the treatment medium to high intensity electric field. The exponential-decay pulse however, makes a characteristic sudden rise in voltage but with a very slow decaying rate leaving behind a long tail section of ineffective and excessive heating. The square wave pulse produces durable and stable peak voltage with high intensity over the entire pulse duration in addition to reducing thermal effect and is therefore mostly preferred to the others. (Jambari, et al. 2011)

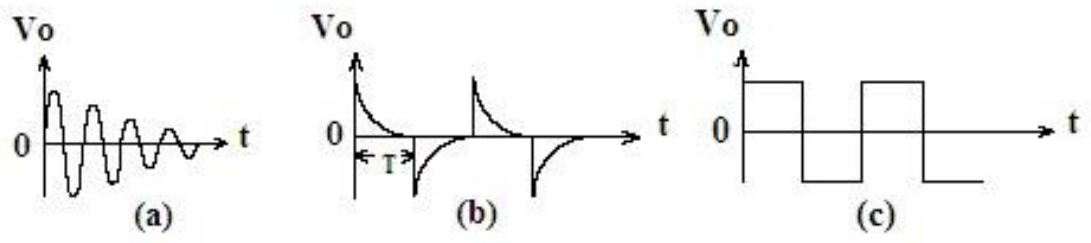

Figure 14. PEF generated waveforms (a) Oscillatory-decay pulse (b) Exponential-decay pulse (c) Square wave (Jambari, et al. 2011).

3.4.3 Treatment conditions in medium

In the category of critical parameters of the sample to be treated by pulsed electric field irradiation that should be considered are the operating temperature and pressure; pH and conductivity of the medium as well as the electrode material. While the conductivity of the treatment medium appears to be central here, it is largely affected by the other factors. An increase in temperature, for instance, would ideally lead to some increase in

the medium conductivity. The medium itself should not possess too low conductivity, as this would hinder the generation of electric fields while too high conductivity leads to outright failure of electric field generation. However, there are not known limits for PEF application; hence, the adoption of practical possibilities. (Raschke 2010)

3.4.4 Solution mixing profile

Making the appropriate choice of mixing profile for a crystallization study is another important factor to the success of the process. The reactor geometry, mixer type and mixer speed are quite significant in this regard. According to Palosaari et al. (2007), the mixing degree in the reactor is the extent of accomplishment of homogeneity in the system. Inefficent mixing gives room for localized supersaturations and poor mass transfer within the reactor thereby making the desired product qualities like size distribution, crystal morphology and purity difficult to control.

With respect to reactor geometry, almost all other reactor types except the flat-bottom ones could readily provide good fluidity. So, the additional consideration for improvement of mixing efficiency is in respect of the need for baffles as well as the determination of required number of agitators and their positioning. In non-seeding crystallization for example, where complete initial dissolution of the sample is required, the choice of appropriate mixer speed that will ensure the realization of this goal is very important. However, as a result of the variation in mixer features, impeller tip speed calculated according to equation (3) offers a comparative basis for the impeller's impact on mixing (Dickey 2005):

$$TIPS = \pi \cdot D \cdot N \quad , \tag{3}$$

where $TIPS$ impeller tip speed
D impeller diameter
N impeller rotation speed.

3.5 Industrial applications of pulsed electric field

An illustration of pulsed electric field application in water processing has been established by a commercialized technology in the United States. This technology, known as, *Flow-Tech Home* softens water through scales removal and prevention over the entire domestic plumbing network through pulsed electric field irradiation induced crystallization. As scaling is the heterogeneous crystallization result of the supersaturation induced by pressure and temperature changes, *Flow-Tech* creates an electric field which favors homogeneous crystallization thereby fulfilling descaling (Fig. 15). This electric field stimulates the formation of seed crystals irrespective of supersaturation and the crystals swim irreversibly along the water flow path together with the descaled particles where they exist. (Flow-Tech Systems, LLC 2014).

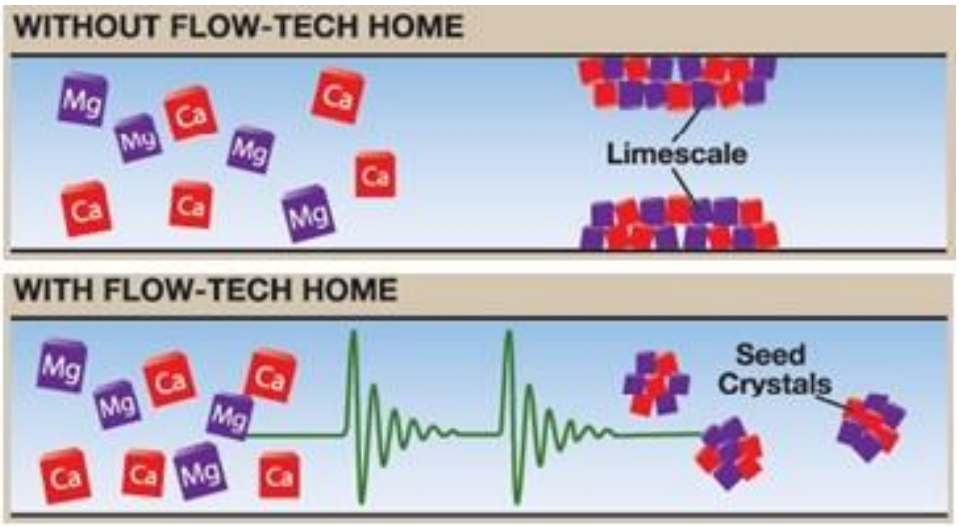

Figure 15. PEF application in water processing (Flow-Tech Systems, LLC 2014).

The economic significance of this technology as a physical water treatment technique include money saving, protection of appliances and fixtures, removal of existing scales and prevention of build-up, sufficiency and improved energy efficiency. Others are lack of maintenance necessity, compactness and space-saving, non-generation of additional effluent load as well as environmental and health friendliness (Plumber's Choice, LLC 2014).

In food processing, pulsed electric field treatment in the purification of sugar beet juice (Loginova et al. 2012) has proven to be more economical and efficient, with respect to reduced concentration of non-sugar impurities, colorants and pectin as well as improved raw juice quality, in comparison to the conventional extraction technique. Similarly, an overall quality improvement with respect to freeze-drying, shape uniformity, visual quality, less shrinkage and reduced freezing time has also been reported in the study of pulsed electric treatment effect on potato freezing (Jalte et al. 2009).

However, in spite of the breakthrough recorded by PEF application in food processing, such challenges as difficulty in bacterial spores inactivation, application for non-homogenous foods and highly viscous fluids, adaptation to air bubbles-entrapping foods, high electric conductivity and limited flowrates as well as damage control of heating effects to some products have posed a huge hindrance to the commercial packaging of this technology (Barbosa-Canovas 2002).

4. ANALYTICAL METHODS OF CRYSTAL PROPERTIES

Several analytical techniques are being employed in the characterization of the crystallized product of glycine with respect to its polymorphic composition studies. Some of these utilized analytical tools are single crystal XRD for investigating single crystal structures; powder XRD for crystallinity verification and polymorphs identification; FTIR analysis for functional groups identification and UV-vis spectrum for optical transmittance measurement. Others include TG/DTA analysis for thermal stability investigation; elemental (CHN) analysis for chemical composition determination (Sankar et al. 2010); Kurtz and Perry method for second harmonic generation behavior or efficiency and DSC for phase transition determination (Anbu Chudar Azhagan & Ganesan 2013). The background principles of the relevant techniques in this study are summarily discussed.

4.1 Powder X-ray Diffraction

X-ray powder diffraction is a nondestructive technique employed in the characterization of crystalline materials' properties like preferred crystal orientations, phases and structural parameters such as average grain size, strain, crystallinity and crystal defects (EAG Inc. 2014). The equipment used is known as X-ray diffractometer (Fig. 16) with core components as X-ray tube, sample holder, X-ray detector and goniometer for maintenance of angle and sample rotation. In its treatment of powder samples of glycine for instance, data is typically collected at 2θ within preset angles of 10 and 60 degrees as would be seen in subsequent XRD patterns from this study.

Figure 16. An image of Bruker D8 Advance X-ray diffractometer.

According to Dutrow & Clark (2013), this technique is based on constructive interference between monochromatic X-rays and a crystal sample. The X-rays interact with the sample rotating at an angle θ to the rays, to generate diffracted rays upon satisfying Bragg's Law which relates the wavelength of electromagnetic radiation to the diffraction angle and the lattice spacing in the crystalline sample. The diffracted X-rays are detected, by mounted detectors rotating at an angle 2θ to the sample, recorded and

converted to count rate readable on a connected electronic device. This generated pattern is then compared with standards from an XRD database for quick identification of the crystalline sample (EAG Inc. 2014).

In addition to this quick check of the obtained patterns with the available library data, identification of glycine polymorphs for instance, can be further compared with the available lliterature data. With different polymorphs existing at distinct peaks, the obtained XRD pattern can be checked and the peaked obtained can be related to the corresponding polymorph. Literature data on PXRD patterns for glycine have shown that the most significant peaks are obtained in the range of 10º - 40º on a 2θ basis. Figure 17 therefore presents the typical PXRD patterns for the different glycine polymorphs.

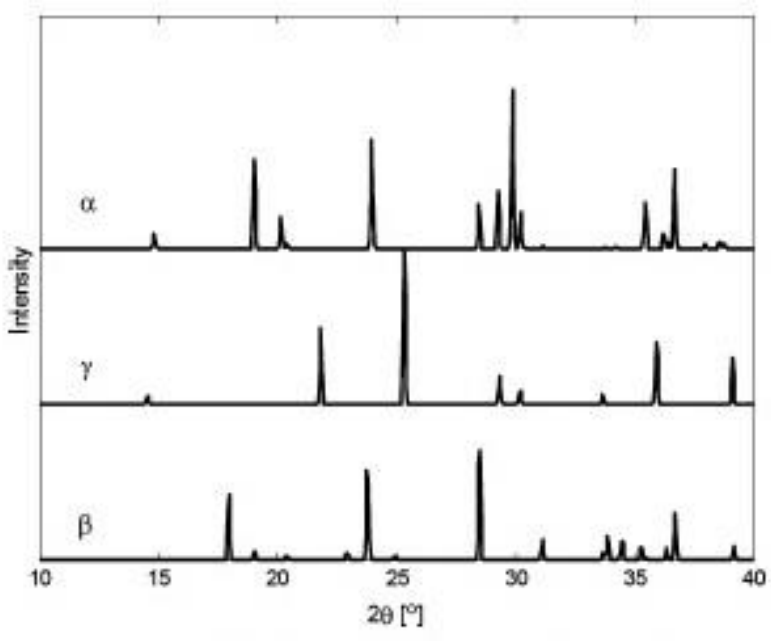

Figure 17. Typical PXRD patterns for the different glycine polymorphs (Louhi-Kultanen et al. 2006)

XRD as an analytical technique is being employed in such industries as aerospace, automobile, medical implants, compound semiconductors, data storage, electronics, lightning, pharmaceuticals, photonics, polymer and solar photovoltaics (EAG Inc. 2014). Some of the identified strength of the method are suitability at ambient

conditions, minimal or no sample preparation requirements, non-destructive, quantitative measurement of phase content and texture orientation, simplicity, availability and time efficiency. Its shortcomings however include non-suitability for amorphous materials, lack of depth profile information, compeling need for standard reference and tendency for peak overlays especially at high angle reflections (EAG Inc. 2014; Dutrow & Clark 2013).

4.2 Fourier Transform Infrared (FT-IR) Spectroscopy

Infrared spectroscopy is the study of interactions between matter, whose component atoms are in continuous vibration with natural frequencies of about 1014 cycles per second, and electromagnetic radiation (Rocky Mountain Laboratories, Inc. 2012). Fourier Transform Infrared Spectroscopy (FTIR) is an analytical technique used to identify organic, polymeric and in some cases, inorganic materials by scanning the sample with infrared emission. During this analysis, an absorbance (or transmittance) spectrum from which unique chemical bonds and molecular structure of the material can be interpreted is generated, with characteristic peaks of the spectrum indicating the presence of those components at higher concentrations. This spectrum is then compared in a reference library program with cataloged spectra for identification of components or for possible match with a spectrum of a known material. (Lab Testing, Inc. 2014).

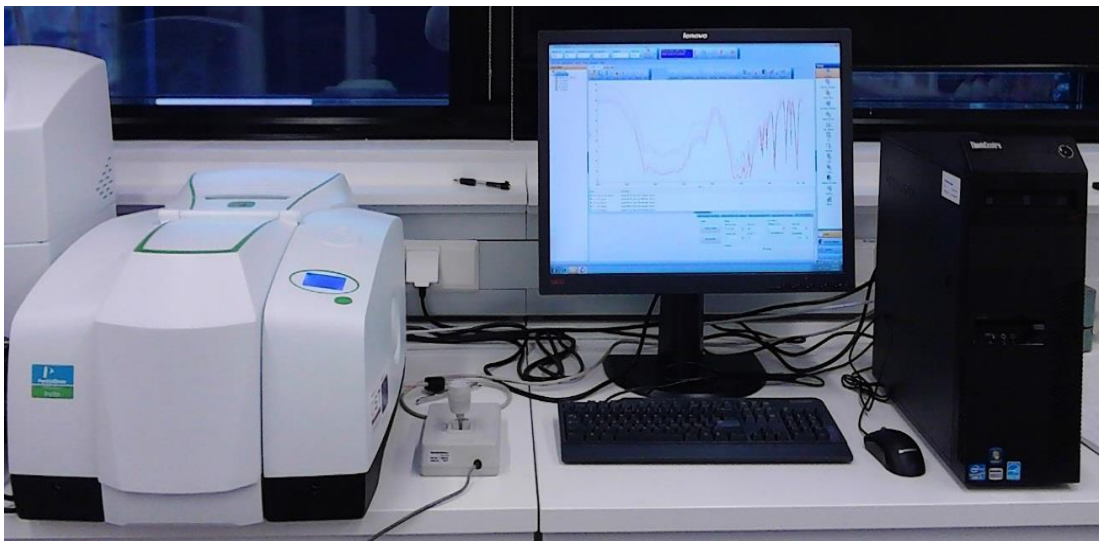

Figure 18. Frontier FT-IR Spectrometry set-up.

FTIR analysis has been put to use for purity assessment and characterization or identification of base polymer composition, additives, organic contaminants and unknown materials generally in such fields as aerospace, automobile, biomedical/biotechnology, compound semiconductors, data storage, defense, electronics, lightning, pharmaceuticals, photonics, polymer solar photovoltaics and telecommunications (EAG Inc. 2014; Lab Testing, Inc. 2014). The merits of this technique include its capability of identifying organic functional groups and often specific organic compounds, broad spectral libraries for compounds identification, non-destructive ability, suitability at ambient conditions and minimal analysis area. Its demerits include limited surface sensitivity, mimimum analysis area, limited inorganic information and the need for standards (EAG Inc. 2014). Figure 19 present typical FTIR spectra of both α- and γ-glycine polymorphs.

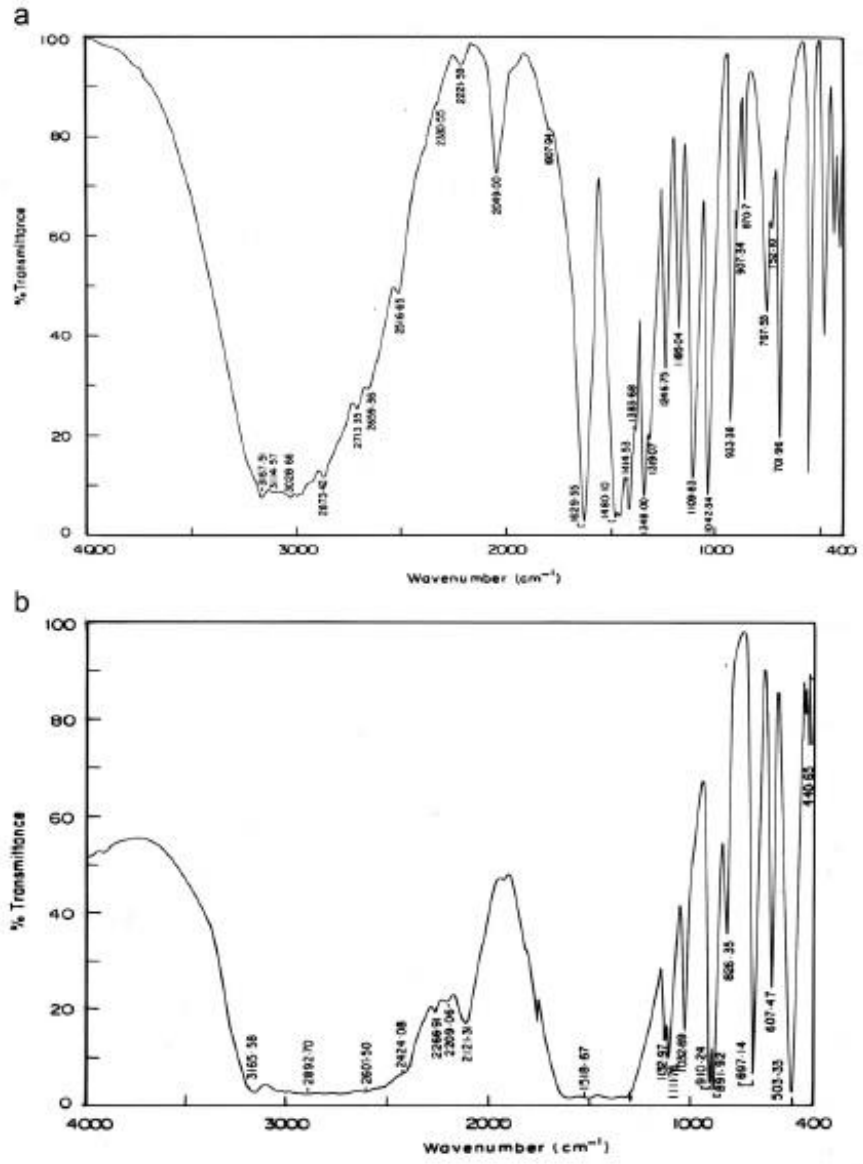

Figure 19. Typical FTIR spectra of (a) α-glycine and (b) γ-glycine polymorphs (Srinivasan et al. 2011).

For the purpose of identification of glycine polymorphs, FTIR spectra obtained, like the PXRD patterns, are perhaps also better compared with existing literature information. This has been mostly presented as absorbance or transmittance (%) as a function of wavenumber (between 4000 and 400 cm^{-1}). With this technique, α-polymorph have been typically characterized by a strong band at 3028 cm^{-1} and absorbed peaks 3167, 1109 and 870 cm^{-1}. γ-polymorph on the other hand have been identified with peaks at 3165, 891, 1132 and 1111 cm^{-1} and also bands at 607, 697, 1518, 1032 and 910 cm^{-1} while not much have been said of β-polymorph in this regard. (Srinivasan et al. 2011)

4.3 Morphologi G3 Imaging

The Morphologi G3 is a particle imaging equipment with capacity ranging from 0.5 microns to several millimeters. It determines the size and shape of particles, in three stages, using the technique of static image analysis. These stages are sample preparation and dispersion; image capture and data analysis. In the sample preparation and dispersion phase, the equipment offers the possibility of direct dispersion of larger particles to the imaging screen while for finer particles, the sample dispersion unit can be utilized to ensure spatial separation of the individual particles and agglomerates with minimal damaging impact. (Malvern Instruments Ltd 2014)

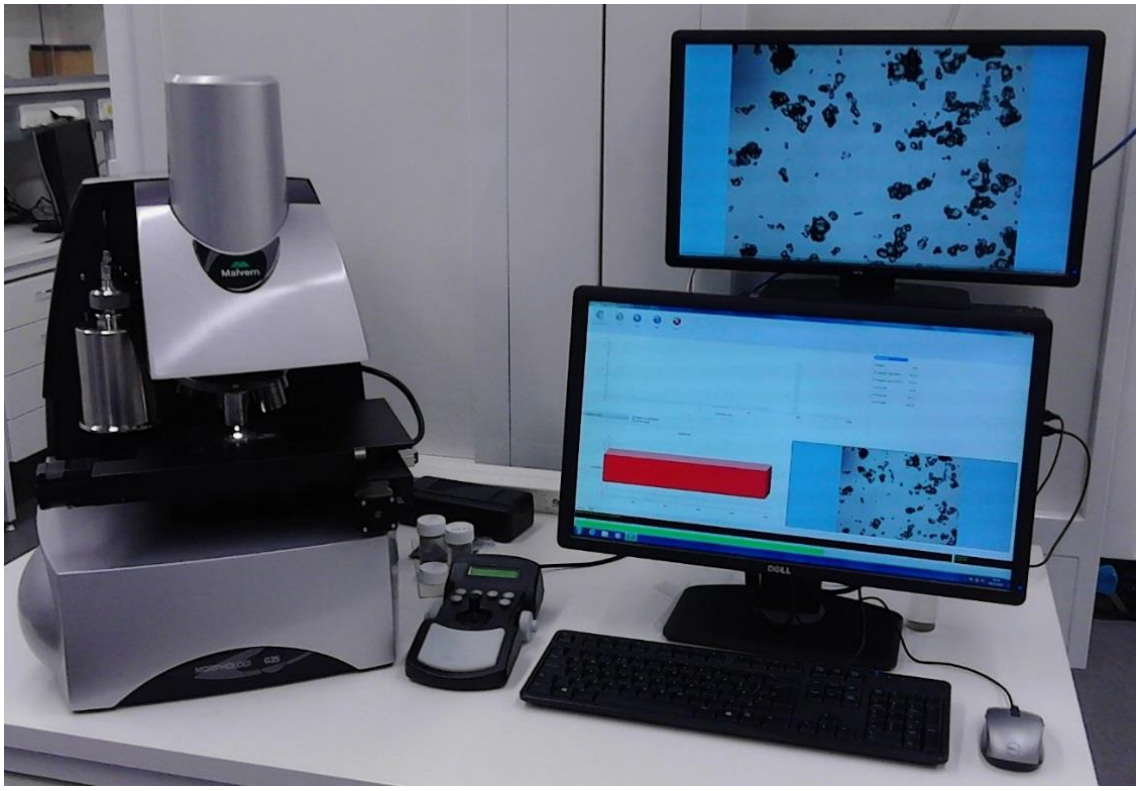

Figure 20. Morphologi G3 particle imaging set-up.

Upon satisfactory dispersion of the particles, the instrument then automatically captures images of individual particles by scanning the sample underneath the microscope optics within the defined imaging area. At the end of the imaging, the instrument has measured a range of morphological properties for each particle. With the aid of the advanced graphing and data classification options offered by the software, extraction of relevant

data from the measurement based on intuitive visual inspection then becomes simplistic. (Malvern Instruments Ltd 2014)

The Morphologi G3 is known for such features as automated control for unattended operation; good reproducibility of results; good quality of microscope imaging that enhances characterization; rapid automatic particle counting on membrane filters as well as intuitive software interface that enhances both visual and statistical interpretation of captured data. It has been deployed in such industrial applications as pharmaceuticals and mineral processing (Malvern Instruments Ltd 2014).

5. MATERIALS AND METHODS

5.1 Materials and equipment

Commercial samples of glycine (99.7% Merck KGaA, Germany), KDP (99.5% Merck KGaA, Germany) and ethanol (99.91% VWR Chemicals, France) were the chemicals utilized in this study. Other materials and equipment include a 250 ml U-bottom-shaped reactor, an electric-motor driven Rushton turbine impeller (Ø2 cm), RC 6 CP LAUDA thermostat, high voltage pulse generator (Wapulec Oy), a mixed signal oscilloscope, Büchner funnel, Whatman 40 ashless filter paper (Ø70 mm) and oven. A Bruker D8 Advance X-ray diffractometer, PerkinElmer Frontier FT-IR spectrometer and Morphologi G3 were used in characterizing the product crystal samples.

5.2 Experimental set-up

The experimental set-up can be seen in Figures 21 and 22. It consisted of a U-bottom-shaped crystallizer vessel (reactor) equipped with electric motor-driven pitched blade turbine impeller with 4 blades. RC 6 CP LAUDA thermostat was connected over the reactor to control the temperature of the crystallization process. Electrodes powered by the high voltage pulse generator were inserted into the reactor for supply of pulse currents which were monitored by the mixed signal oscilloscope via its probe. The post-

crystallization experiment processes involved are filtration, drying and product characterization.

Figure 21. An image of the experimental set-up excluding the mixed signal oscilloscope monitor.

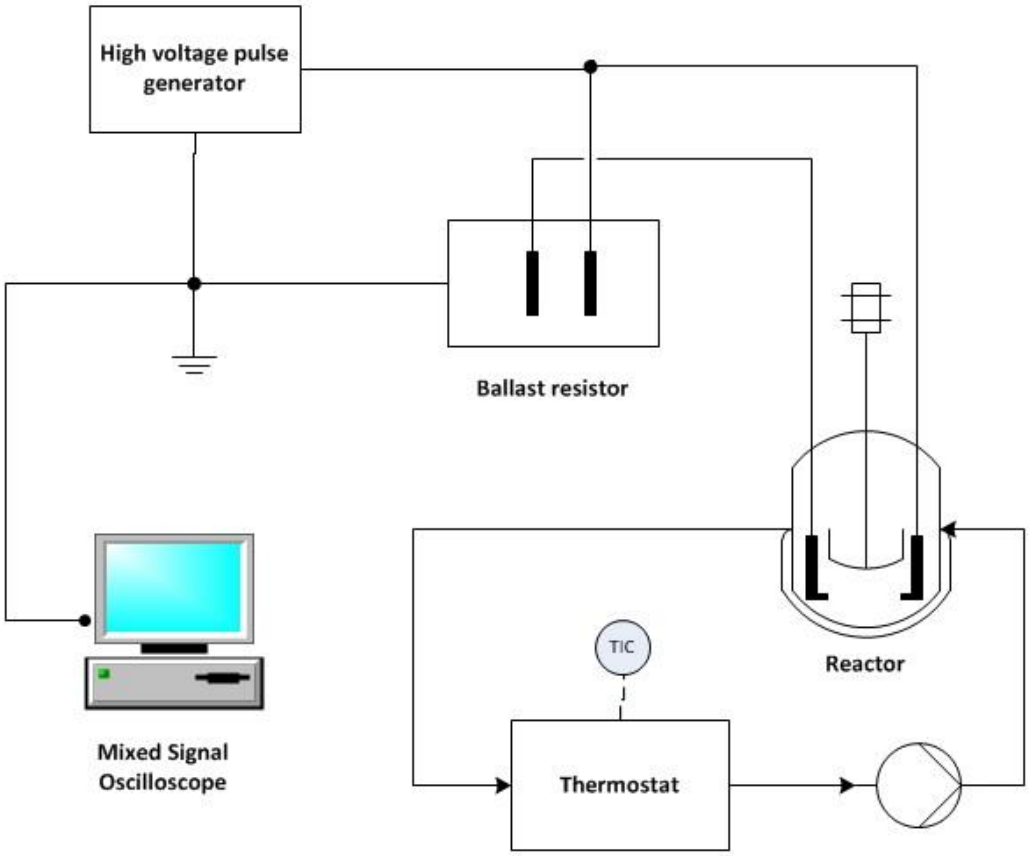

Figure 22. Flowsheet of the cooling crystallization study set-up.

Table 1 presents the pulse parameters obtained for the three different pulse settings of 2, 3 and 4 while their corresponding oscillograms as utilized in the glycine experiments are presented in subsequent Figures 23-25.

Table 1. Pulse parameters used in glycine experiments.

Parameter	Pulse setting 2	Pulse setting 3	Pulse setting 4
Effective voltage, kV	8.8	8.2	8.8
Period, ms	3.4	1.05	6.9
Frequency, Hz	294	950	145

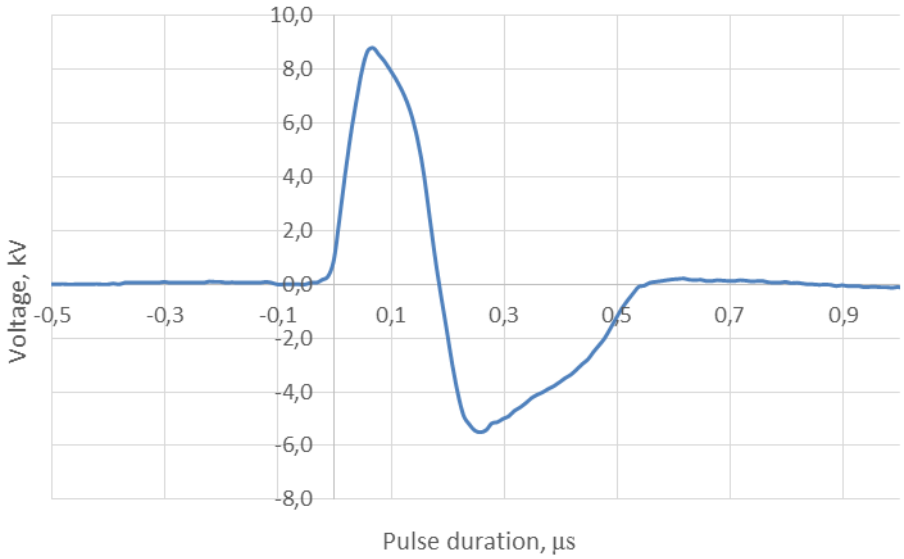

Figure 23. Oscillogram of the pulse setting 2 (294 Hz frequency) applied in glycine experiment.

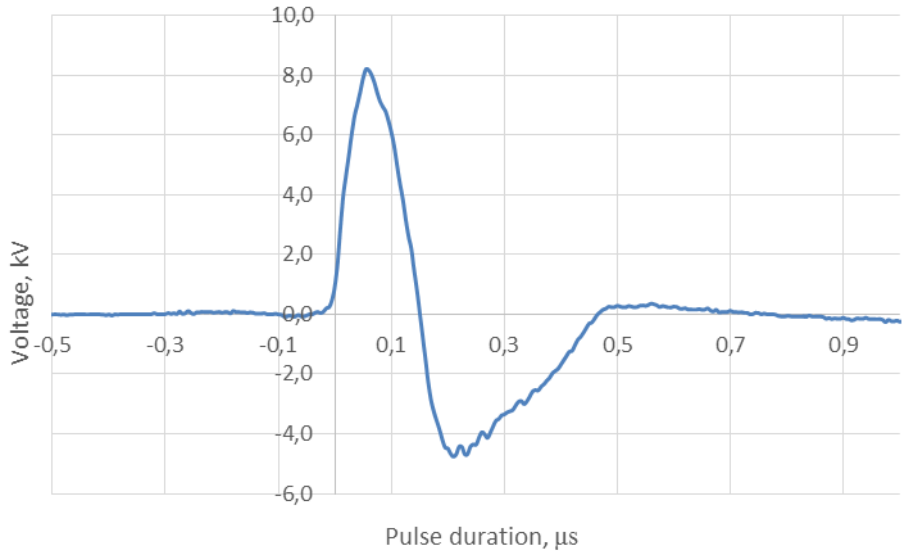

Figure 24. Oscillogram of the pulse setting 3 (950 Hz frequency) applied in glycine experiment.

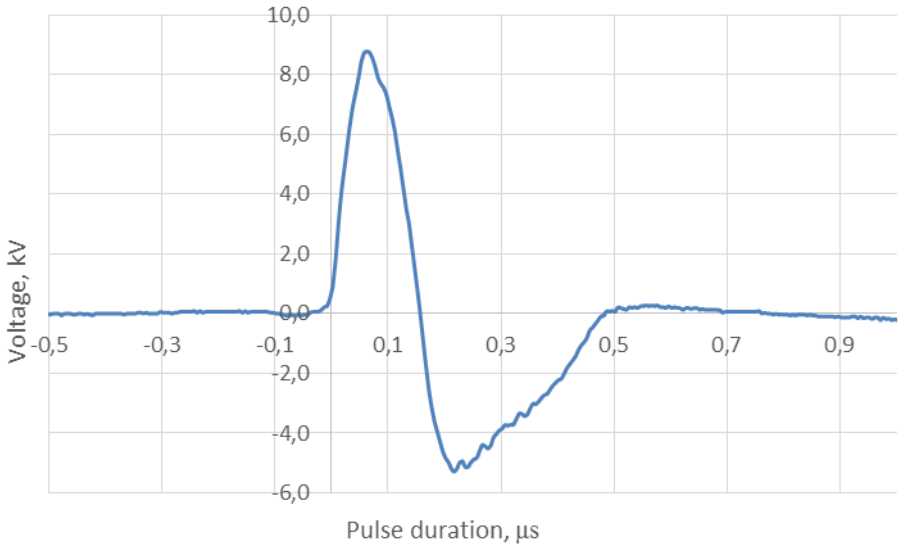

Figure 25. Oscillogram of the pulse setting 4 (145 Hz frequency) applied in glycine experiment.

5.3 Experimental procedure

An aqueous solution of glycine was prepared from 27g of the commercial glycine sample and 100ml of deionized water according to its solubility data (Table 2). The solid glycine particles were dissolved in the deionized water at 35 ºC (corresponding to saturated aqueous solution at 30 ºC) with an impeller speed of 600 rpm for one hour. This temperature regulation was provided by the thermostat that was connected to the crystallizer jacket. At the end of the dissolution phase, the reactor content was cooled to saturation temperature of 30 ºC.

Table 2. Solubility data on glycine and KDP (Mullin 2001).

Compound	**Solubility (g of anhydrous compound per 100g of water), ^{0}C**							
	0	10	20	30	40	60	80	100
Glycine	14.2	18.0	22.5	27.0	33.0	45.0	57.0	70.0
KDP	15.9	18.3	22.6	27.7	33.5	50.0	70.4	

With the electrodes already immersed into the crystallizer, the pulsed electric field was applied when the saturation temperature was achieved, and was sustained for the remaining part of the experiment which covered further cooling of the solution to 20 ºC

and a two-hour ageing duration. Three different cooling profiles of 5 ºC/h, 10 ºC/h and 20 ºC/h were utilized, therefore corresponding to 2 h, 1 h and 0.5 h cooling times. With the supplied average voltage of 8.8 kV in DC form, three different pulse frequencies (299, 950 and 145 Hz) were applied over a treatment gap (distance between electrodes) of 2 cm to each of these cooling profiles. One experiment without PEF was also conducted for each cooling profile in order to provide sufficient grounds for comparison.

At the end of the crystallization experiment, the reactor content was filtered under vacuum by Büchner funnel with about 10 ml of cautious ethanol rinsing. This caution was informed by the knowledge of anti-solvent action of ethanol on glycine. The filtered crystals were then dried in the oven at 100 ºC overnight and the dried product was weighed to confirm compliance with theoretical yield.

To further verify the impact of the pulsed electric field application on crystallization, commercial KDP sample was also tested by using 10 ºC/h cooling profile at reduced frequency of 50 Hz. This was so because it was impossible to operate at higher frequency due to KDP's higher electric conductivity than that of glycine. All other processes were the same as with the glycine studies. The product crystals were then analyzed for variation in polymorphic composition, crystal morphology and particle size distribution.

5.4 Characterization of product particles

Three different analytical methods were used in this study. They were powder X-ray diffraction, Fourier transform infrared spectrometry (FT-IR) and Morphologi G3 particle imaging techniques. While PXRD and FT-IR were used to study the possibility of differences in the original sample and crystallized product particles with respect to their polymorph contents, Morphologi G3 was used to observe the variance in the particle shapes and size distribution. All analysis were carried out at ambient pressure and room temperature.

The PXRD analysis was carried out on a Bruker D8 Advance X-ray diffractometer with variable rotation and optics primary settings of 10.0/min and 20 mm respectively. The X-ray generator power rating of 1600 W, corresponding to voltage and current set values of 40 kV and 40 mA, was used. LYNXEYE detector type was used and the measurements were taken in 2θ range of 10º – 60º with an increment of 0.01 and with the samples carefully dispersed on the Si (silicon) sample holder. The obtained spectra were then identified with the available library data.

PerkinElmer Frontier FT-IR spectrometer was used to execute the FT-IR analysis of the samples in the spectral range of 400 – 4000 cm^{-1} using the KBr pellet method. This method required prior molding of tablets from about 0.3 g of KBr and 3 mg of the product samples. With front internal and 20 scans set as the beam location and accumulations respectively, KBr spectra was taken and set as background for the measurements. The product sample measurements were then taken and the eventual spectra were refined by baseline correction and normalization before conducting a search of the spectra with the available library data.

The particle shapes and size distribution was investigated on Morphologi G3 particle imager. Due to the large size of the studied crystal samples, the sample dispersion unit was considered not useful, and therefore, the samples were dispersed directly onto the plate. With magnification of 2.5, all the dispersed samples were scanned. With the goal of targeting individual crystals as best as possible, solidity and convexity filter parameters with values of 0.95 each were used to refine the raw scan results in each case.

6. RESULTS AND DISCUSSION

The application of pulsed electric field in this study was a deliberate approach to determine its relevance or otherwise to the modification of commercial glycine sample with respect to crystal morphology and size. The driving forces expectedly are the pulse

frequency and the electric field intensity, calculated illustratively from the average applied voltage of 8.8 kV used in this work according to equation (1):

$$E = \frac{8.8kV}{2cm} = 4.4kV/cm \quad (4)$$

This use of high voltage pulse current is accompanied by a measurable heating effect which appeared to be suppressed by the thermostat-controlled water filling the crystallizer jacket. With knowledge of the initial aqueous solution conditions (i.e. temperature is 15 °C and pressure is 101325 Pa) and the observed rise in temperature of the aqueous solution within 30 minutes, this heating effect can nonetheless be estimated according to equation (2):

$$P = 0.127kg \cdot \frac{4185.5J}{kg \cdot K} \cdot (28 - 15.5)K \cdot \frac{1}{1800\ s} = 3.69\ W \quad (5)$$

As this study was done without seeding, attention was paid to the mixing regime of the solution in order to ensure complete dissolution of the solid particles. The corresponding tip speed to the 600 rpm impeller speed used in this study is therefore determined according to equation (3) as follows:

$$TIPS = 3.142 \cdot 0.02m \cdot 10s^{-1} = 0.63m/s \quad (6)$$

The cooling profile of the thermostat-controlled coolant was monitored, both digitally and manually, in relation to the solution temperature as can be seen in Figure 26, shows that the latter followed the former quite steadily with little lagging. Cooling rate of 10 ºC/h was used for this demonstration but repeated patterns were observed with other cooling rates in the subsequent experiments. Figures 27 and 28 depict the coolant and solution cooling profiles (including the first 30 minutes of the ageing phase).

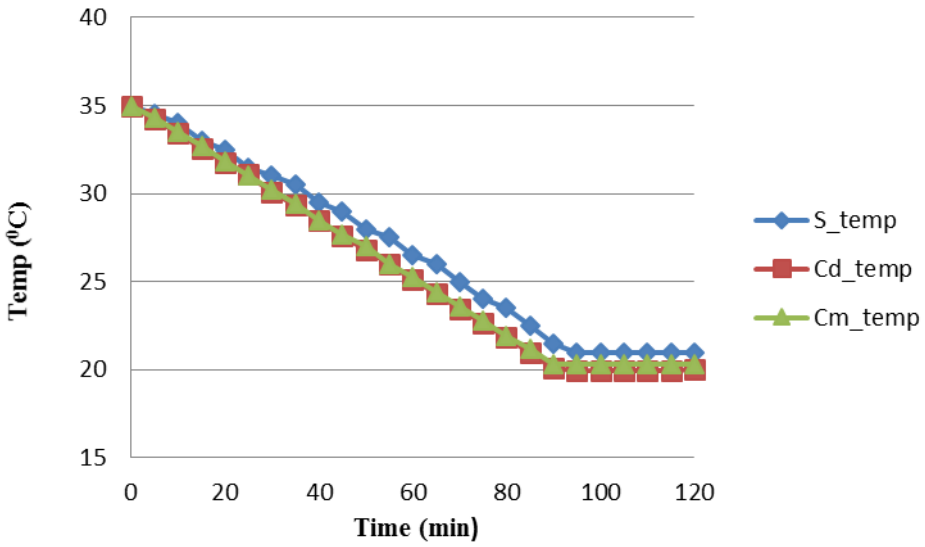

Figure 26. Comparison of the solution and coolant cooling profiles at 10 ^{0}C/h. S_temp is the solution temperature, Cd_temp is the digitally displayed coolant temperature and Cm_temp is the coolant temperature determined manually.

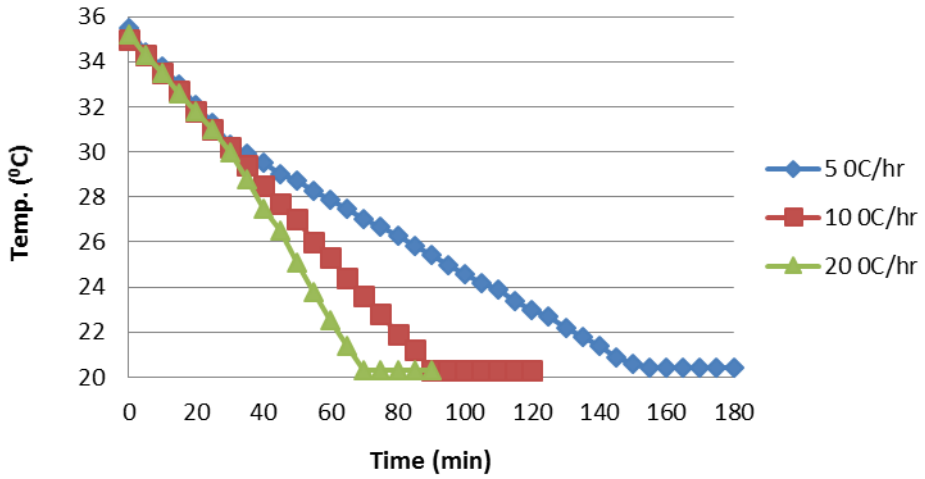

Figure 27. Coolant cooling profiles at different cooling rates of 5, 10 and 20 °C/h.

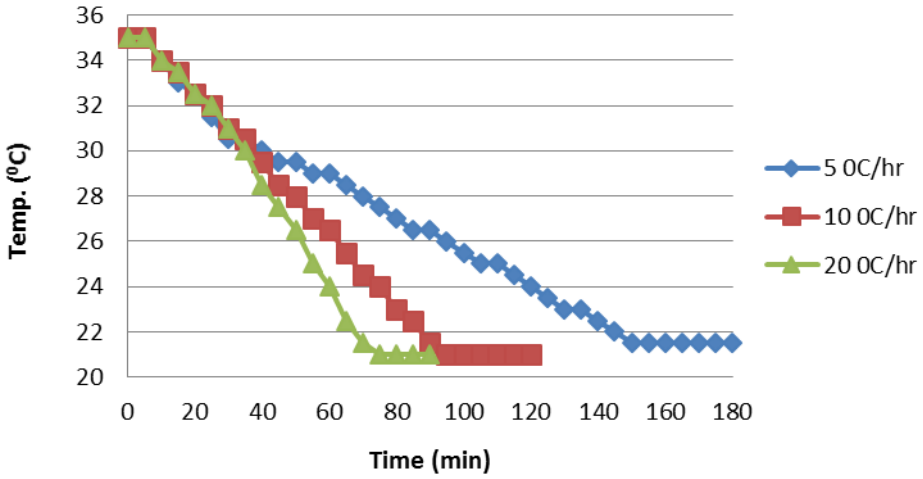

Figure 28. Solution cooling profiles at different cooling rates of 5, 10 and 20 °C/h.

In the cooling crystallization experiments of glycine, secondary crystallization was observed on the walls of the crystallizer, at the topmost layer of the solution, in the form incrustations and also around the blades of the impeller (Fig. 29). This phenomenon was observed to have the largest effect when no pulse frequency was applied. The near absence of this effect in KDP crystallization therefore suggests that the glycine particles under study may possess some surface charge which facilitates this mechanism. Unfortunately, the zeta potentials of the aqueous solutions were not monitored in this work and this made better understanding of the situation fairly difficult.

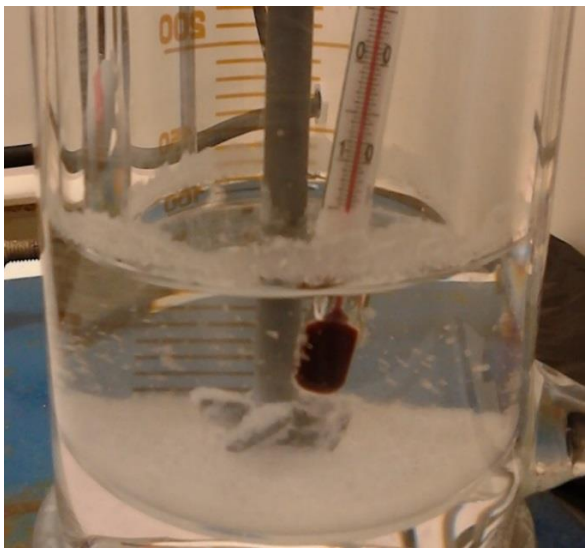

Figure 29. Secondary crystallization observed in glycine experiments.

Details of the experimental data and results reported as average values from two experiments are presented in Table 3. The highlighted part (the last two columns) refer to the KDP verification experiments while the others are for the glycine experiments carried out. The table classifies the glycine experiments conducted at different pulse frequencies into the different cooling rates used. It further presents the temperature at which the first crystals were observed and the product yield obtained in each case. In the case of KDP experiments however, only the 10 ºC/h cooling rate was used.

Table 3. Experimental data and results of glycine experiments and KDP verification experiments (highlighted in the last two columns).

Temperature range (°C)	Cooling rate (°C/h)	Effective voltage (kV)	Frequency (Hz)	Period (ms)	Impeller speed (rpm)	Yield (g)	First crystal appearance (°C)
35-20	20	8.8	145	6.9	600	4.528	20 (+10 mins)
35-20	20	8.2	950	1.05	600	4.762	20 (+10 mins)
35-20	20	8.8	294	3.4	600	5.055	20 (+20 mins)
35-20	20	-	-	-	600	4.921	20 (+30 mins)
35-20	10	8.8	145	6.9	600	5.284	26
35-20	10	8.2	950	1.05	600	5.021	26
35-20	10	8.8	294	3.4	600	4.741	22.5
35-20	10	-	-	-	600	5.155	21.5
35-20	5	8.8	145	6.9	600	5.139	29
35-20	5	8.2	950	1.05	600	5.177	28
35-20	5	8.8	294	3.4	600	5.664	27
35-20	5	-	-	-	600	5.263	23.5
35-20	10	1.4	50	20	600	4.731	23
35-20	10	-	-	-	600	0.568	20 (+60 mins)

As can be seen from Table 3, the application of pulsed electric field showed a narrowing effect on the metastable zone width of both glycine and KDP samples studied. Comparing both, it is obvious that the metastable zone width of KDP is broader than that of glycine. This is evident by the attainment of the theoretical yield of 4.5 g for glycine while the 5.1 g required for KDP could not be realized under the same circumstance. In the absence of PEF however, 0.568 g yield of KDP was realized as against the 4.731 g obtained under electric field application. Nucleation of crystal particles was observed, by visual inspection, earlier with higher electric pulse frequency application. Another contributing factor to this result was the cooling rate. At slower

cooling rates of 5 ºC/h and 10 ºC/h, first crystal appearance was noticed at 23.5 ºC and 21.5 ºC in the absence of pulsed electric current and at higher temperature when PEF was applied while at the fastest cooling rate of 20 ºC/h, no crystal was observed before transition into the ageing phase of the crystallization.

No significant impact on the pH of the aqueous solutions was noticed as a consequence of the dc-electric field application as could be seen in Table 4. And particularly with respect to glycine, the closeness of this value to its isoelectric point (pH 6.0) at which the average charge of a glycine molecule is zero, according to Aber et al. (2005), suggests the existence of the molecules under study as neutral zwitterions in the solution. This assumption was further supported by the formation of crystals in the bulk of the solution. But if the glycine species present were significantly charged, these charged species would have migrated to the electrode with the opposite charge, therefore leading to nucleation and growth of crystals on the electrode(s) instead.

Table 4. Determined pH values of aqueous solutions at the start (before PEF application) and at the end (after PEF application) of the experiments.

	Glycine		KDP	
	Start	End	Start	End
pH	6.29	6.24	4.07	4.03
Temp (^{0}C)	20.0	20.3	20.3	20.5

FT-IR analysis of the product crystal particles did not suggest significant changes with respect to morphology between the obtained crystals and the raw material (original sample). Comparison of the obtained spectrum for each product sample with that of the raw material however showed some minor shifts in the spectra of the PEF-treated crystals when compared to that of the raw material. This most significant difference observed by this technique was that at about 1042 cm^{-1}, an absorbed peak in the raw material and the crystal products obtained without PEF did not exist particularly in PEF-crystallized products at the slowest cooling rate of 5 ºC/h. This pattern was observed to be most significant with 294 Hz treated sample. This difference, according to Srinivasan et al. 2011, suggests the presence of γ-polymorph in the PEF-treated samples.

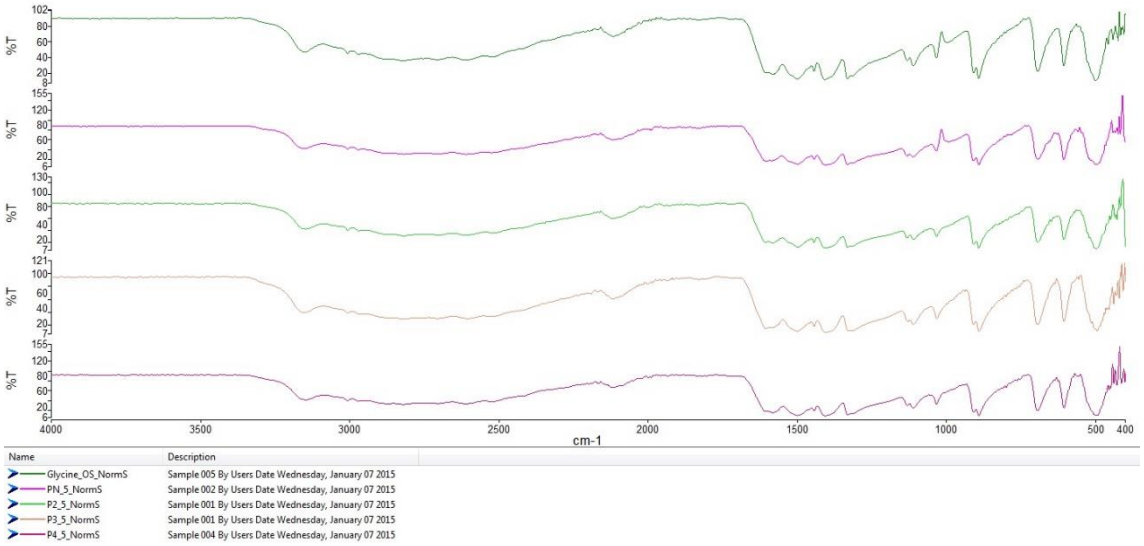

Figure 30. Split display of FT-IR spectra demonstrating PEF effect at 5 ºC/h cooling rate. From top to bottom are the spectra obtained for the glycine raw material, crystal product of the experiment conducted without PEF (PN) and crystals products of pulse settings 2 (294 Hz), 3 (950 Hz) and 4 (145 Hz) respectively.

The PXRD pattern obtained from the original sample supported earlier observation by the previous technique that β-glycine polymorph was present beside α-glycine polymorph. A comparison of the individual product sample spectrum with that of the raw material showed that β-glycine polymorphs were mostly obtained with distinct peaks at 31.3º, 34º (Liu et. al. 2008; Louhi-Kultanen et al. 2006), 48.8º and 49.3º at the slowest cooling rate of 5 ºC/h without the application of pulse electric field. The use of ethanol rinsing at the end of filtration and storage at dry ambient may have also contributed to the sustenance of the metastability of this polymorph according to Devi et al. (2014).

The PXRD analysis also revealed that γ-glycine polymorphs were obtained in the product samples subjected to PEF application. The biggest effect was observed in the product of the sample treated with 294 Hz at the slowest cooling rate. In this particular result, characteristic γ-glycine polymorphs peaks were recorded at 22.5º, 25.5º, 30.3º, 39.3º (Liu et al. 2008; Louhi-Kultanen et al. 2006), 53.7º (Devi & Srinivasan 2013) and 57º (Srinivasan & Arumugan 2007). It is therefore suspected that control of glycine

polymorphism may indeed be possible under stronger electric field intensity as reported by Aber et al. (2005). This can be achieved under the same experimental circumstance by reducing the PEF treatment gap. Figure 31 presents a comparative illustration of the effect of the applied electric pulse current at the slowest cooling rate used. The unmarked peaks relate to α-polymorph while β-polymorph identification is marked by yellow arrows and γ-polymorph identification is marked by green arrows where they were observed most.

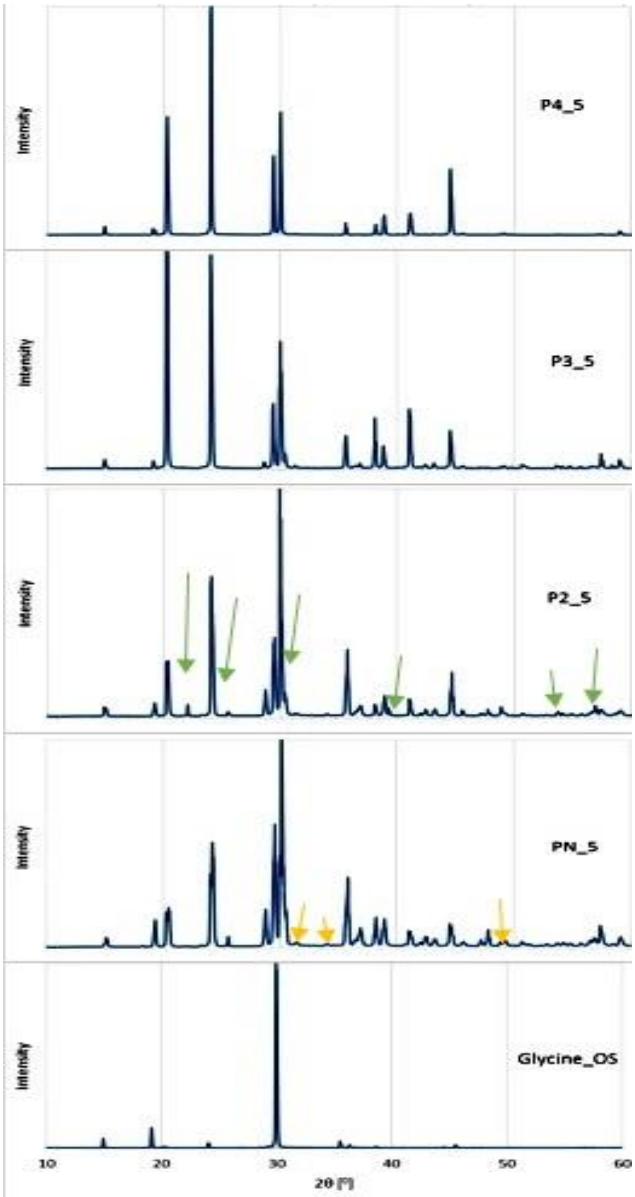

Figure 31. Comparative PXRD patterns demonstrating PEF effect at 5 ºC/h cooling rate. PN refers to the experiment done without PEF while P2, P3 and P4 refer to those carried out on pulse settings 2 (294 Hz), 3 (950 Hz) and 4 (145 Hz). The green arrows identify γ-polymorph while the yellow markers identify β-polymorph in the samples they were found most.

Table 5 summarizes the results of the crystal particles characterization carried out on the Morphologi G3 particle imager. It presents the results of the crystallized glycine particles according to the pulse conditions while the data obtained for the KDP crystallized sample by PEF can be seen alongside its original sample (raw material) in the bottom two columns. The data was drawn on CE Diameter basis (i.e. the diameter of a circle with the same area as the particle). In the rows of the table are the number of particles, the mean value and the standard deviation from each analyzed sample. Also included in the table is a representation of the values below which 10, 50 and 90 % of the data set for each measurement exists and these are represented by the 10^{th}, 50^{th} and 90^{th} percentiles respectively.

Table 5. Measurement results from Morphologi G3 according to pulse conditions. PN refers to the experiments conducted without PEF while P2, P3 and P4 refers to those done with pulse settings 2 (294 Hz), 3 (950) and 4 (145). KDP_OS is the KDP raw material while KDP_CC refers to its PEF-crystallized product.

Property	No. of Particles	CED Mean (µm)	CED S.D (µm)	10 Percentile (µm)	50 Percentile (µm)	90 Percentile (µm)
Glycine_OS	22206	449.45	42.22	172.8	390.85	780.55
PN_5	23810	180.2	18.12	33.96	145.8	329.1
PN_10	11932	376.5	53.51	109.6	294.3	784.2
PN_20	4093	497.1	58.23	179.4	472.7	871.1
P2_5	1578	160.4	42.66	74.57	145.2	287.6
P2_10	3993	769.8	65.58	130.5	416.6	1557
P2_20	6252	398.7	49.24	119.4	322.6	872.2
P3_5	11867	392.6	36.27	94.72	379.8	619.5
P3_10	3869	553.9	115.41	248.8	518.6	935.4
P3_20	7272	458.3	76.58	187.9	452	709.5
P4_5	19236	549.7	48.91	171.7	547.9	981.6
P4_10	5196	382.2	66.05	177.3	366.2	598.1
P4_20	14396	527.3	53.88	154.8	466	982.9
KDP_OS	6838	281.4	73.68	132.8	255.2	478.9
KDP_CC	14884	102.6	24.36	42.03	84.83	174.6

In order to make a better understanding of the available data from the characterization of the samples by Morphologi G3 particle imager as presented in Table 5, Table 6 was drawn from the data plot (Fig. 31) obtained for each measurement (Appendix IV) in terms of HS circularity and Elongation values. HS (high sensitivity) Circularity is the squared value of the circumference of equivalent circle area as the particle divided by

the perimeter of the particle while Elongation is the opposite of aspect ratio (1 - Aspect ratio) and Aspect ratio is the ratio of the width of the particle to its length.

Table 6. Summary of the analytical parameters (CE Diameter, HS Circularity and Elongation) drawn from data plot of each measurement.

Parameter	CE Diameter (μm)	HS Circularity	Elongation
Glycine_OS	100 - 1000	0.70 - 0.95	0.0 - 0.6
PN_5	10 - 600	0.25 - 1.00	0.0 - 0.9
PN_10	20 - 1000	0.20 - 0.95	0.1 - 0.9
PN_20	40 - 1000	0.25 - 0.85	0.2 - 0 9
P2_5	30 - 350	0.25 - 0.95	0.5 - 0.9
P2_10	40 - 1100	0.30 - 0.95	0.4 - 0.9
P2_20	30 - 1000	0.30 - 0.90	0.1 - 0.9
P3_5	20 - 900	0.20 - 0.95	0.3 - 0.9
P3_10	80 - 1040	0.25 - 0.80	0.3 - 0.9
P3_20	70 - 900	0.22 - 0.90	0.5 - 0.9
P4_5	50 - 1040	0.20 - 0.85	0.4 - 0.9
P4_10	70 - 800	0.25 - 0.80	0.4 - 0.9
P4_20	45 - 1030	0.25 - 0.87	0.3 - 0.9
KDP_OS	40 - 850	0.65 - 0.95	0.0 - 0.6
KDP_CC	15 - 400	0.65 - 0.95	0.0 - 0.7

These results do not suggest that the application of pulsed electric field impacted significantly on the crystal size distribution of the end-product but the effect of cooling rate in this regard may have been pronounced. A broadening of the crystal size distribution of the crystallization products was noticed when compared with that of the raw material. While the crystal particles of the commercial glycine sample used were found to be in the range of 100-1000 μm, those obtained from the experiments showed a downward shift of this lower bound with values in the range of 10-50 μm. The use of the slowest cooling rate appeared to favor the formation of the smallest particles.

The crystal products obtained from the experiments seemed to be within similar size range irrespective of the use of PEF. From the classification of these sizes into mean, 10^{th}, 50^{th} and 90^{th} percentiles as detailed in Table 5, the unclear impact of PEF on the product crystal products may have been further established. However, the lower bound of HS Circularity value was found to reduce from 0.7 to about 0.25 while the upper

limit of the Elongation was observed to have increased from 0.6 to 0.9 (Table 6) when comparing the original glycine sample to the obtained crystallization products.

These support the observation made earlier in respect of the broadened crystal size distribution. They also confirm the formation of round particles, suggestive of the presence of γ-glycine polymorphs, and an increase in the population of the existent longer crystals in the crystallized products. A closer look at the parameters obtained for the crystallized sample at 294 Hz and 5 ºC/h (P2_5), at which point γ-glycine polymorphs are suspected to have been attained the most, shows elongation value of 0.5 – 0.9. This means that the population of long crystals was highest in this sample and the tendency of obtaining needle-like γ-glycine polymorphs under PEF and high supersaturation, according to Aber et al. (2005), may have been responsible for this.

Figure 32 shows the particle images of the glycine raw material and the typical crystallized product sample. As mentioned earlier, the particles of the raw material are quite round while those obtained under cooling crystallization, irrespective of the use of PEF, are rather long. In Figure 33 however, is a comparative characterization data plot of glycine raw material (Glycine_OS1), the crystallized product without PEF (PN_5) and the crystallized samples at 294 Hz (P2_5), 950 Hz (P3_5) and 145 Hz (P4_5) at the cooling rate of 5 ºC/h. This characterization data plots formed the basis for the formulation of Table 6.

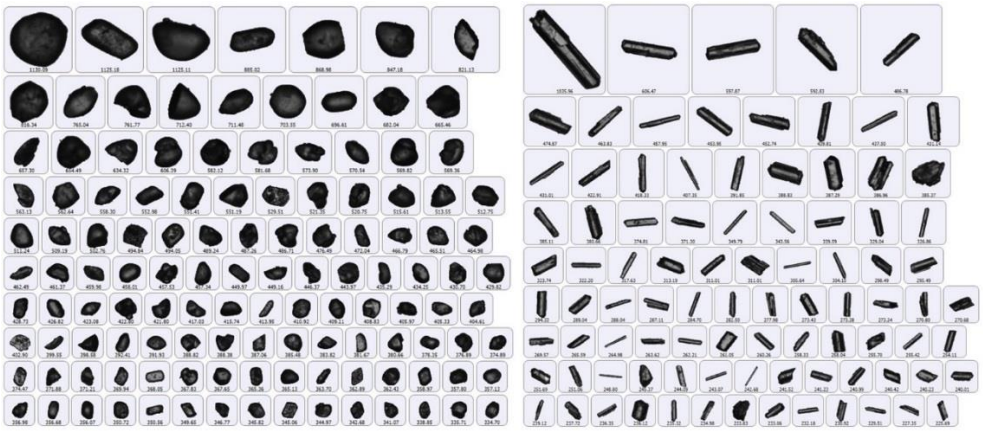

Figure 32. Comparison of the microscopic images (x2.5) of glycine raw material particles (left) with those obtained under cooling crystallization (right).

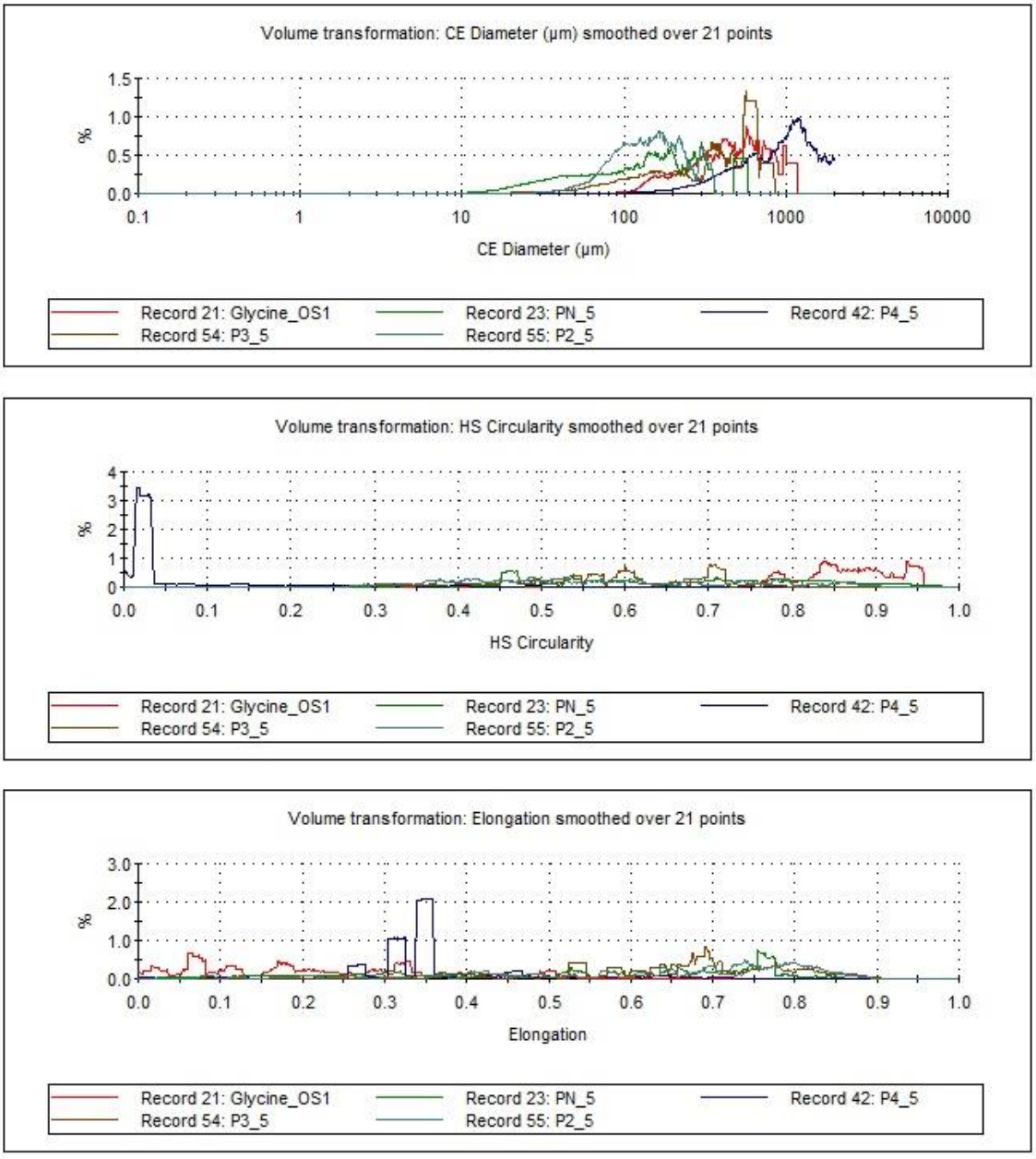

Figure 33. Morphologi G3 comparative characterization data plot of glycine raw material (Glycine_OS1), the crystallized product without PEF (PN_5) and the crystallized samples at 294 Hz (P2_5), 950 Hz (P3_5) and 145 Hz (P4_5) at 5 ºC/h cooling rate.

Since it had been established that pulsed electric field irradiation impacted on metastability in this study, it was expected that the crystal size distribution of the particles should be narrower with increasing pulse frequency application, but this was not the case. To this extent, two scenarios are suspected to have played out. The first is that the ageing period of two hours kept was too long that it nullified the earlier

achieved PEF effect since the electric field was kept till the end of the experiment. The second could be that although the use of higher pulse frequency induced nucleation faster, its energy supply was least sustained as its pulse wave pattern would suggest. This second reason may also be responsible for the observation of the biggest PEF effect, with respect to the shift in product composition in the direction of γ-glycine polymorphs, at 294 Hz applied frequency as earlier mentioned.

7. CONCLUSION

The impact of pulsed electric field application on the cooling crystallization of glycine was studied in this work, with three different pulse frequencies and three cooling rates as main variables. Commercial glycine sample was mainly used while KDP was also partly utilized in order to gain a better insight into the obtained results that were been observed in the glycine experiments. The different pulse frequencies applied are 294 Hz, 950 Hz and 145 Hz while the cooling rates used are 5 ºC/h, 10 ºC/h and 20 ºC/h. An experiment was carried out additionally without PEF irradiation at each cooling rate with the aim of establishing adequate comparison of obtained results. It was however expected that the use of PEF under these conditions should impact on the crystal morphology and the size distribution of the crystallized product particles.

The outcome of this study showed that the use of pulsed electric field did not affect in any meaningful way on the pH of the aqueous glycine solution as well as on its crystal size distribution. However, some argument being advanced in literature about the possibility of obtaining γ-glycine polymorphs from the near pure α-polymorphs raw material under high electric field intensity was substantiated. The obtained results, majorly by PXRD, showed as increase in γ-glycine polymorph content of the product with increasing electric field strength. The most significant effect was recorded on application of pulse frequency of 294 Hz at the slowest cooling rate of 5 ºC/h. The metastable zone width of the compounds studied was also significantly impacted by the pulsed electric field as nucleation of crystal particles began earlier with increasing electric pulse frequency applied.

In addition to contributing to the control of end products polymorphic composition as highlighted, the choice of cooling rate was also found to be critical to enhancing induction of crystallization and to the control of particle size distribution which may be of great interest in pharmaceuticals. At the slowest cooling rate, nucleation was observed much earlier than at faster cooling rates. The size distribution of the crystallized particles was generally wider towards the lower limit when compared with the raw material. This effect was more pronounced at the slowest cooling rate which produced particles as small as 10-30 μm from the raw material whose smallest particle was about 100 μm.

Further studies may focus on the application of stronger electric field intensity with the goal of establishing the critical parameters for which γ-glycine polymorphs could be attained in specific compositions. Attention may therefore be given to the determination of supersaturation and zeta-potentials of the solution, the choice agitation and duration of ageing as these have been identified in literature as likely contributing factors.

REFERENCES

Aber, J. E., Arnold, S., Garetz, B. A. & Myerson, A. S. 2005. Strong dc electric field applied to superstaurated aqueous glycine solution induces nucleation of the γ polymorph. *American Physical Society: Physical Review Letters,* vol. 94(145503), pp. 1-4.

Anbu Chudar Azhagan, S. & Ganesan, S. 2013. Crystal growth, structural, optical, thermal and NLO studies of γ-glycine single crystals. *Optik,* vol. 124, pp. 6456-6460.

Barbosa-Canovas, G. 2002. Food Safety Magazine. [Online document]. [Accessed 14 August 2014]. Available at: http://www.foodsafetymagazine.com/magazine-archive1/augustseptember-2002/key-goals-of-emerging-technologies-for-inactivating-bacteria/

Boldyreva, E.V., Drebushchak, V.A., Drebushchak, T.N., Paukov, I.E., Kovalevskaya, Y.A., Shutova, E.S. 2003. Polymorphism of Glycine. Thermodynamic aspects. Part I: Relative stability of the polymorphs. *Thermal Analysis and Calorimetry,* vol. 73, pp. 409-418.

Bonnin-Paris, J., Bostyn, S., Havet, J. & Fauduet, H. 2011. Determination of the metastable zone width of glycine aqueous solutions for batch crystallizations. *Chemical Engineering Communications,* vol. 198, pp. 1004-1017.

Cueva, O. A. 2009. Pulsed electric field influences on acid tolerance, bile tolerance, protease activity and gowth characteristics of Lactobacillus Acidophilus LA-K. Master's Thesis, Louisiana State University, School of Animal Sciences.

Devi, K. R., Gnanakamatchi, V. & Srinivasan, K. 2014. Attainment of unstable β nucleation of glycine through novel swift cooling crystallization process. *Journal of Crystal Growth,* vol. 400, pp. 34-42.

Devi, K. R. & Srinivasan, K. 2013. The role of charge compensation on the nucleation of α and γ polymorphs of glycine from aqueous solutions. *Journal of Crystal Growth,* vol. 364, pp. 89-94.

Devi, K. R. & Srinivasan, K. 2014. Towards a better understanding of the nucleation behavior of α and γ polymorphs of glycine from aqueous solution in the presence of

selective additives by charge compensation mechanism. *Journal of Crystal Growth,* vol. 401, pp. 227-232.

Dickey, D. 2005. Chemical Processing. [Online document]. [Accessed 11 December 2014]. Available at: http://www.chemicalprocessing.com/articles/2005/519/

Dutrow, B. L. & Clark, C. M. 2013. Montana State University, Bozeman. [Online document]. [Accessed 13 November 2014]. Available at: http://serc.carleton.edu/research_education/geochemsheets/techniques/XRD.html

EAG Inc. 2014. Evans Analytical Group. [Online document]. [Accessed 13 November 2014]. Available at: http://www.eag.com/mc/x-ray-diffraction.html

EBSCO Publishing 2013. Heart Health Articles. [Online document]. [Accessed 10 November 2014]. Available at: http://www.lifescript.com/health/centers/heart_health/alternative_treatments/glycine.aspx

Flow-Tech Systems, LLC 2014. Flow-Tech Home. [Online document]. [Accessed 11 November 2014]. Available at: http://flowtechhome.com/

Jalte, M., Lanoiselle, J., Lebovka, N. & Vorobiev, E. 2009. Freezing of potato tissue pre-treated by pulsed electric fields. *LWT - Food Science and Technology,* vol. 42, pp. 576-580.

Jambari, H., Azli, N. A. & Mohamed-Piah, M. 2011. Comparison of pulsed electric field generation techniques for microbial inactivation application. *Journal of Theoretical and Applied Information Technology,* vol. 33, issue 1, pp. 22-31.

Kumar, R. A., Vizhi, R. E., Vijayan, N. & Babu, D. R. 2011. Structural, dielectric and piezoelectric properties of non-linear optical γ-glycine single crystals. *Physica B,* vol. 406, pp. 2594-2600.

Lab Testing, Inc. 2014. Laboratory Testing. [Online document]. [Accessed 13 November 2014]. Available at: http://www.labtesting.com/services/polymer-testing/ftir-analysis/

Liu, Z., Zhong, L., Ying, P., Feng, Z. & Li, C. 2008. Crystallization of metastable β-glycine from gas phase via the sublimation of α or γ form in vacuum. *Biophysical Chemistry,* vol. 132, pp. 18-22.

Loginova, K., Loginov, M., Vorobiev, E. & Lebovka, N. 2012. Better lime purification of sugar beet juice obtained by low temperature aqueous extraction assisted by pulsed electric field. *LWT - Food Science and Technology,* vol. 46, pp. 371-374.

Louhi-Kultanen, M., Karjalainen, M., Rantanen, J., Huhtanen, M. & Kallas, J 2006. Crystallization of glycine with ultrasound. *International Journal of Pharmaceutics,* vol. 320, pp. 23-29.

Malvern Instruments Ltd, 2014. Malvern. [Online document]. [Accessed 8 December 2014]. Available at: http://www.malvern.com/en/products/product-range/morphologi-range/morphologi-g3/default.aspx

Mikhaylin, S., Nikonenko, V., Pourcelly, G. & Bazinet, L. 2014. Intensification of demineralization process and decrease in scaling by application of pulsed electric field with short pulse/pause conditions. *Journal of Membrane Science,* vol. 468, pp. 389-399.

Mitchell, N. A., O'Ciardha, C. T. & Frawley, P. J., 2011. Estimation of the growth kinetics for the cooling crystallization of paracetamol and ethanol solutions. *Journal of Crystal Growth,* vol. 328, pp. 39-49.

Mullin, J. 2001. Crystallization. Fourth ed. Oxford: Butterworth-Heinemann.

Nii, S. & Takayanagi, S. 2014. Growth and size control in anti-solvent crystallization of glycine with high frequency ultrasound. *Ultrasonics Sonochemistry,* vol. 21, pp. 1182-1186.

Palosaari, S., Louhi-Kultanen, M. & Sha, Z. 2007. Industrial Crystallization. In: Mujumdar, A. S. edited. Handbook on Industrial Drying. Third ed. Florida: CRC Press, pp. 1203-1224.

Pearson, N. 2014. TutorVista. [Online document]. [Accessed 11 August 2014]. Available at: http://chemistry.tutorvista.com/biochemistry/biological-molecules.html

Plumber's Choice, LLC 2014. Plumber's Choice. [Online document]. [Accessed 11 November 2014]. Available at: http://www.plumberschoicewater.com/

Radácsi, N. 2012. Process intensification in crystallization: Submicron particle generation using alternative energy forms. Doctoral thesis. Delft University of Technology, Holland.

Raschke, D. 2010. Pulsed electric fields - Influence on physiology, structure and extraction processes of the oleaginous yeast Waltomyces lipofer. Doctoral thesis. Technical University of Berlin, Faculty of Process Sciences.

Rocky Mountain Laboratories, Inc. 2012. Rocky Mountain Labs. [Online document]. [Accessed 13 November 2014]. Available at: http://www.rockymountainlabs.com/fourier-transform-infrared-spectroscopy-ftir.htm

Sankar, S., Manikandan, M., Gopal Ram, S.D., Mahalingam, T. & Ravi, G. 2010. Gel growth of α and γ glycine and their characterization. *Journal of Crystal Growth,* vol. 312, pp. 2729-2733.

Srinivasan, T. P., Indirajith, R. and Gopalakrishnan, R. 2011. Growth and characterization of α and γ-glycine single crystals. *Journal of Crystal Growth*, vol. 318, pp. 762-767.

Srinivasan, K. 2008. Crystal growth of α and γ glycine polymoprhs and their polymorphic phase transformations. *Journal of Crystal Growth,* vol. 311, pp. 156-162.

Srinivasan, K. & Arumugan, J. 2007. Growth of non-linear optical γ-glycine single crystals and their characterization. *Optical Materials,* vol. 30, pp. 40-43.

Therapeutic Research Faculty 2009. Natural Medicines Comprehensive Database. [Online document]. [Accessed 10 November 2014].Available at: http://www.webmd.com/vitamins-supplements/ingredientmono-1072-glycine.aspx?activeingredientid=1072&activeingredientname=glycine

U.S. Food and Drug Administration 2011. FDA. [Online document]. [Accessed 12 November 2014].Available at: http://www.fda.gov/Food/FoodScienceResearch/SafePracticesforFoodProcesses/ucm101662.htm

Verma, T. 2012. Slideshare. [Online document]. [Accessed 14 August 2014]. Available at: http://www.slideshare.net/trish070892/pef-ppt?related=4

Yuki Gosei Kogyo Co. Ltd 2006. [Online document]. [Accessed 10 November 2014]. Available at: http://www.yuki-gosei.co.jp/en/special/glycine08.html

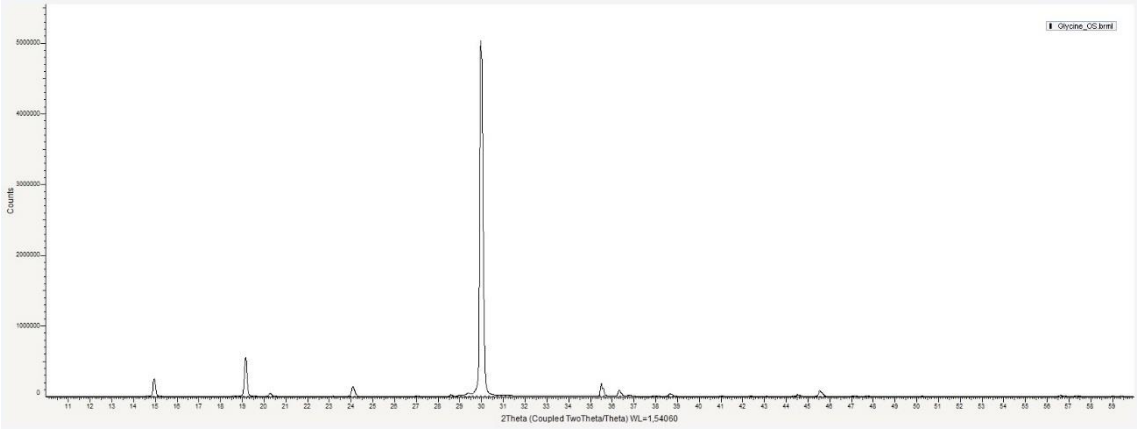

Figure 1. PXRD spectrum for glycine raw material sample.

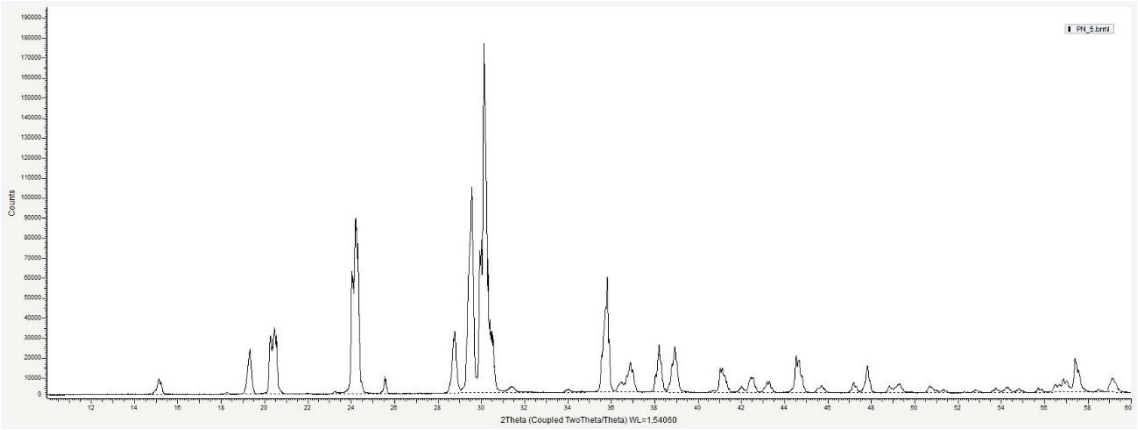

Figure 2. PXRD spectrum for crystallized product without PEF at 5 ºC/h.

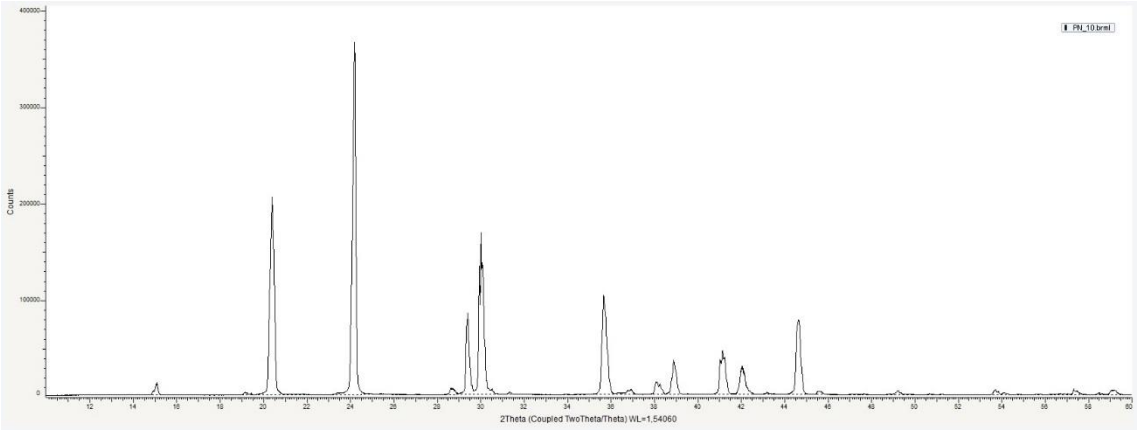

Figure 3. PXRD spectrum for crystallized product without PEF at 10 ºC/h.

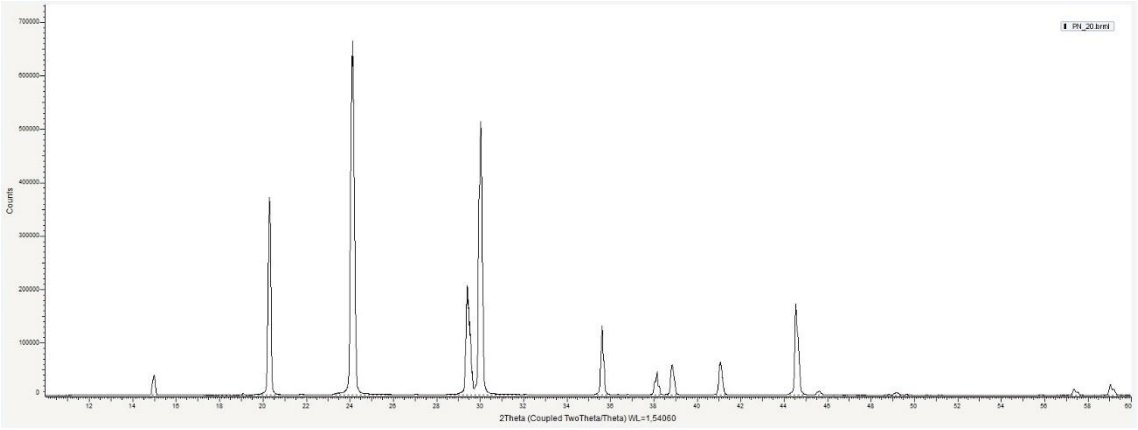

Figure 4. PXRD spectrum for crystallized product without PEF at 20 ºC/h.

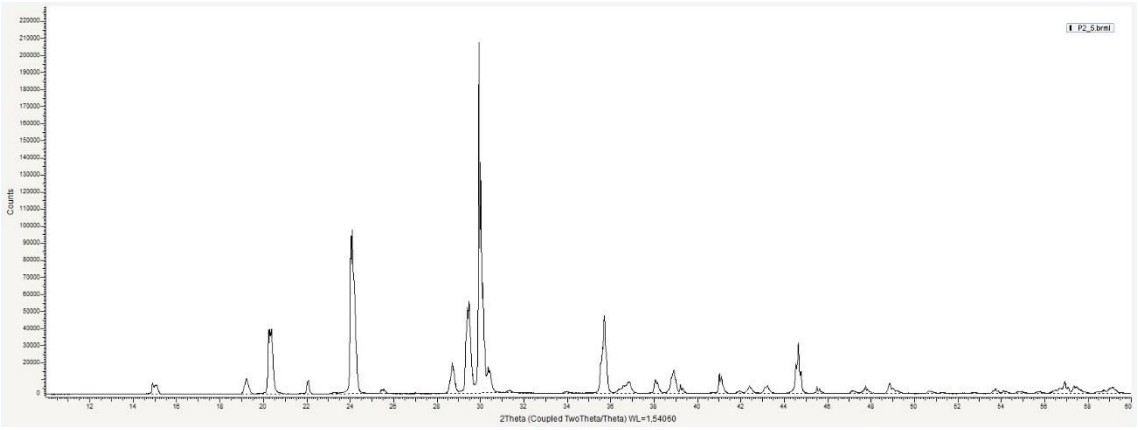

Figure 5. PXRD spectrum for crystallized product at 294 Hz and 5 ºC/h.

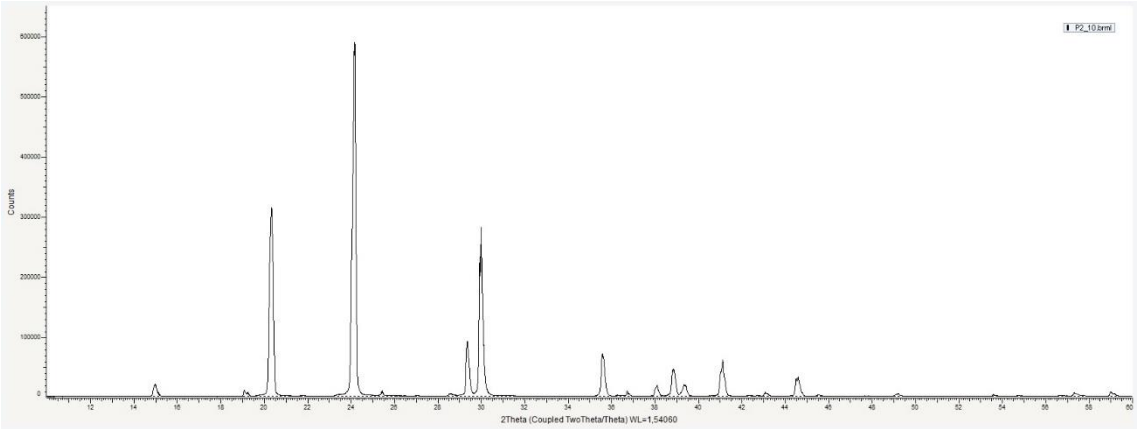

Figure 6. PXRD spectrum for crystallized product at 294 Hz and 10 ºC/h.

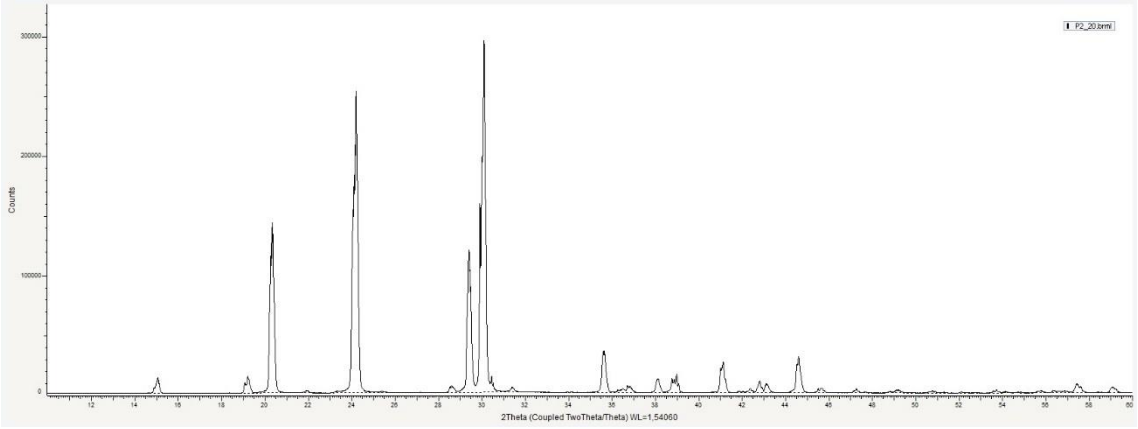

Figure 7. PXRD spectrum for crystallized product at 294 Hz and 20 ºC/h.

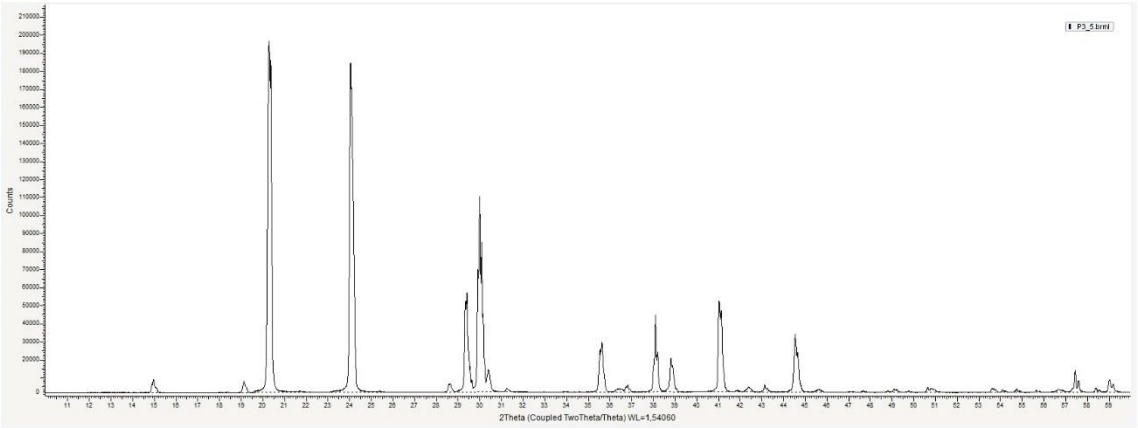

Figure 8. PXRD spectrum for crystallized product at 950 Hz and 5 ºC/h.

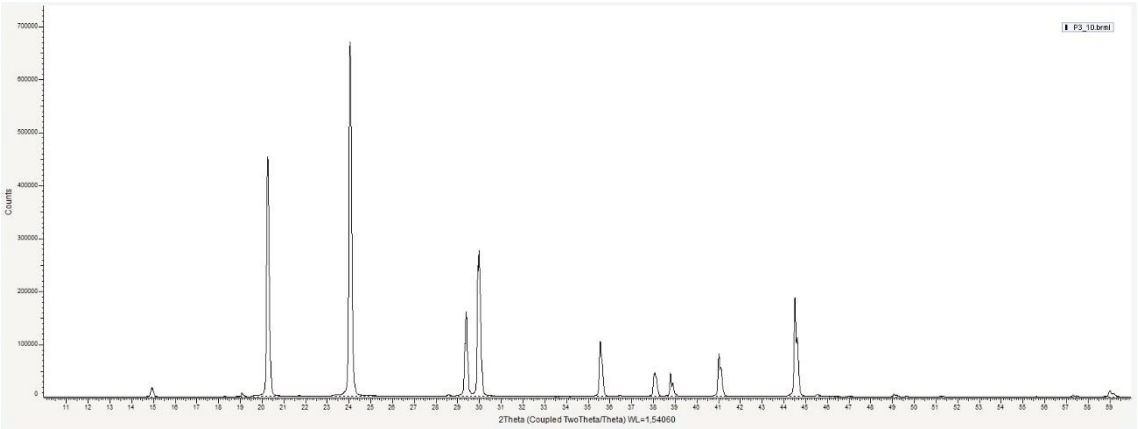

Figure 9. PXRD spectrum for crystallized product at 950 Hz and 10 ºC/h.

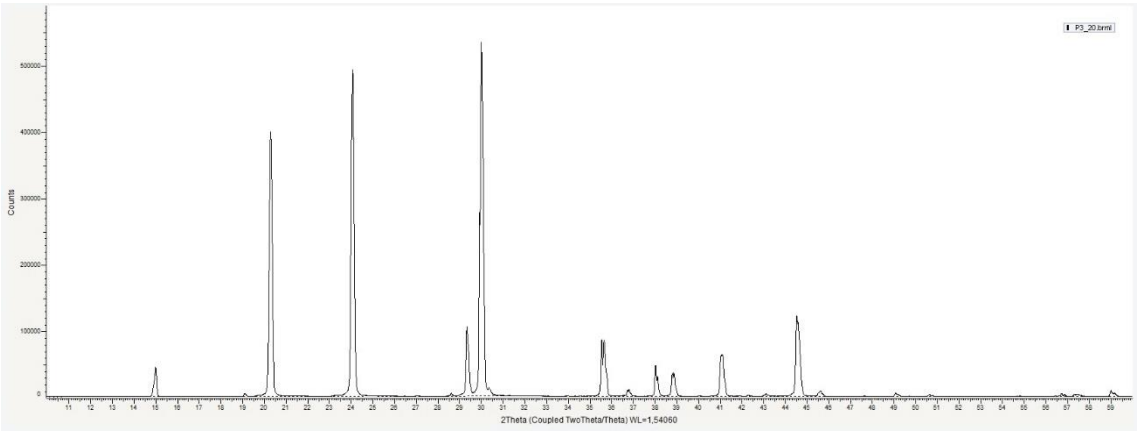

Figure 10. PXRD spectrum for crystallized product at 950 Hz and 20 ºC/h.

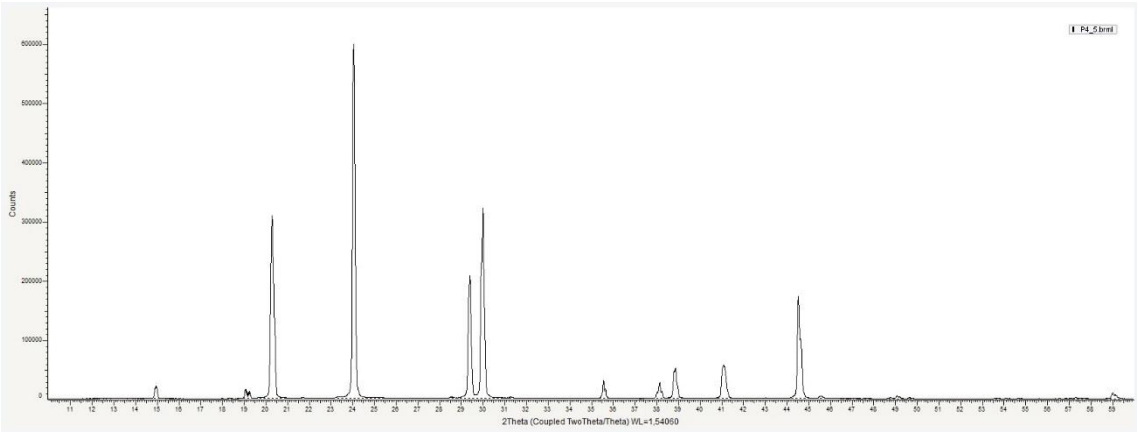

Figure 11. PXRD spectrum for crystallized product at 145 Hz and 5 ºC/h.

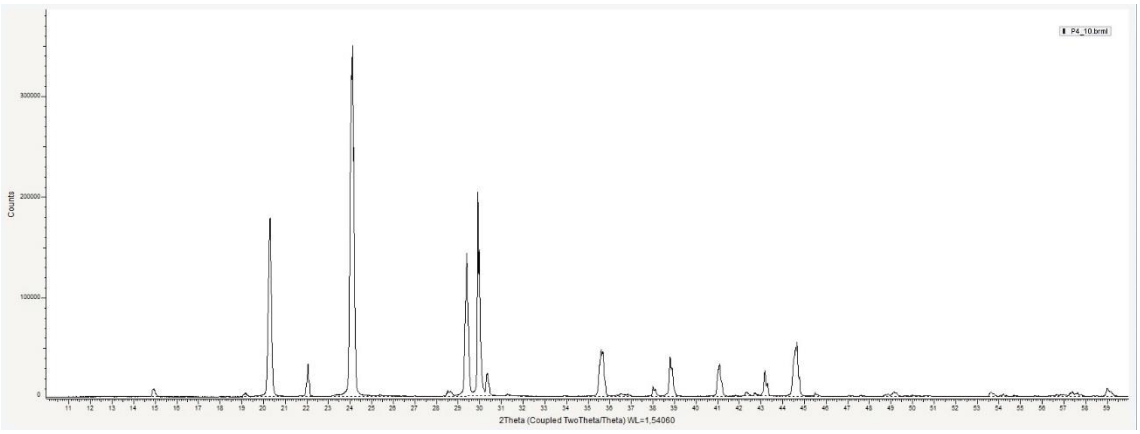

Figure 12. PXRD spectrum for crystallized product at 145 Hz and 10 ºC/h.

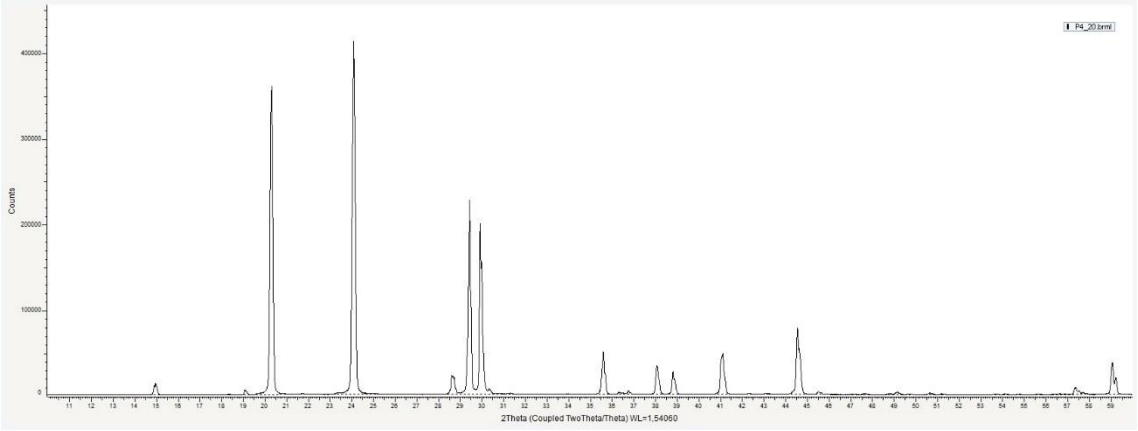

Figure 13. PXRD spectrum for crystallized product at 145 Hz and 20 ºC/h.

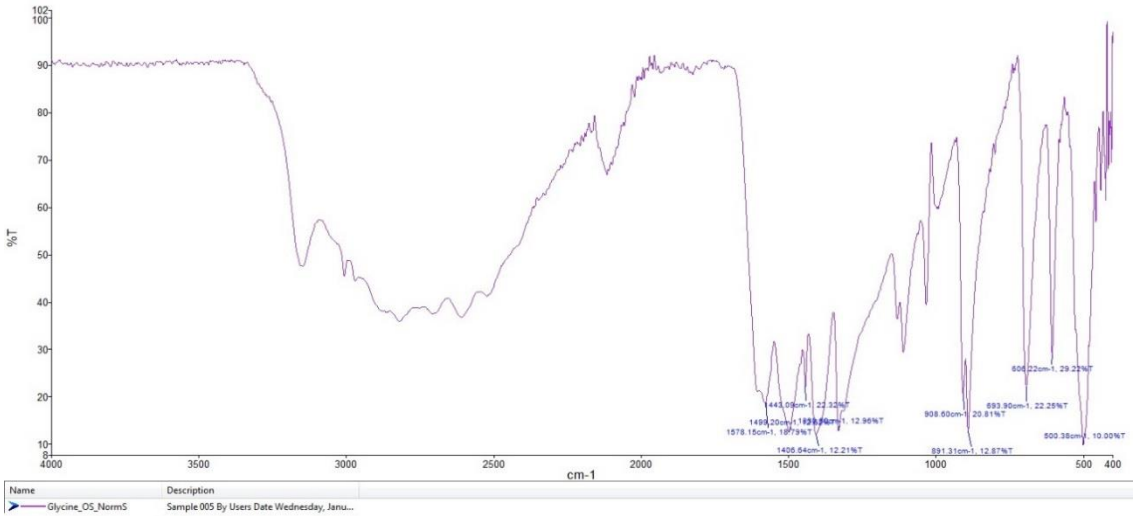

Figure 1. FT-IR spectrum for glycine raw material sample.

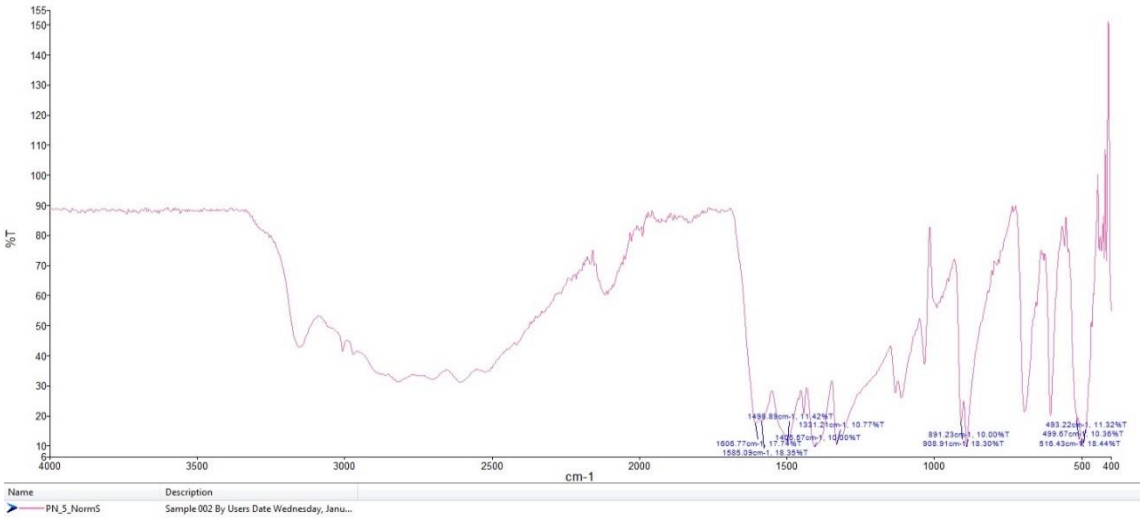

Figure 2. FT-IR spectrum for crystallized product without PEF at 5 ºC/h.

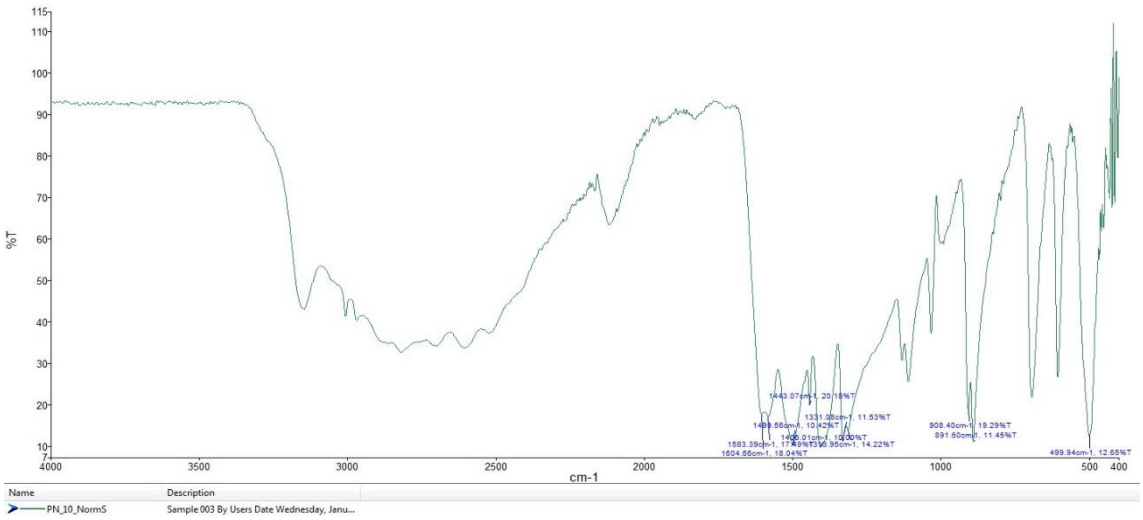

Figure 3. FT-IR spectrum for crystallized product without PEF at 10 ºC/h.

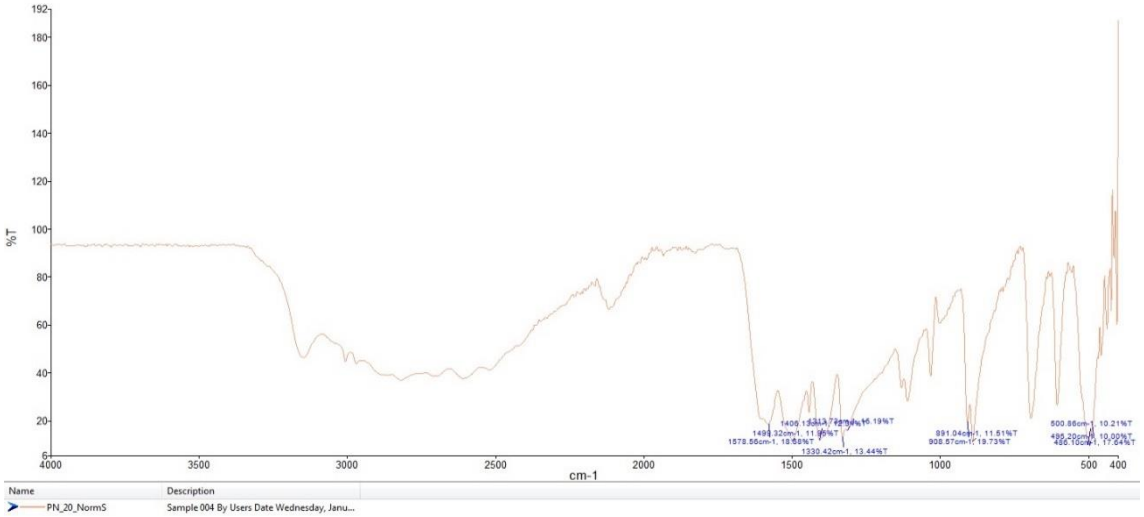

Figure 4. FT-IR spectrum for crystallized product without PEF at 20 ºC/h.

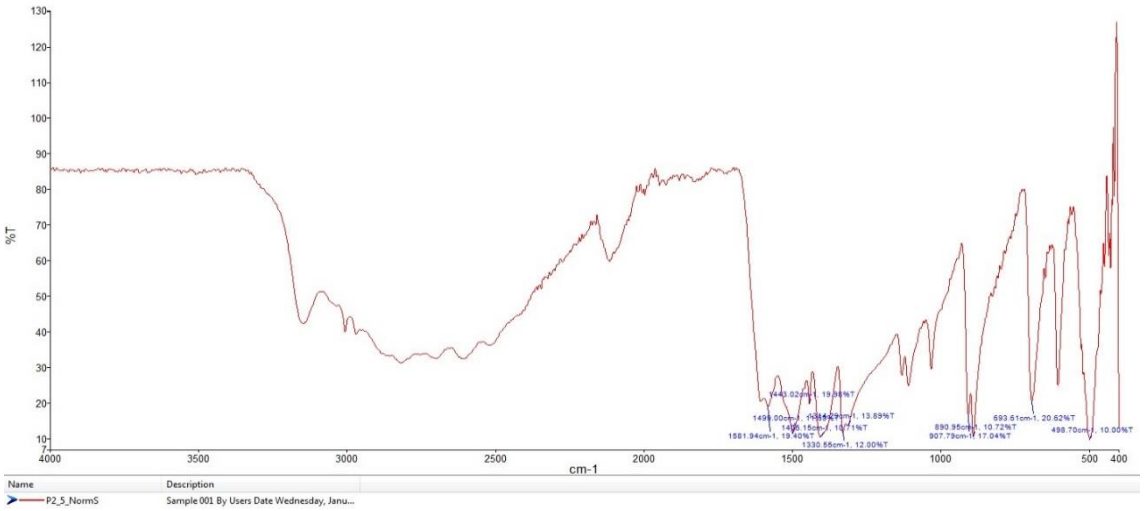

Figure 5. FT-IR spectrum for crystallized product at 294 Hz and 5 ºC/h.

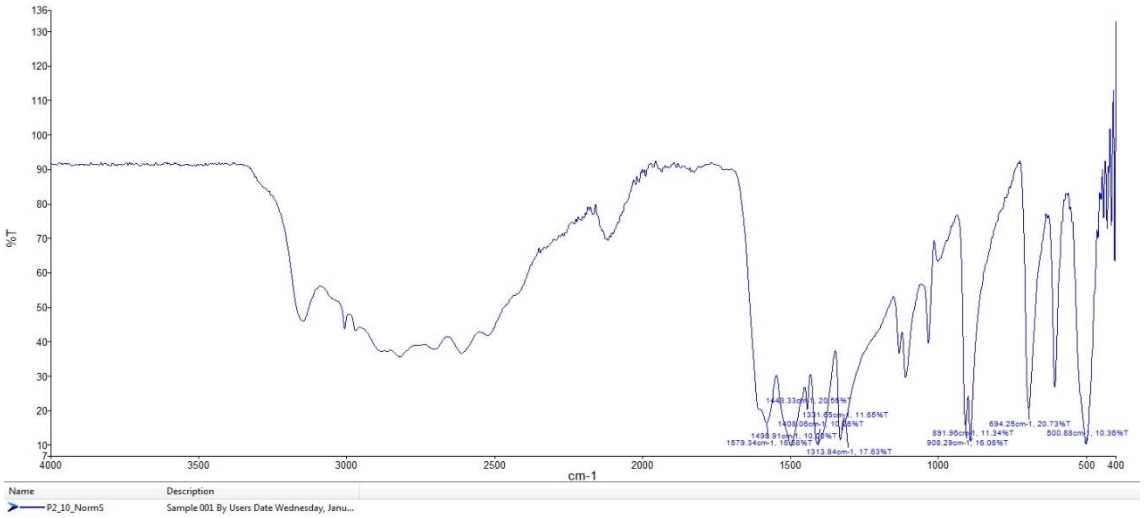

Figure 6. FT-IR spectrum for crystallized product at 294 Hz and 10 ºC/h

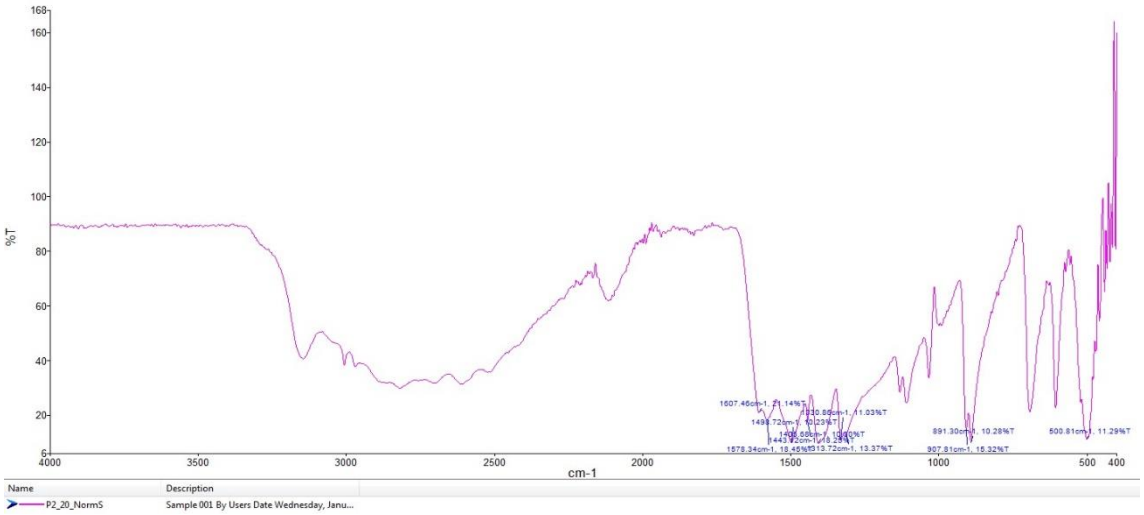

Figure 7. FT-IR spectrum for crystallized product at 294 Hz and 20 ºC/h.

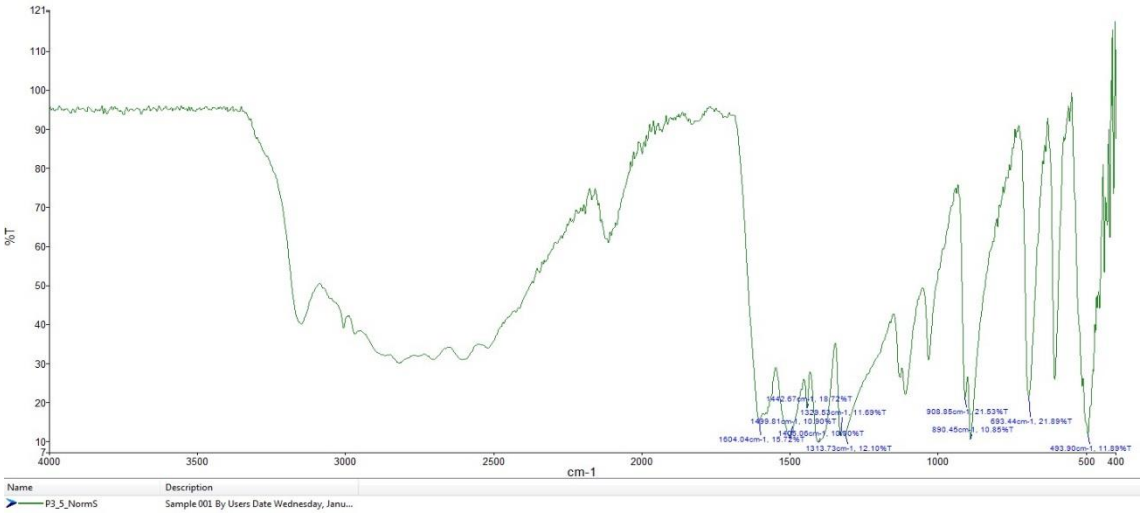

Figure 8. FT-IR spectrum for crystallized product at 950 Hz and 5 ºC/h.

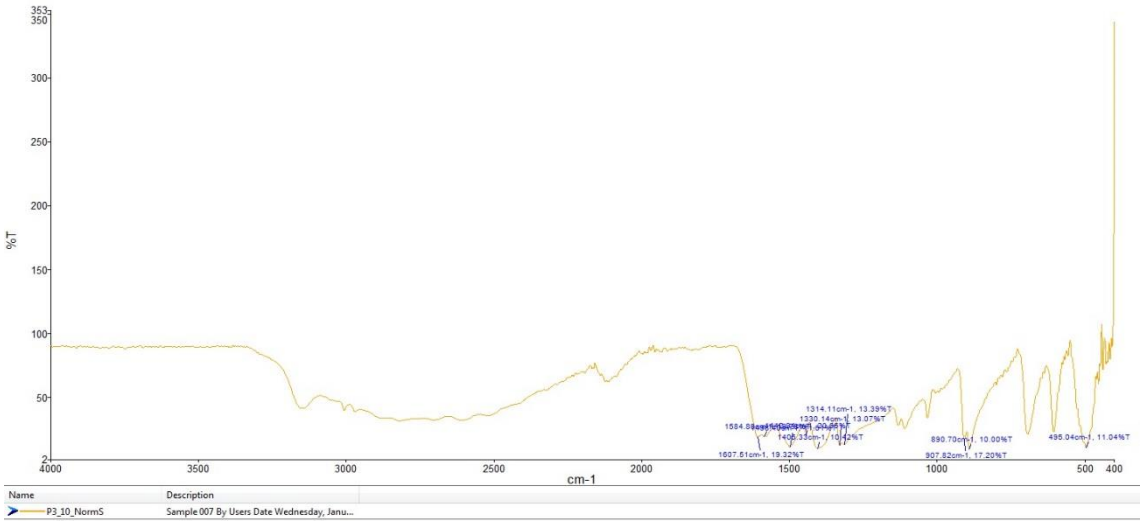

Figure 9. FT-IR spectrum for crystallized product at 950 Hz and 10 ºC/h.

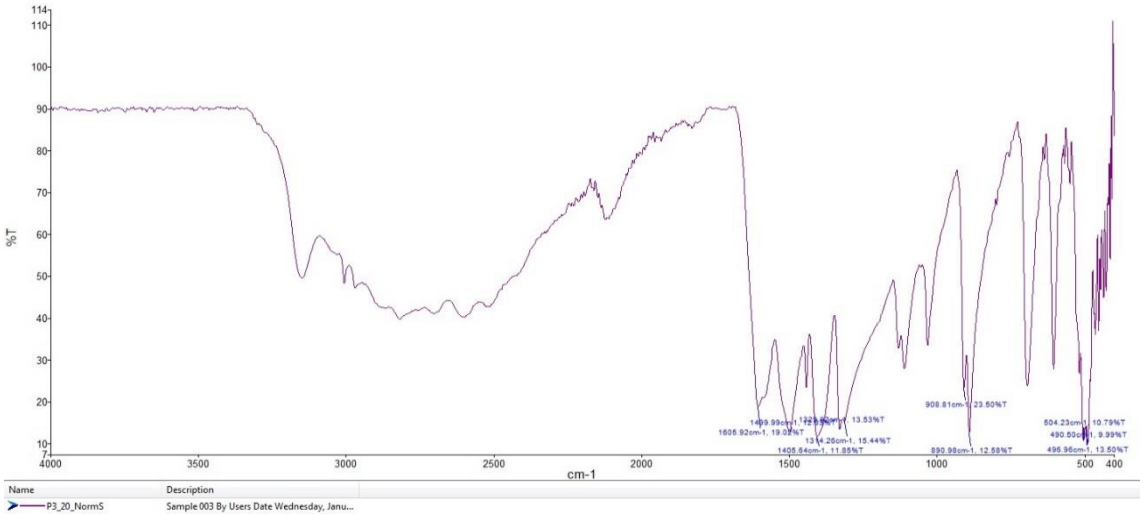

Figure 10. FT-IR spectrum for crystallized product at 950 Hz and 20 ºC/h.

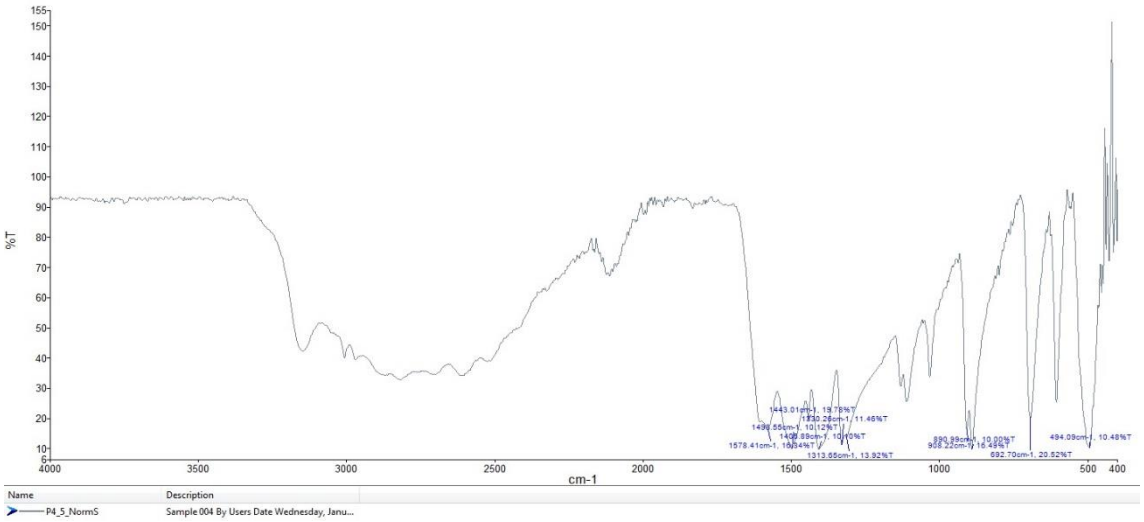

Figure 11. FT-IR spectrum for crystallized product at 145 Hz and 5 ºC/h.

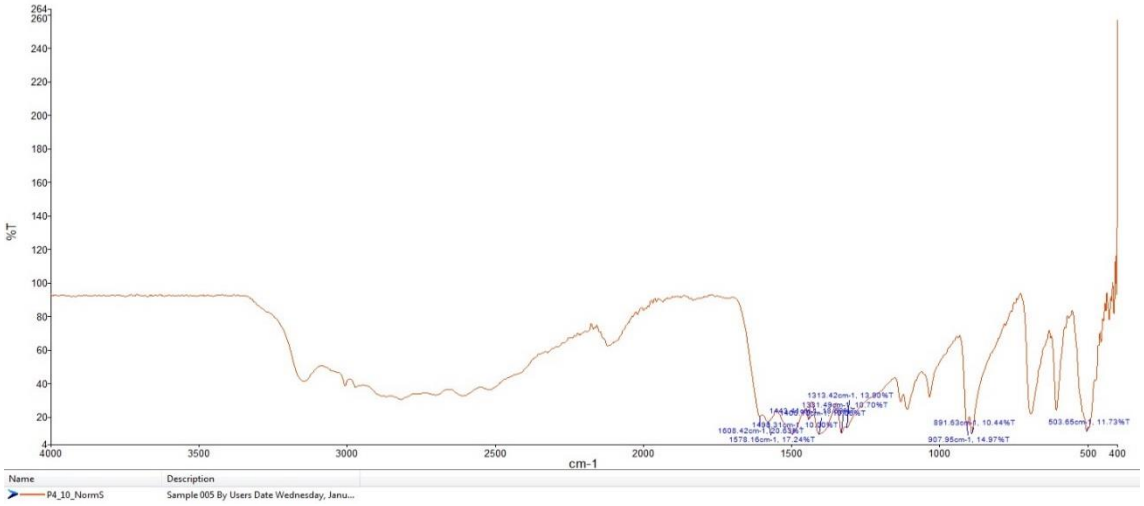

Figure 12. FT-IR spectrum for crystallized product at 145 Hz and 10 ºC/h.

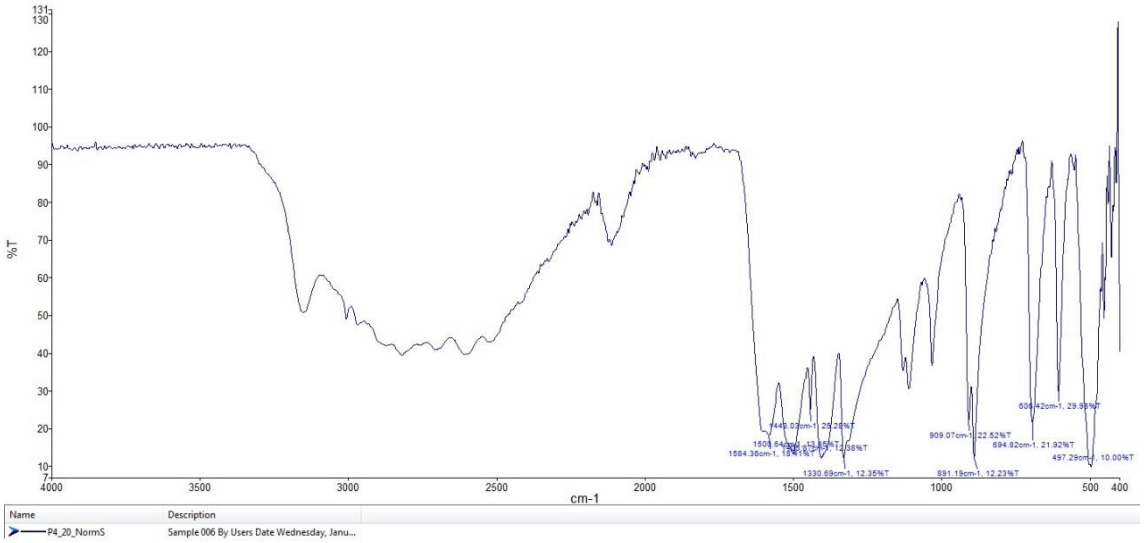

Figure 13. FT-IR spectrum for crystallized product at 145 Hz and 20 ºC/h.

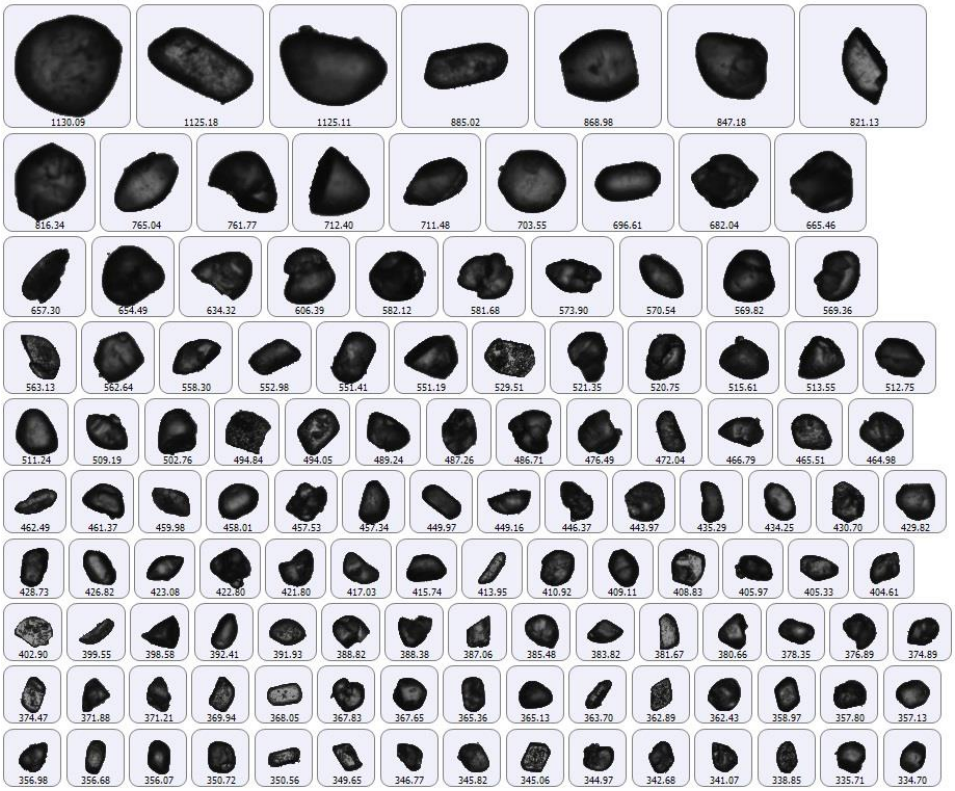

Figure 1. Particle images (x2.5) for glycine raw material sample.

Figure 2. Particle images (x2.5) for crystallized product without PEF at 5 ºC/h.

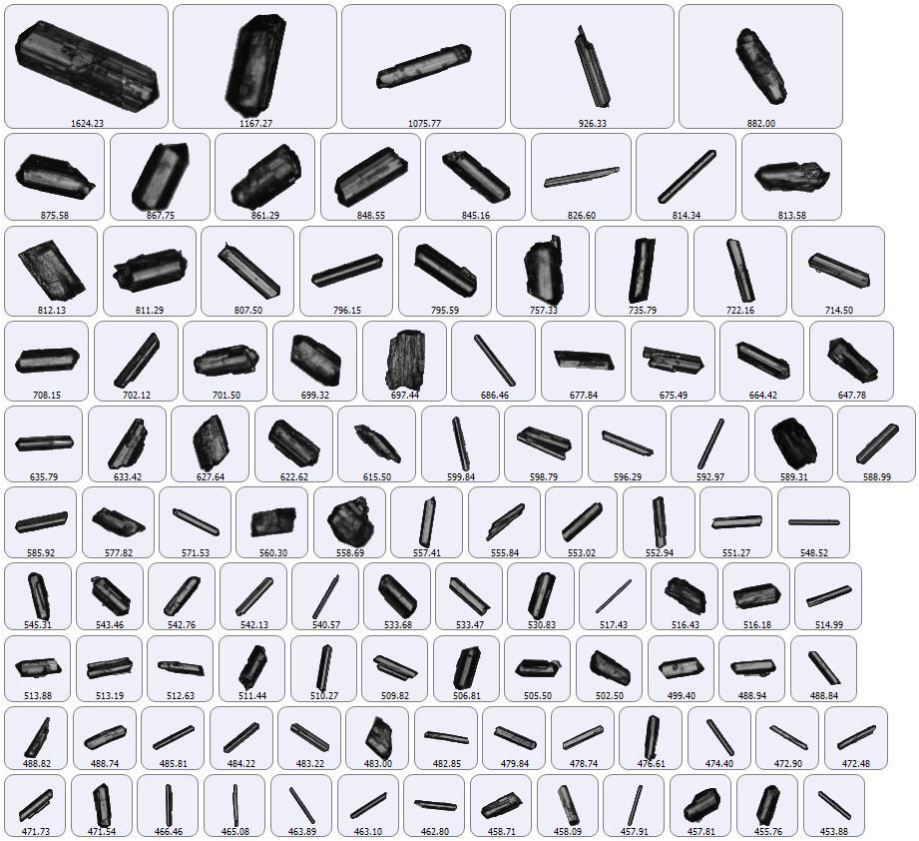

Figure 3. Particle images (x2.5) crystallized product without PEF at 10 ºC/h.

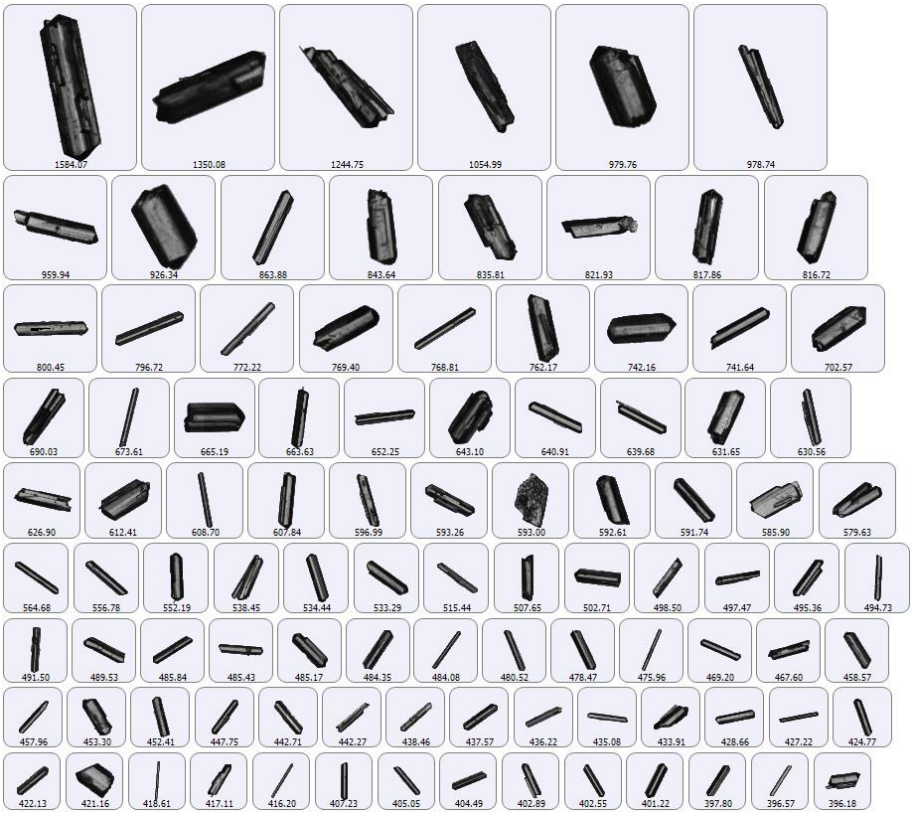

Figure 4. Particle images (x2.5) for crystallized product without PEF at 20 ºC/h.

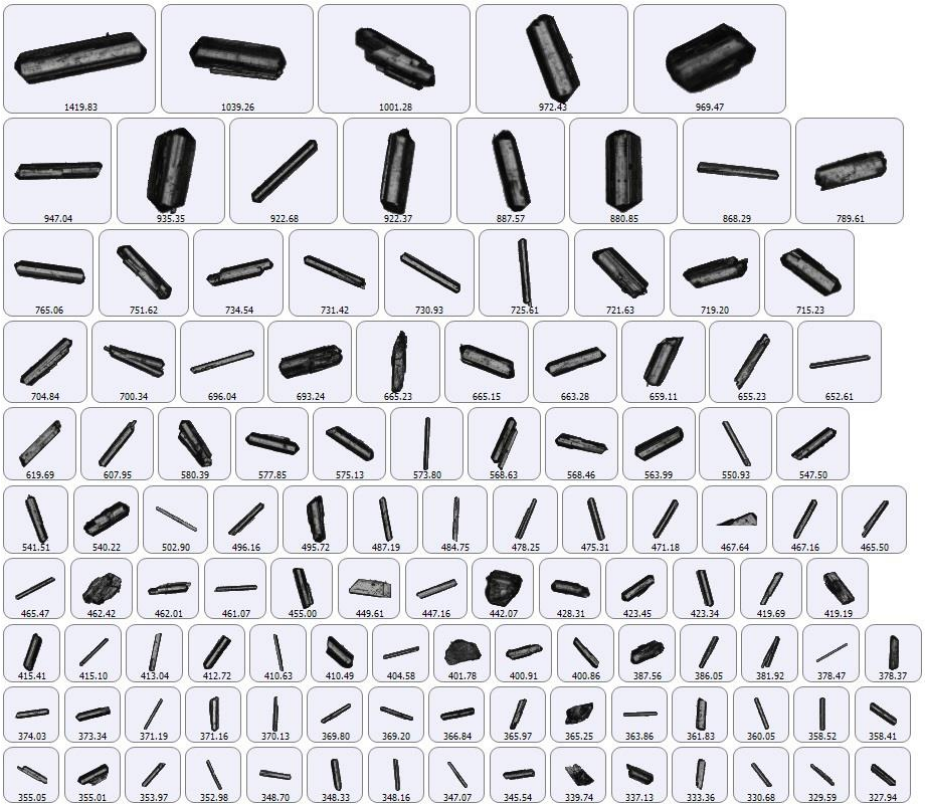

Figure 5. Particle images (x2.5) for crystallized product at 294 Hz and 5 ºC/h.

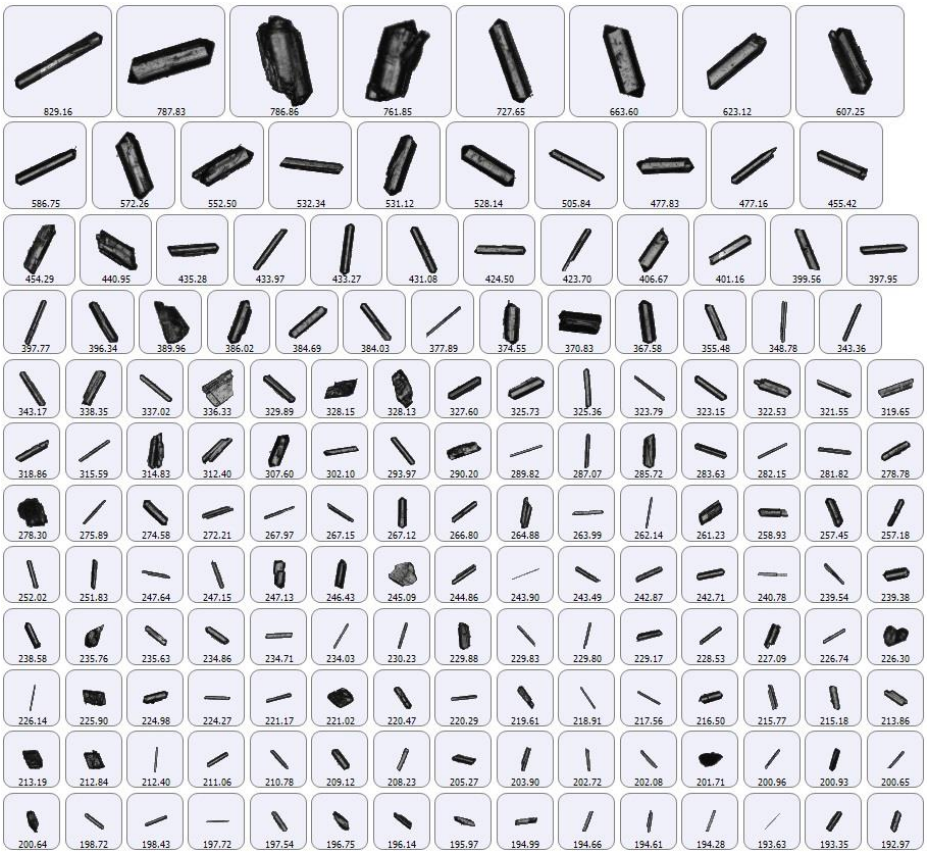

Figure 6. Particle images (x2.5) for crystallized product at 294 Hz and 10 ºC/h

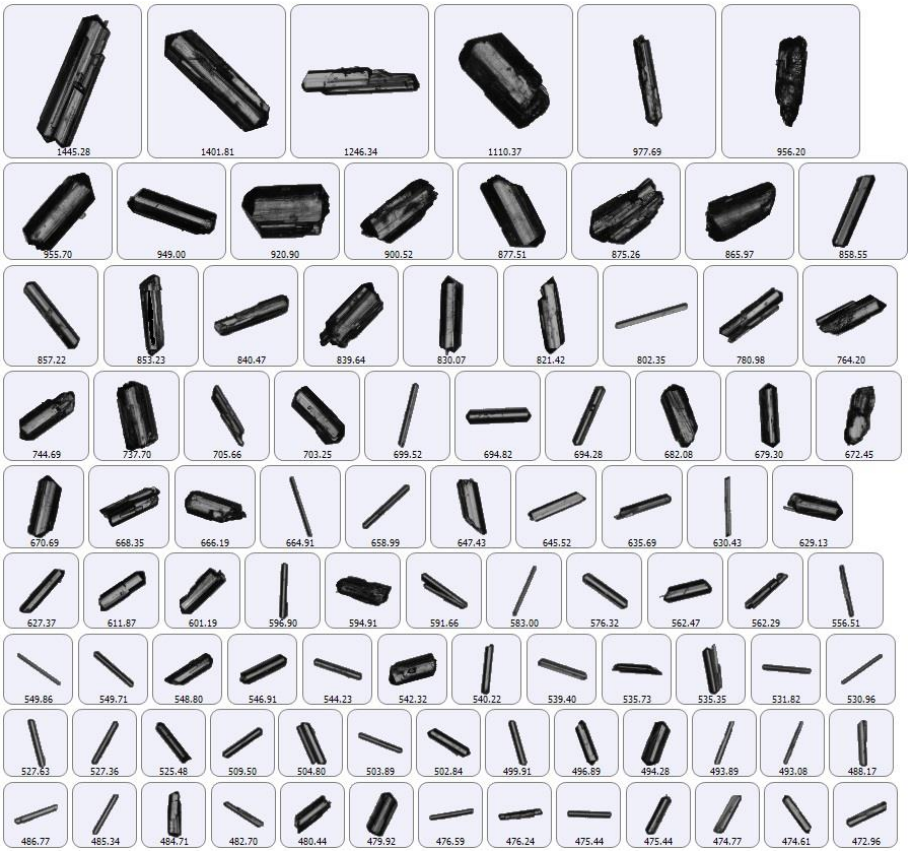

Figure 7. Particle images (x2.5) for crystallized product at 294 Hz and 20 ºC/h.

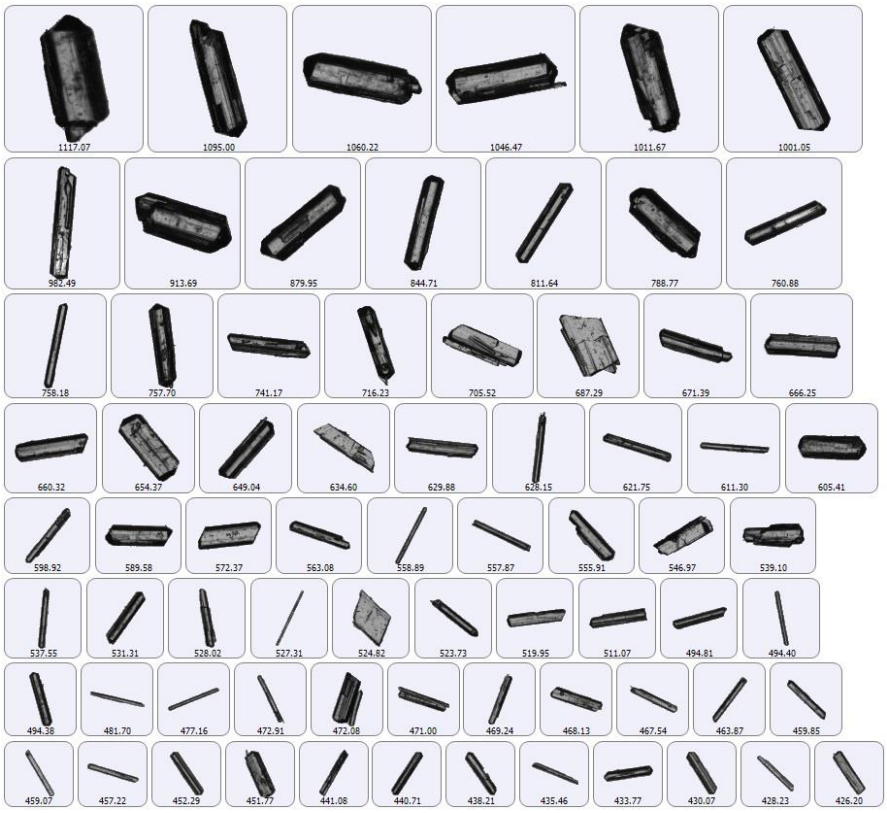

Figure 8. Particle images (x2.5) for crystallized product at 950 Hz and 5 ºC/h.

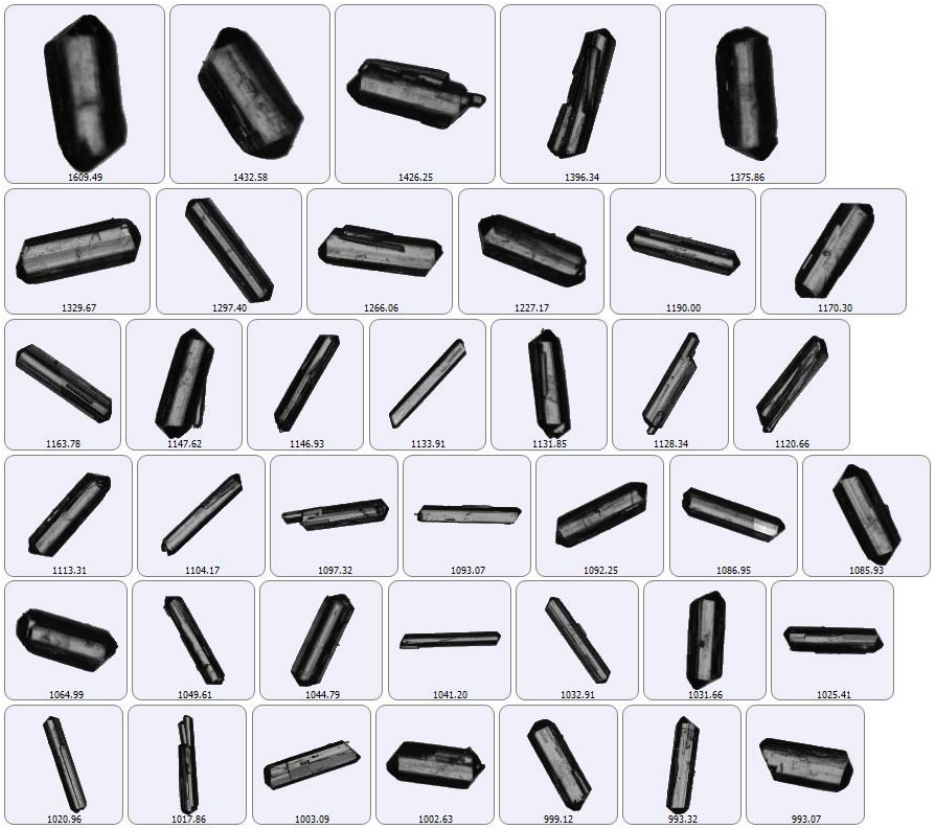

Figure 9. Particle images (x2.5) for crystallized product at 950 Hz and 10 ºC/h.

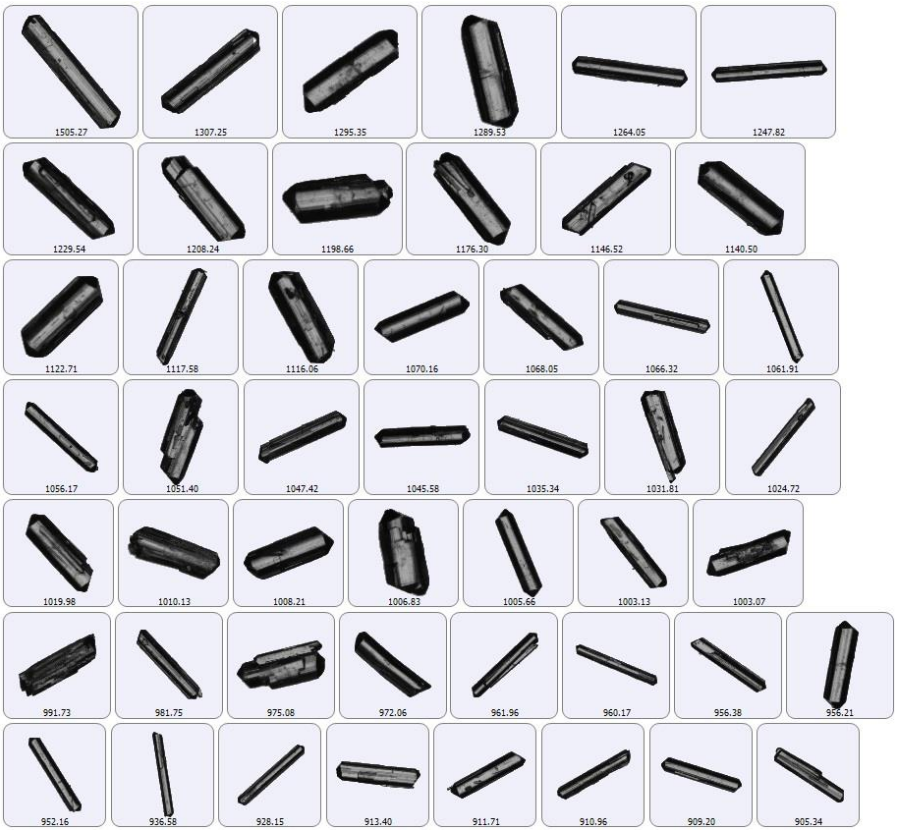

Figure 10. Particle images (x2.5) for crystallized product at 950 Hz and 20 ºC/h.

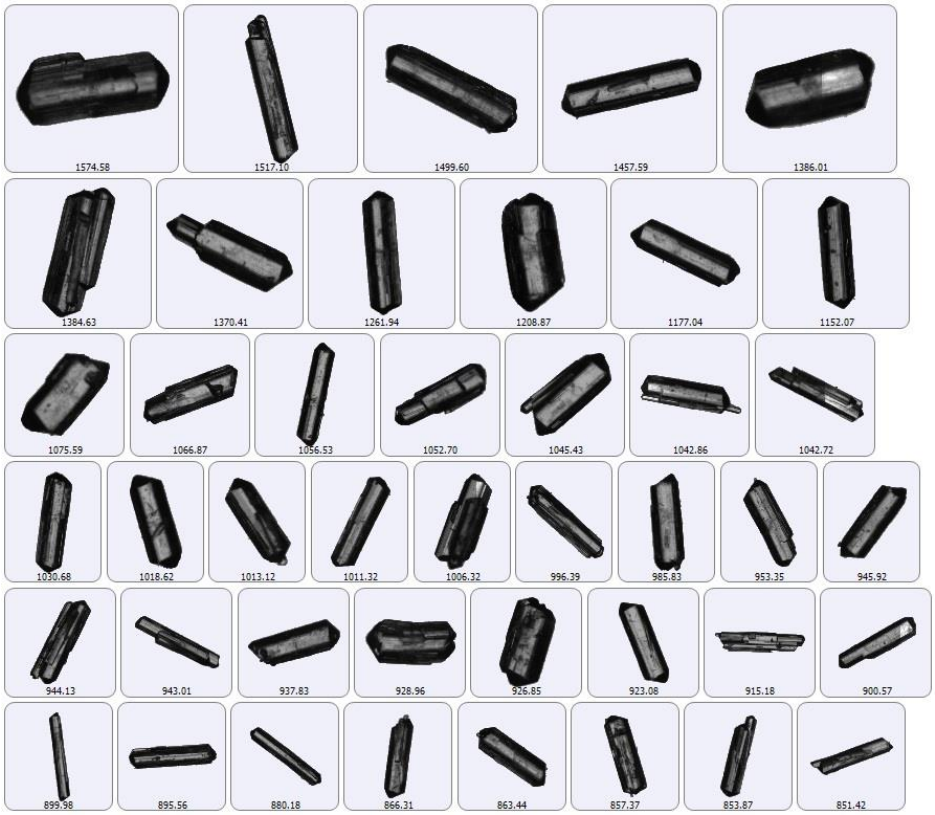

Figure 11. Particle images (x2.5) for crystallized product at 145 Hz and 5 ºC/h.

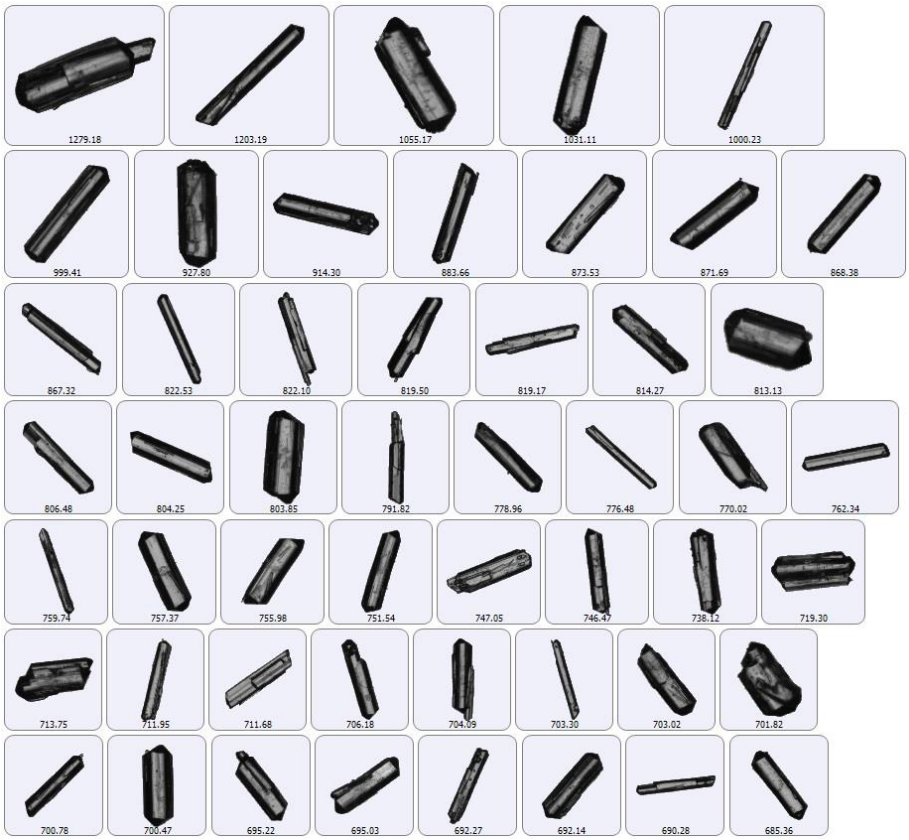

Figure 12. Particle images (x2.5) for crystallized product at 145 Hz and 10 ºC/h.

Figure 13. Particle images (x2.5) for crystallized product at 145 Hz and 20 ºC/h.

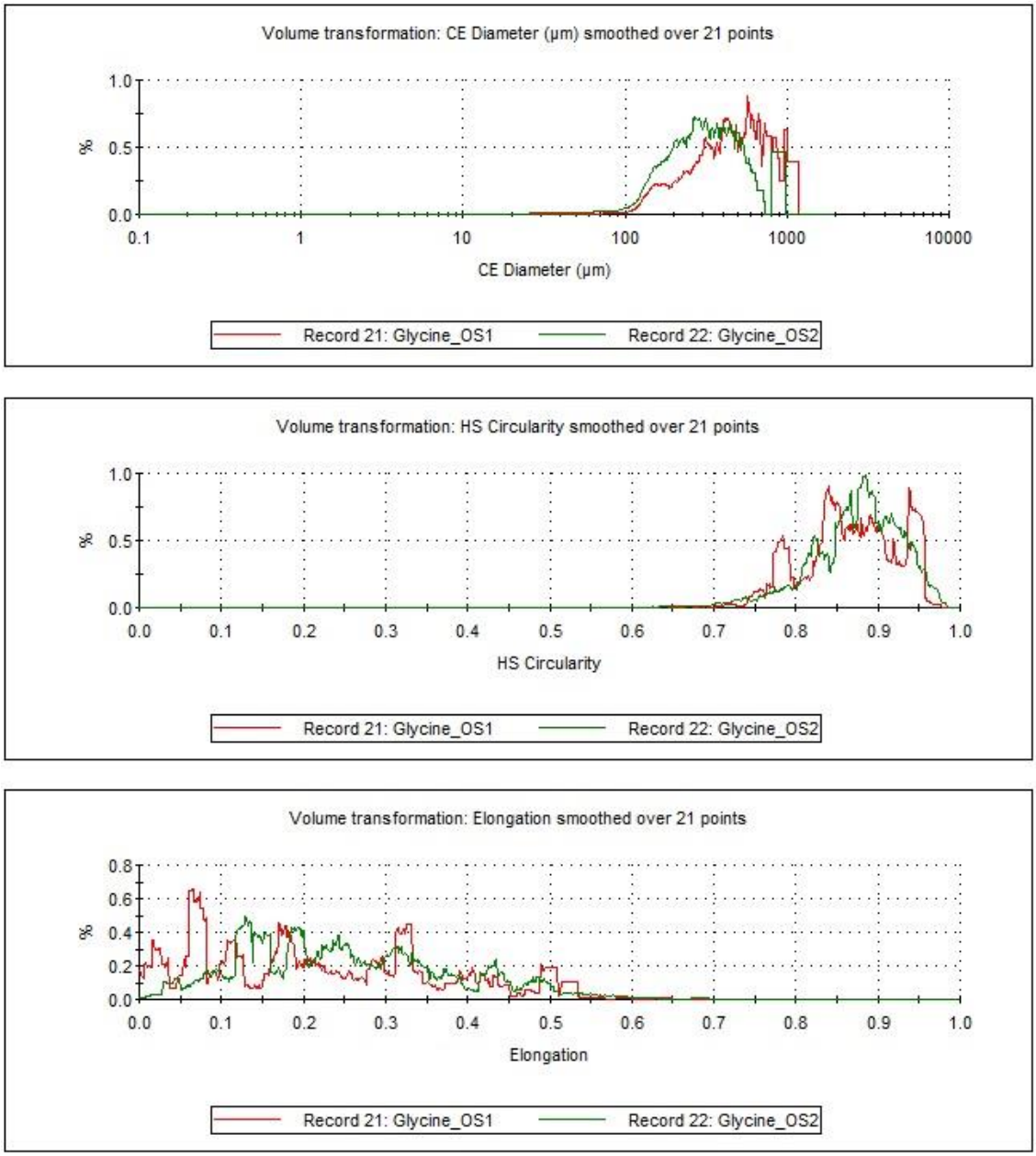

Figure 1. Particle characterization data plot (repeated measurement) for glycine raw material.

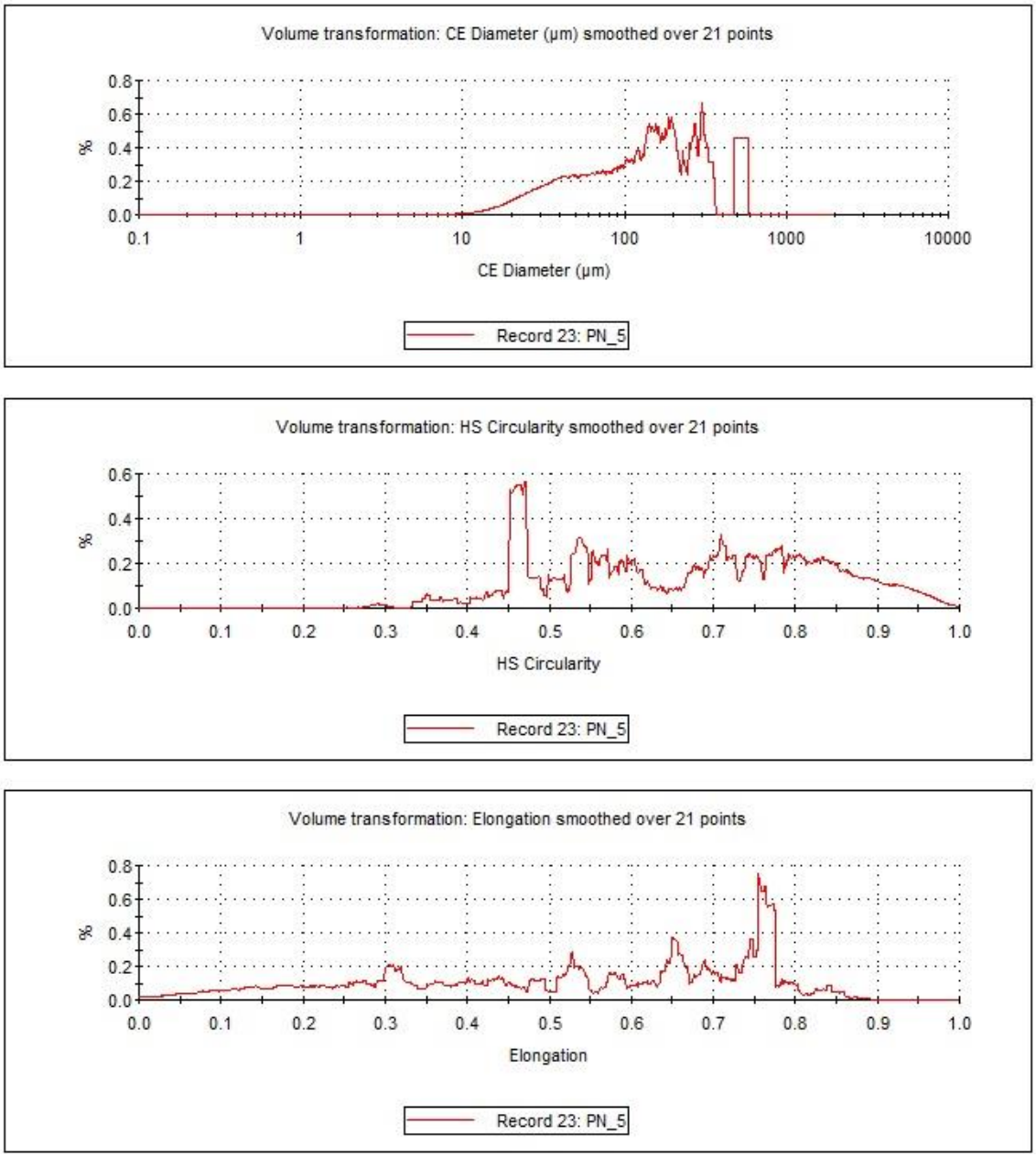

Figure 2. Particle characterization data plot for crystallized product without PEF at 5 ºC/h.

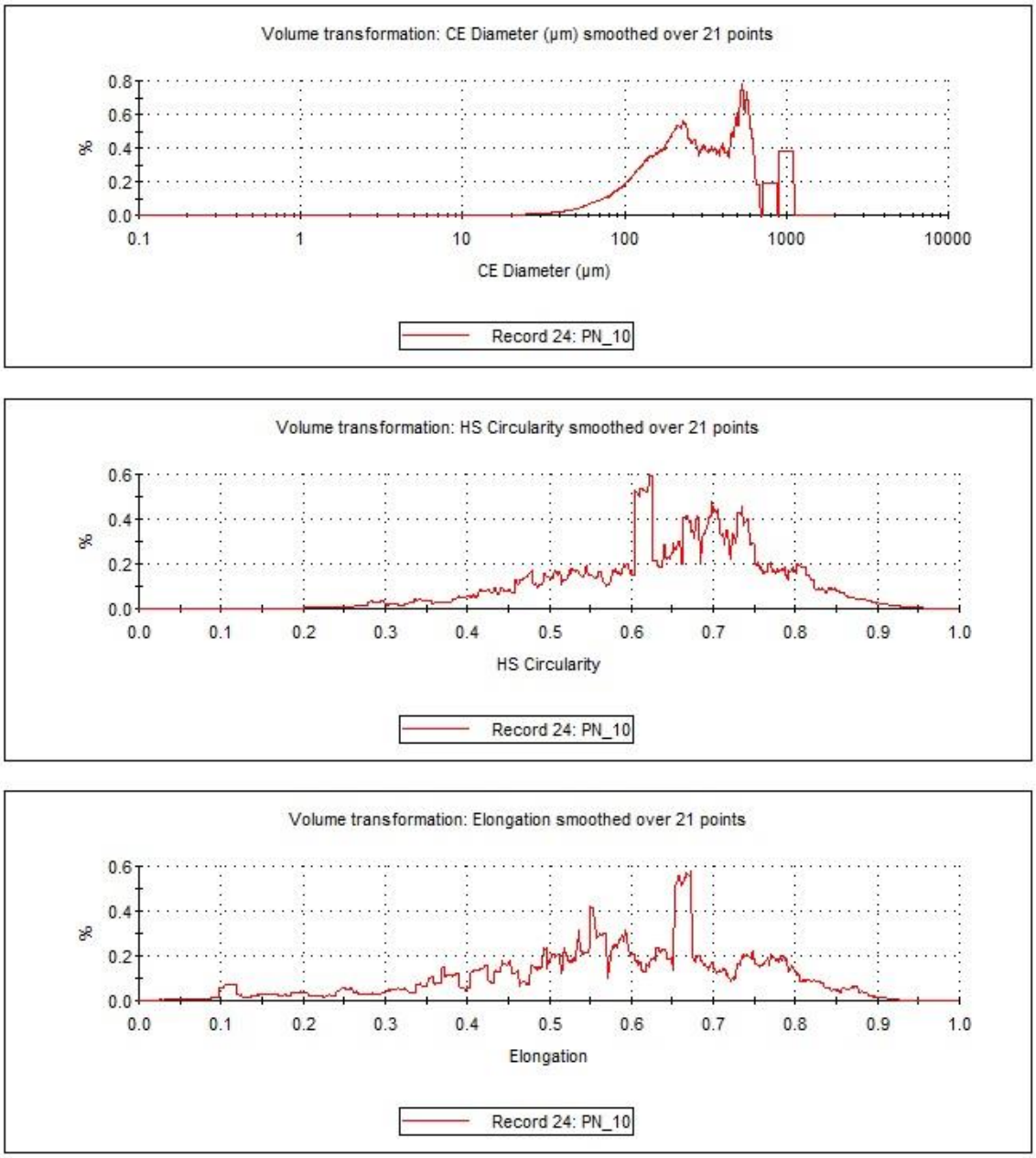

Figure 3. Particle characterization data plot for crystallized product without PEF at 10 ºC/h.

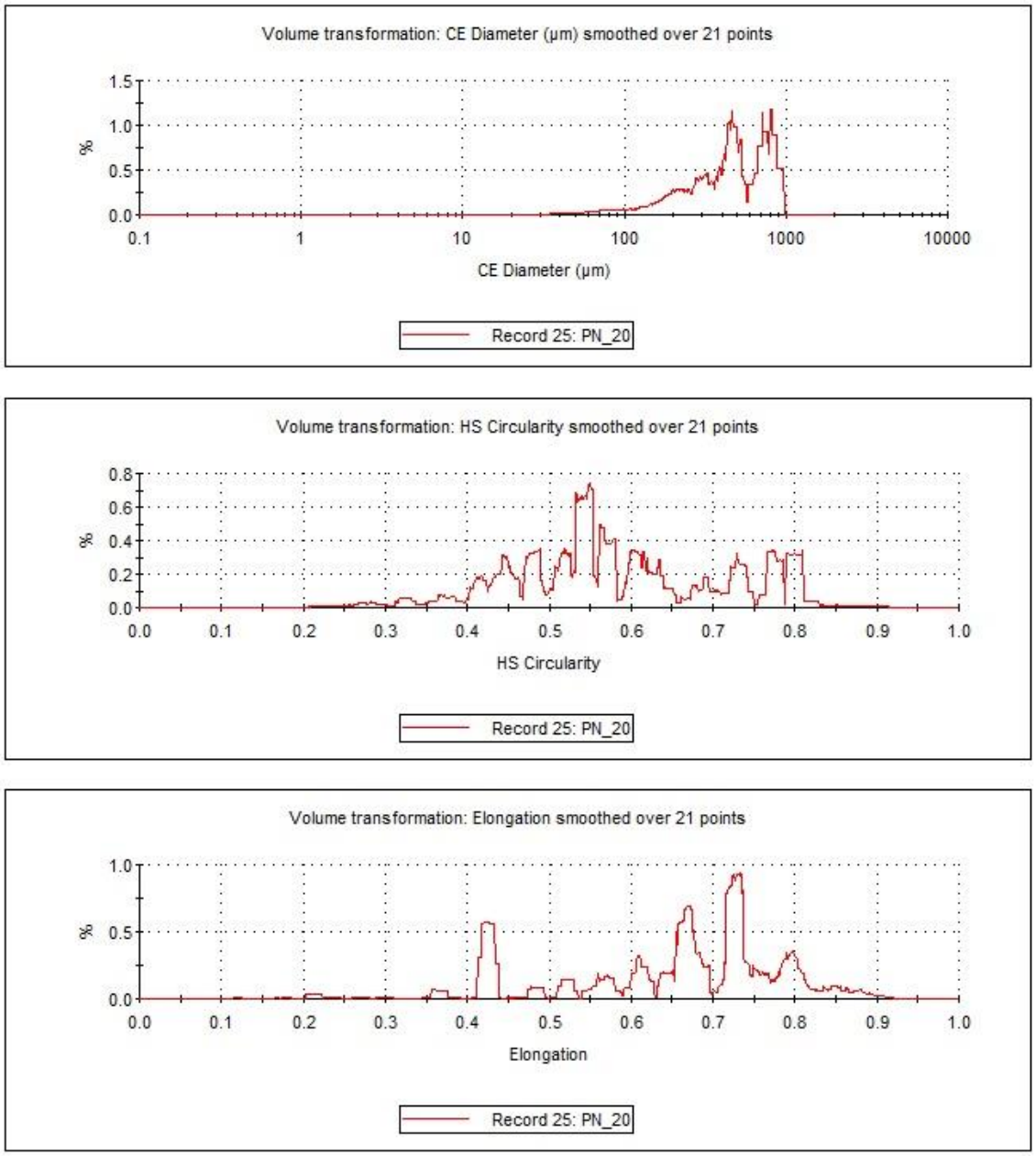

Figure 4. Particle characterization data plot for crystallized product without PEF at 20 ºC/h.

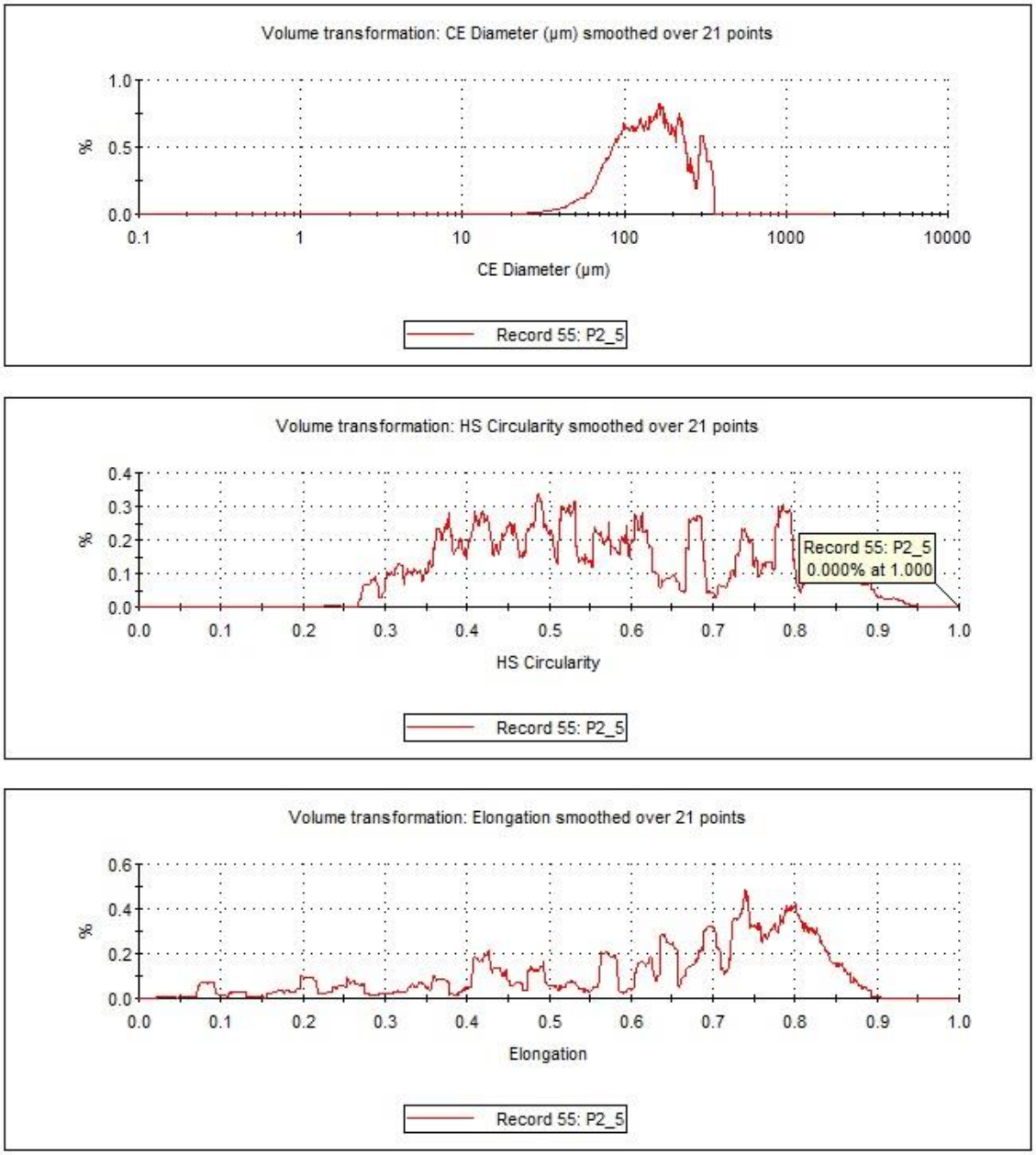

Figure 5. Particle characterization data plot for crystallized product at 294 Hz and 5 ºC/h.

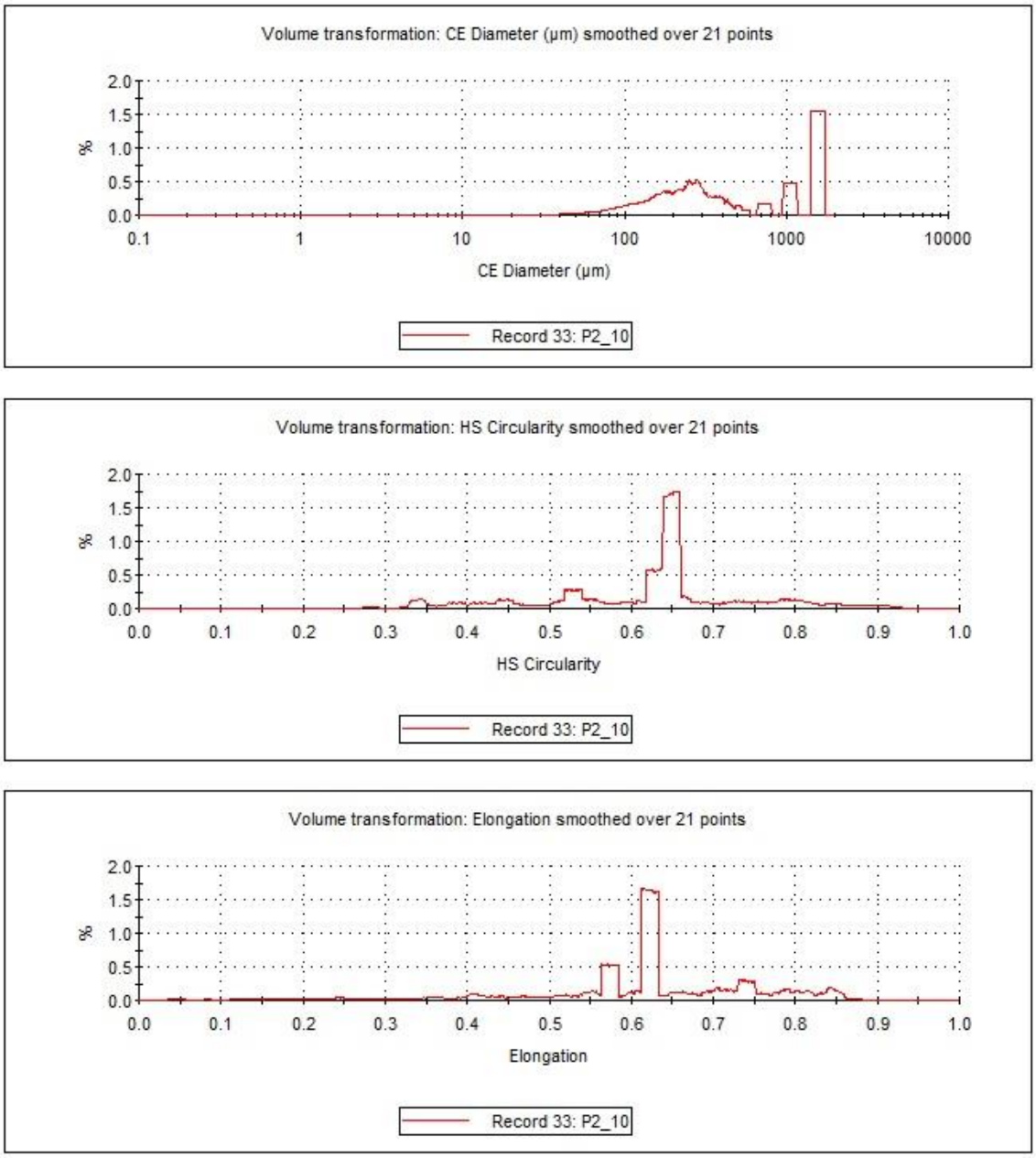

Figure 6. Particle characterization data plot for crystallized product at 294 Hz and 10 ºC/h.

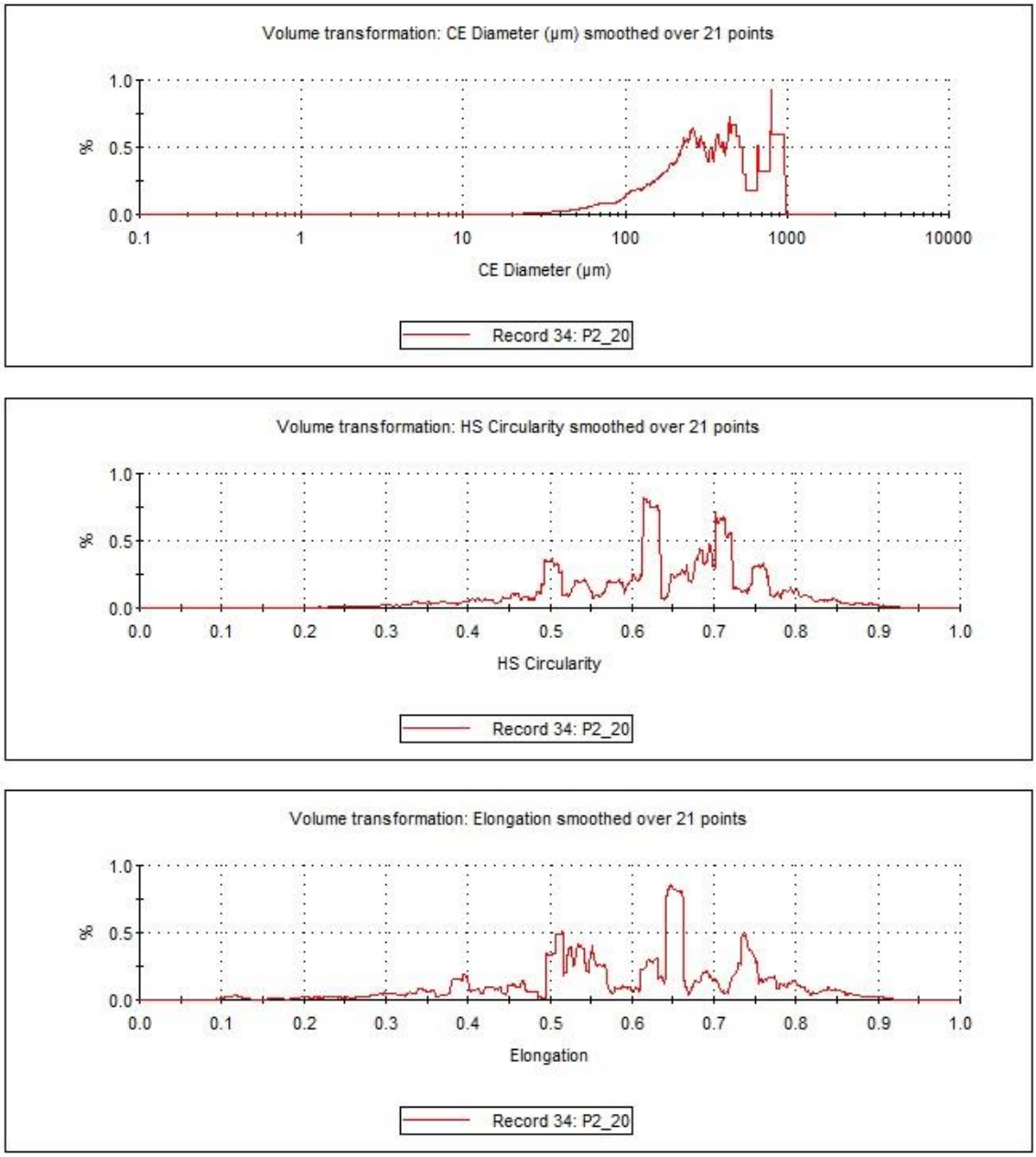

Figure 7. Particle characterization data plot for crystallized product at 294 Hz and 20 ºC/h.

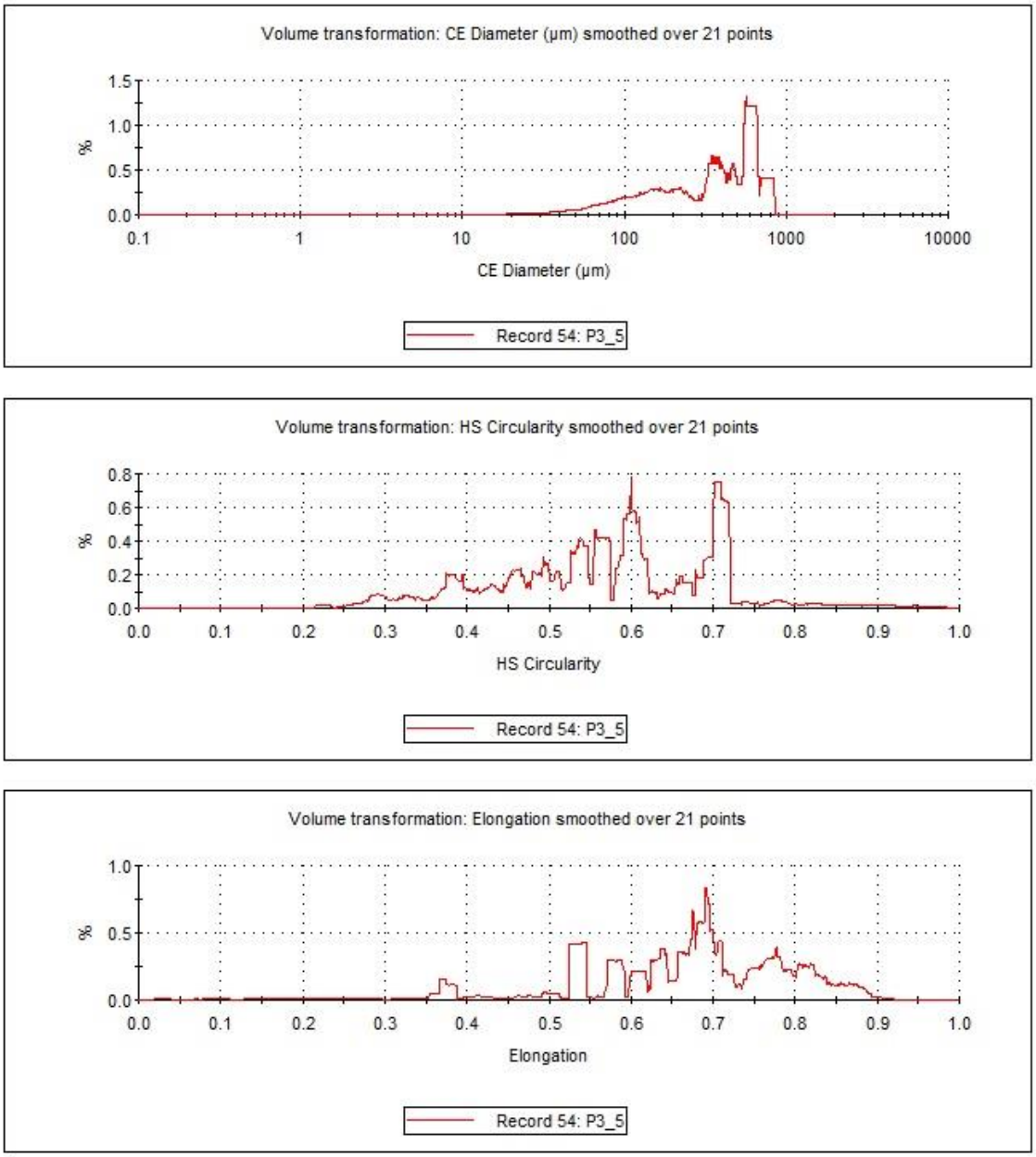

Figure 8. Particle characterization data plot for crystallized product at 950 Hz and 5 ºC/h.

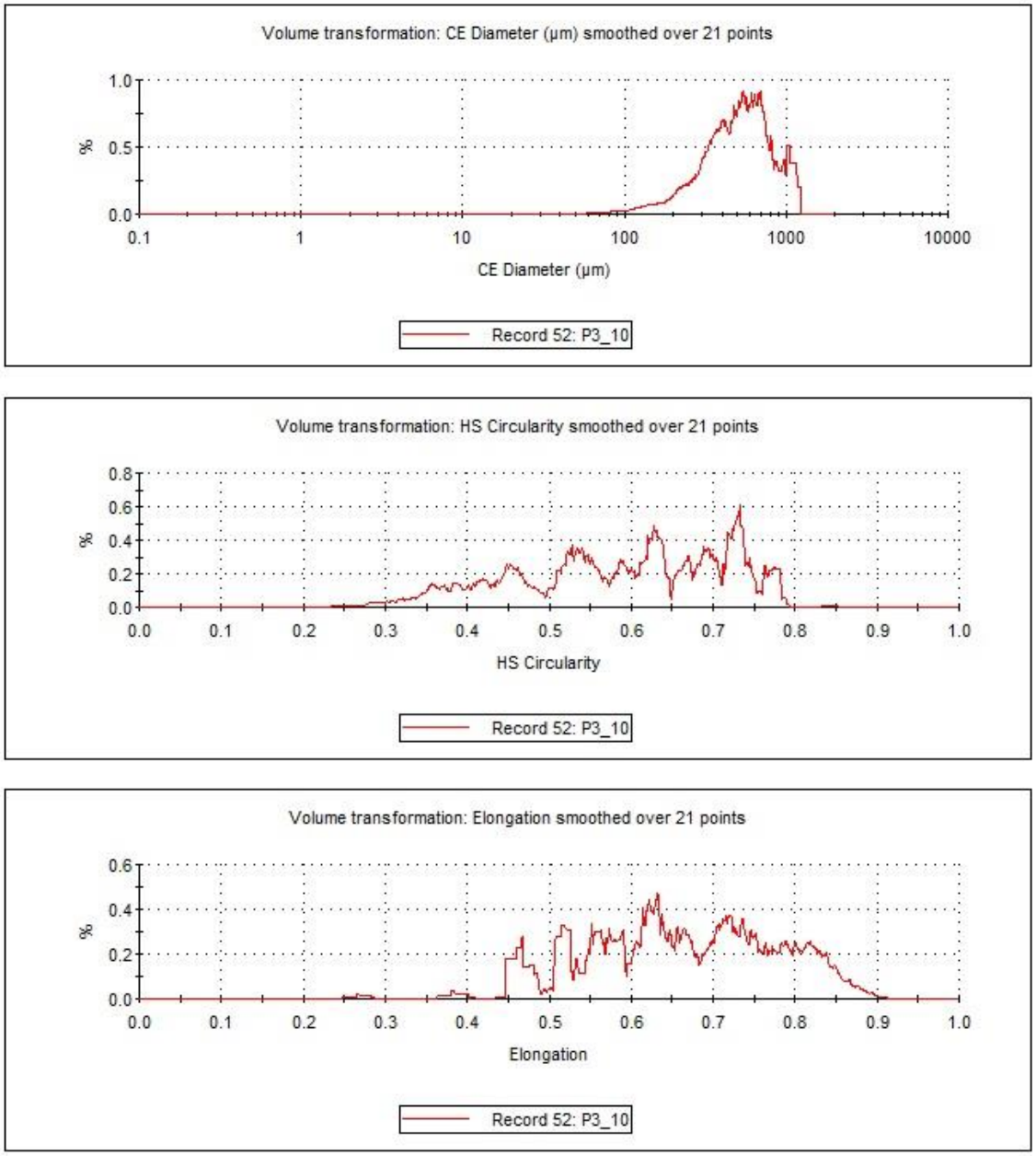

Figure 9. Particle characterization data plot for crystallized product at 950 Hz and 10 ºC/h.

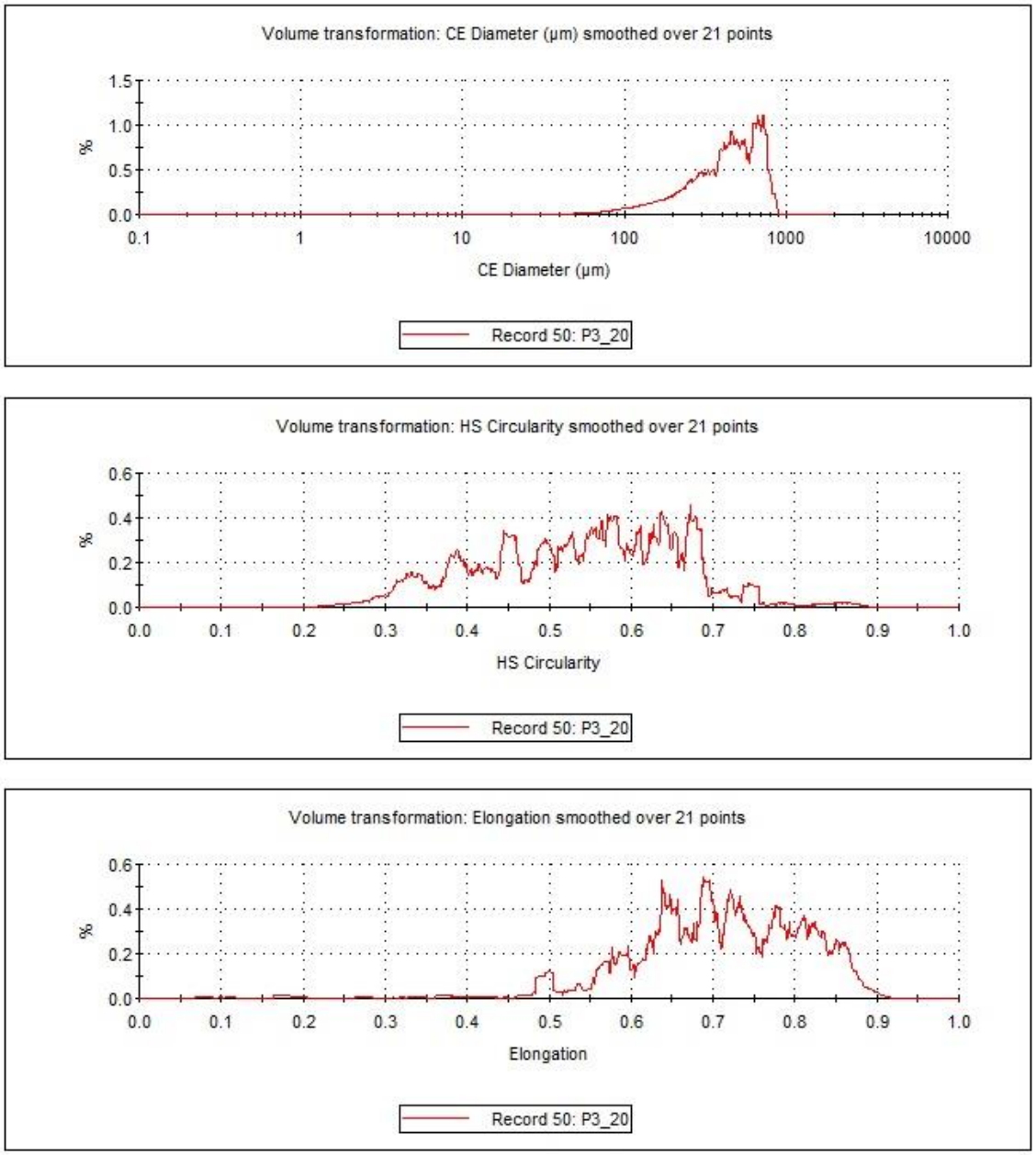

Figure 10. Particle characterization data plot for crystallized product at 950 Hz and 20 ºC/h.

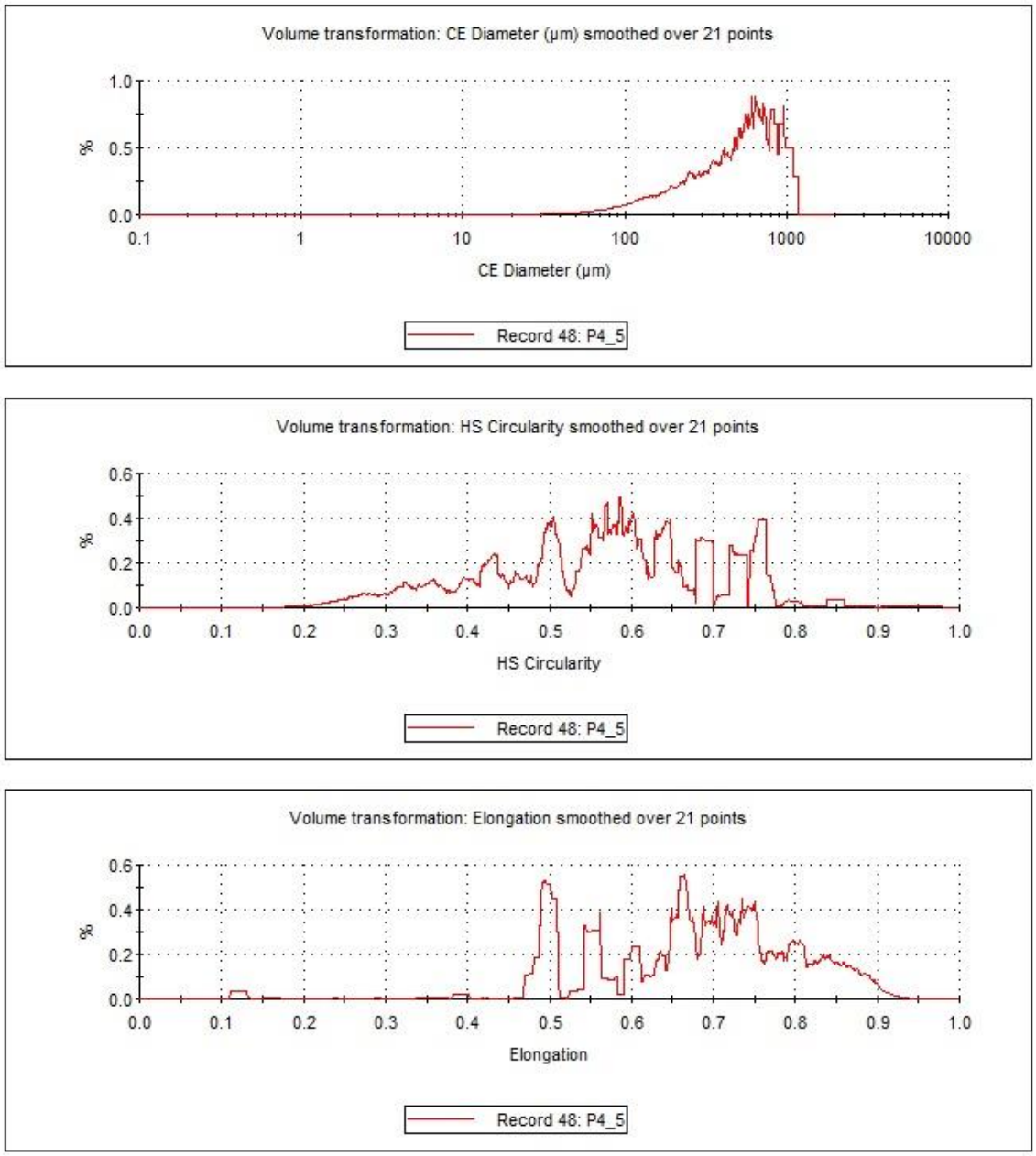

Figure 11. Particle characterization data plot for crystallized product at 145 Hz and 5 ºC/h.

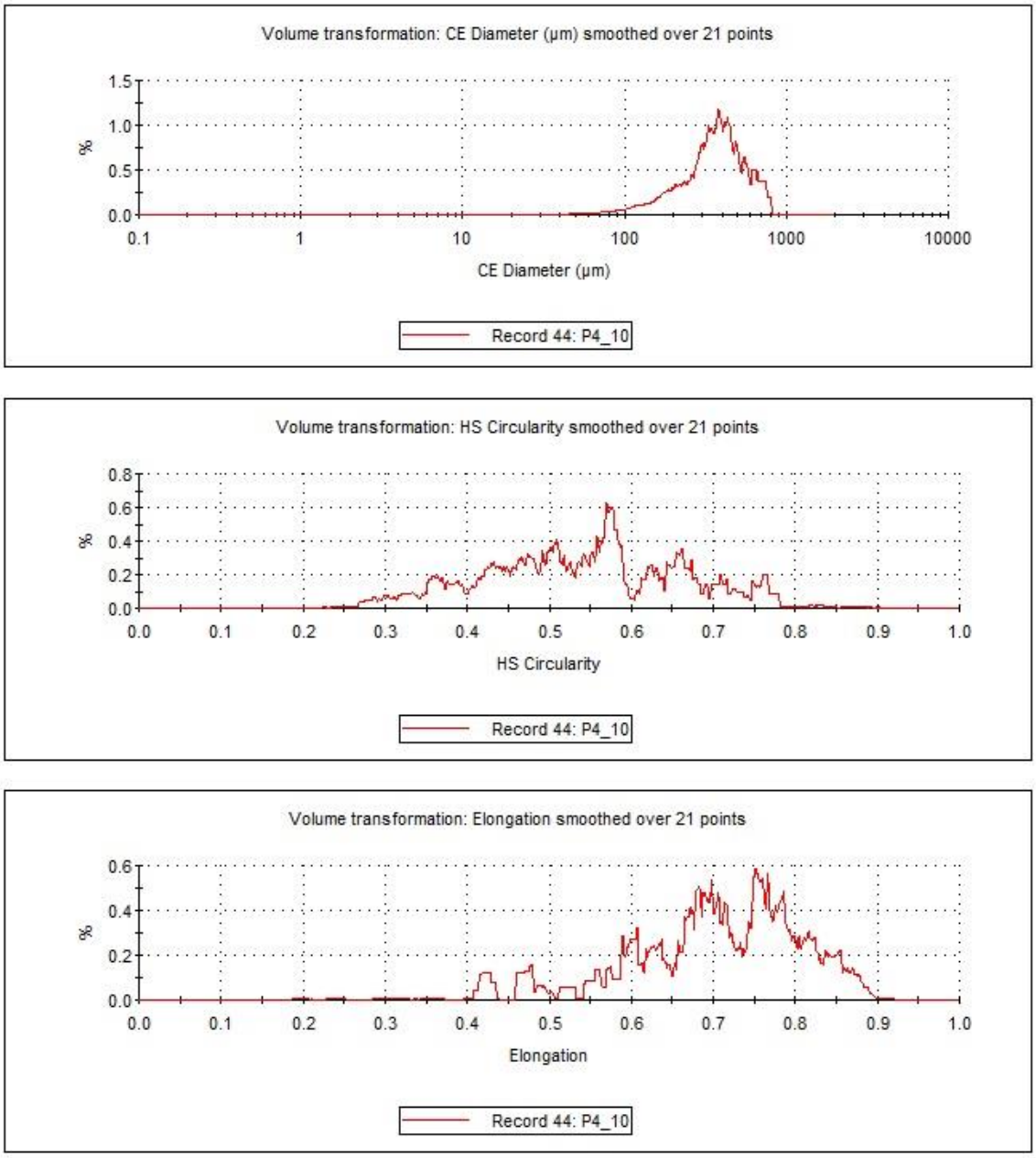

Figure 12. Particle characterization data plot for crystallized product at 145 Hz and 10 ºC/h.

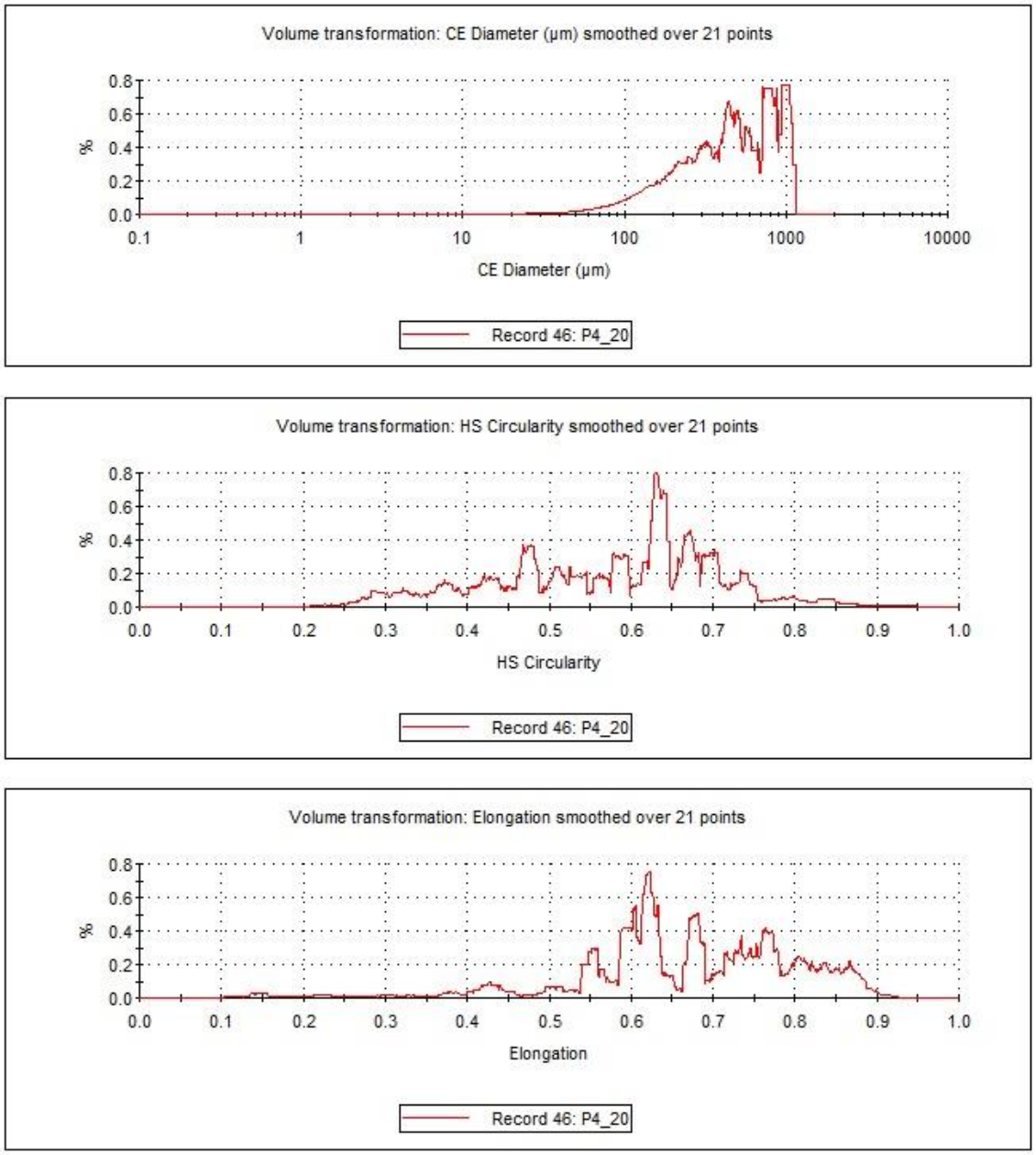

Figure 13. Particle characterization data plot for crystallized product at 145 Hz and 20 ºC/h.